DESIGN AND ANALYSIS OF SIW FILTER AND ANTENNA

A thesis submitted to

Delhi Technological University

for the Award of Degree of

Doctor of Philosophy

In

Electronics and Communication Engineering

by

SUDARSHAN KUMAR

(Roll No. 2K17/PHD/EC/10)

Under the Supervision of

Dr. ASOK DE

Professor

ELECTRONICS AND COMMUNICATION ENGINEERING DEPARTMENT

DELHI TECHNOLOGICAL UNIVERSITY

(Formerly Delhi College of Engineering)

Bawana Road, Delhi – 110042 India

August, 2023

DECLARATION

I hereby declare that the research work reported in this thesis entitled "**Design and Analysis of SIW Filter and Antenna**" for the award of the degree of Doctor of Philosophy in Electronics and Communication Engineering has been carried out by me under the supervision of Prof. Asok De in the Department of Electronics and Communication Engineering at Delhi Technological University, New Delhi.

The research work embodied in this thesis, except where otherwise indicated, is my original research. This thesis has not been submitted by me earlier in part or full to any other University or Institute for the award of any degree or diploma. Furthermore, this thesis does not contain other person's data, graphs, or other information unless specifically acknowledged and cited.

Date:

(Sudarshan Kumar)

Roll No. 2K17/PHD/EC/10

Department of ECE

Delhi Technological University,

New Delhi 110042, India

Delhi Technological University
(Formerly Delhi College of Engineering)
Shahbad Daulatpur, Bawana Road,
New Delhi 110042, India

This is to certify that the research work embodied in the thesis entitled "**Design and Analysis of SIW Filter and Antenna**" submitted by **Mr. Sudarshan Kumar** with roll no. **(2K17/PHD/EC/10)** is the result of her original research carried out in the Department of Electronics and Communication Engineering, Delhi Technological University, New Delhi, for the award of **Doctor of Philosophy** under the supervision of **Prof. Asok De**.

It is further certified that this work is original and has not been submitted in part or fully to any other University or Institute for the award of any degree or diploma.

This is to certify that the above statement made by the candidate is correct to the best of my knowledge.

(Prof. Asok De)

Supervisor

Professor

Department of ECE

Delhi Technological University

New Delhi-110042

ACKNOWLEDGEMENT

Begin by expressing my heartfelt gratitude to the Almighty, the source of all wisdom and knowledge, for guiding me throughout this Ph.D. journey. I am deeply thankful for the strength, inspiration, and blessings I have received from above, which have sustained me during moments of doubt and difficulty. The unwavering faith and belief in divine guidance have been my constant companions, reminding me that all things are possible with God's grace.

I am profoundly grateful to everyone who has supported and contributed to the successful completion of my Ph.D. thesis. This journey has been both challenging and rewarding, and I am immensely thankful for the encouragement, guidance, and assistance I have received along the way.

First and foremost, I would like to express my heartfelt gratitude to my esteemed supervisor, Prof. Asok De, for their unwavering support, expertise, and invaluable guidance throughout the entire research process. Their profound knowledge, insightful feedback, and constant motivation have been instrumental in shaping this thesis and enhancing my research skills. I am truly indebted to them for their mentorship and patience.

I would like to extend my appreciation to Prof. O. P. Verma, Head of the Department of ECE and Prof. Neeta Pandey, DRC Chairperson, along with the entire faculty members, researchers, and staff at Delhi Technological University, New Delhi. Their continuous support and guidance have provided me with an intellectually stimulating environment and a wealth of knowledge throughout my Ph.D. journey. Engaging in discussions, attending seminars, and participating in conferences organized by them have broadened my horizons and significantly influenced the development of my research.

I am equally grateful to my late mother, Angoori Devi, whose unwavering support, love, and encouragement during my formative years laid the foundation for my academic pursuits. Though she is no longer with us, her memory remains a guiding light, and I am forever grateful for the values and life lessons she imparted.

I am equally grateful to my father, Shri Prem Singh Manav, for his unconditional love, constant encouragement, and unwavering belief in my abilities. His guidance, wisdom, and sacrifices have been instrumental in shaping my character and fostering a passion for learning.

I am also deeply grateful to my loving wife, Ms. Monu, for her understanding, patience, and constant support during the challenging phases of this journey. Her presence and encouragement have been my motivation to overcome obstacles and persevere in pursuit of excellence.

Furthermore, I would like to express my gratitude to my children, Aanya, Avika, and Aarav, for bringing joy, laughter, and a sense of purpose to my life. Their innocent smiles and understanding during times of long study hours have been a source of inspiration, reminding me of the significance of this endeavour.

I extend my heartfelt appreciation to Prof. Neelam Sharma (Director), Prof. S. S. Deswal (Dean Academics), and Prof. Sunil Mathur (HOD ECE) from the Maharaja Agrasen Institute of Technology, New Delhi, for their constant support and inspiration.

Lastly, I am grateful to all the individuals who have participated in my study, providing their time, expertise, and valuable insights. Their contributions have enriched the findings of this research and made a significant impact on the field.

Completing this Ph.D. thesis would not have been possible without the collective support and contributions of all the individuals mentioned above, as well as those who may have inadvertently been omitted. I extend my sincerest gratitude to everyone who has played a role, no matter how big or small, in shaping my academic journey.

Thank you all for your belief in me, your unwavering support, and your contributions to this research. I am truly humbled and forever grateful.

Place: New Delhi (India) **(Sudarshan Kumar)**

DEDICATIONS

This thesis is dedicated to all my family members

Contents

ABSTRACT

The rapid advancements in microwave and millimeter-wave systems have necessitated the development of efficient transmission line technologies. Substrate-integrated waveguide (SIW) has emerged as a popular solution, offering a compelling compromise between the losses associated with planar transmission lines and the cost and size challenges of conventional metallic waveguides. In this thesis, we explore the design and analysis of SIW, SIW filters, and antennas. By utilizing a dielectric substrate with conductors acting as ground planes, SIW combines the benefits of planar transmission lines and metallic waveguides, making it an attractive choice for various high-frequency applications. This thesis presents a comprehensive investigation into the potential of SIW technology for designing and optimizing filters and antennas suitable for millimeter-wave systems and wireless communication.

The work is structured into eight chapters, each contributing unique insights into SIW technology. The introductory chapter provides an overview of SIW's fundamental geometry and various types, such as Half-Mode Substrate Integrated Waveguide (HMSIW), Substrate Integrated Folded Waveguide (SIFW), and Substrate Integrated Rectangular Waveguide (SIRW). Different analysis techniques employed for SIW, including mode matching, full-wave simulation, and other numerical methods, are explored, along with the motivation, objectives, and overall structure of the thesis.

A literature survey is conducted in the subsequent chapter, providing a comprehensive review of existing research and studies related to SIW and its applications. This survey not only highlights the state-of-the-art developments in the field but also identifies gaps and opportunities for further advancements.

Chapters focusing on specific aspects of SIW technology follow, including the design and analysis of sinusoidally modulated SIW, step-sized SIW using mode matching techniques, and a compact sinusoidally modulated SIFW. These chapters provide detailed insights into the characteristics and performance of SIW-based components, such as their frequency responses, dispersion properties, and filter behaviors. Additionally, a novel SIW-based antenna optimized for self-diplexing applications is introduced, along with the design of three

distinct HMSIW components: an HMSIW, an HMSIW band-pass filter, and an HMSIW leaky wave antenna. These antenna designs showcase the versatility and potential of SIW technology for wireless communication systems, offering advantages in terms of compactness, efficiency, and multi-frequency operation.

The conclusive chapter summarizes the essential discoveries, results, and contributions of the research. It also outlines potential avenues for future exploration and study within the field, presenting directions for further investigation and advancement. The thesis concludes by emphasizing the significance of SIW technology in enabling the development of advanced millimeter-wave systems and wireless communication networks.

Overall, this thesis contributes valuable insights into the design and analysis of SIW filters and antennas, offering new possibilities for enhancing the performance and efficiency of communication systems in millimeter-wave and wireless applications. The research presented in this work serves as a valuable resource for those who are working in the field of high-frequency engineering and wireless communication technologies.

List of Figures

List of Tables

List of Abbreviations

2 D	2 Dimension
3 D	3 Dimension
5G	Fifth Generation
BI-RME	Boundary Integral Resonant Mode Expansion
CPW	Coplanar Waveguide
CSRR	Complementary Split Ring Resonator
CST	Computer Simulation Technology
CST-MWS	Computer Simulation Technology-Microwave Studio
DGS	Defected Ground Structure
EBG	Electronic Band Gap
EM	Electromagnetic
GCPW	Grounded Coplanar Waveguide
HFSS	High Frequency Structure Simulator
HMSIW	Half Mode Substrate Integrated Waveguide
FDTD	Finite Difference Time Domain
FEM	Finite Element Method
FHMSIW	Folded Half Mode Substrate Integrated Waveguide
FMSIW	Full Mode Substrate Integrated Waveguide
FSIW	Folded Substrate Integrated Waveguide
FWEM	Full- Wave Electromagnetic Modelling
IF	Intermediate Frequency

IOT	Internet of Things
LAN	Local Area Network
LO	Local Oscillator
LTCC	Low Temperature Co -fired Ceramics
LWA	Leaky Wave Antenna
MB	Mega Bytes
MOM	Method of Moments
MM	Millimeter Wave
MMT	Mode Matching Technique
NFC	Near Field Communication
N/W	Network
PCB	Printed Circuit Board
PEC	Perfect Electric Conductor
PMC	Perfect Magnetic Conductor
RF	Radio Frequency
RWG	Rectangular Waveguide
SMSIW	Sinusoidally Modulated Substrate Integrated Waveguide
SMSIFW	Sinusoidally Modulated Substrate Integrated Folded Waveguide
SIW	Substrate Integrated Waveguide
SIWs	Substrate Integrated Waveguides
SIFW	Substrate Integrated Folded Waveguide
SIRW	Substrate Integrated Ridge Waveguide

SISW	Substrate Integrated Slab Waveguide
TE	Transverse Electric
TM	Transverse Magnetic
Wi-Fi	Wireless Fidelity
Wi-Fi 6 E	Wireless Fidelity 6 Extended

CHAPTER 1

Introduction

Wireless communication underwent a significant revolution and advancement, transforming the way we connect and communicate in our modern world. It has become an integral part of various domains, including telecommunications, networking, mobile computing, Internet of Things (IOT) and more. Wireless communication use electromagnetic waves to transmit information. These electromagnetic waves, including radio waves, microwaves, or even light waves, transmit the encoded data between the transmitting device and the receiving device. The range of wireless communication can vary greatly, depending on the specific technology and application. Short-range wireless communication is commonly employed for devices in close proximity, such as Bluetooth for connecting peripherals to a computer or NFC (Near Field Communication) for contactless transactions. Wi-Fi is another widely used wireless technology that facilitates rapid communication over limited to moderate distances within a local area network (LAN). For longer distances, technologies like cellular networks come into play. Mobile devices can communicate with cellular networks through a network of cellular towers or base stations, allowing voice and data to be transmitted across long distances. These networks allow mobile devices to stay connected and communicate seamlessly as users move within their coverage area.

Wireless communication has opened up new possibilities and transformed various industries. It has facilitated the proliferation of smartphones, enabling ubiquitous access to voice calls, text messages, and internet services. Additionally, wireless technologies have empowered the growth of IOT, enabling the interconnection of various devices and sensors to exchange data wirelessly and automate processes. Furthermore, wireless communication plays a vital role in areas such as satellite communications, radio broadcasting, wireless sensor networks, and even interplanetary communications, expanding the frontiers of human exploration and connectivity.

As technology continues to advance, the field of wireless communication is expected to witness further innovations, including faster data rates, improved reliability, and expanded coverage areas. These advancements will likely fuel the development of new applications and transformative technologies, bringing about even more connectivity and convenience in our daily lives.

On December 12, 1901, Marconi successfully sent a wireless signal by using radio waves to send a straightforward Morse code signal from Cornwall, England (Poldhu), almost 2,100 miles distant, to a receiving station in St. John's, Newfoundland. This transmission proved that electromagnetic waves could be sent over great distances, as it took place between Poldhu, England, and Newfoundland, Canada. The efficacy of a communication system's users in transmitting and receiving energy in the suitable fashion influences both the specific subsystems and the system's entirety. To capture the intended signal, the receiver is equipped with a filter, and an antenna serves the dual purpose of transmitting and receiving electrical energy. As a consequence of this, these two components constitute very essential aspects of a wireless communication system.

A device known as a filter is created to allow the flow of signals at specific frequencies, while concurrently attenuates signals magnitude at other frequencies. An optimal filter exhibits zero attenuation within the desired frequency range, resulting in no loss of signal, and provides infinite attenuation outside that range. The linear characteristics of the ideal filter apply solely to the desired frequencies. Nevertheless, real-world filters may display slight deviations from this ideal behaviour due to inherent limitations. Conversely, an antenna functions as a device utilized for both the transmission and reception of electromagnetic waves. Fig. 1.1 shows an example of wireless communication system.

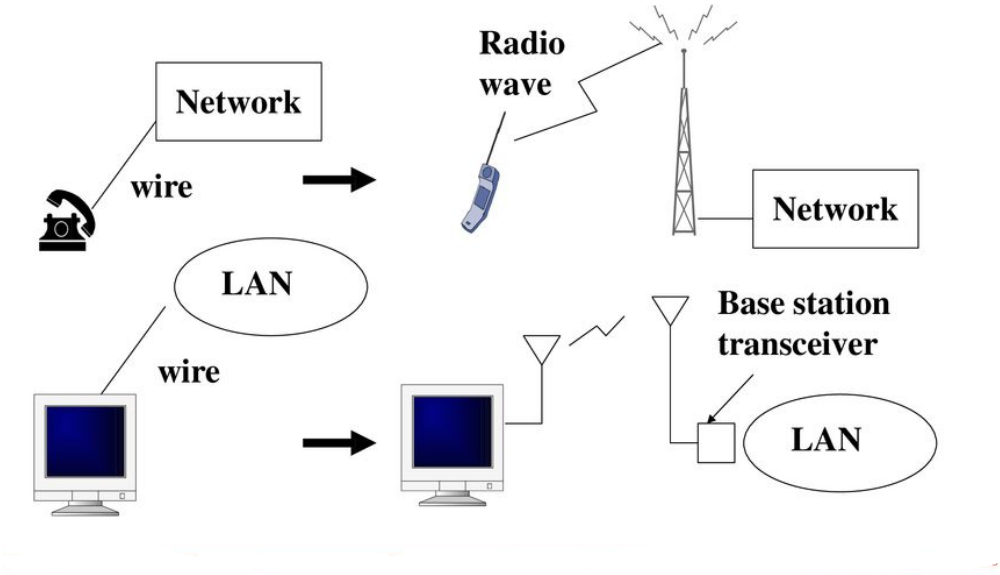

Figure 1.1 Wireless communications System

Rectangular waveguide (RWG) components excel in microwave systems due to their exceptional performance characteristics. In comparison to microstrip line components, these components exhibit superior system performance, yet the cost of these components is high and their size is too large to meet the latest compactness techniques.

In 1994, a Japanese research paper described the SIW structure for the first time. Subsequently, the research team led by Ke.Wu at École Polytechnique de Montréal in Canada played a crucial role in advancing SIW technology and components, thanks to their pioneering investigations in the field. From 2001 to 2007, they conducted research specifically focused on SIW, publishing several important works related to SIW technology and its applications. During their research, Ke Wu and his group extensively investigated the design and characteristics of SIW, utilizing PCB and LTCC technologies. Their endeavours substantially contributed to driving the contemporary progress of SIW technology. Before the term "Substrate Integrated Waveguide" came into use, various similar structures resembling SIW were independently developed. SIW is commonly acknowledged as a planar alternative to the traditional RWG. In [2], a parallel-plate waveguide with similarities to SIW was presented, and [3] introduced a laminated waveguide resembling SIW. However, it was the collaborative efforts of Ke Wu and a team of researchers that played a pivotal role in shaping SIW technology and its subsequent advancements. Their studies and publications between 2001 and 2007 contributed significantly to the understanding and practical

implementation of SIW technology and components. Since its introduction, SIW technology has become highly prevalent in various fields of application, especially millimeter-wave communication system. Additionally, it has significantly contributed to the advancement of high-frequency circuits and systems. Its planar and compact nature, coupled with its impressive power-handling characteristics and minimal signal loss, make SIW a compelling choice for a wide range of radio frequency and microwave engineering applications [4-7].

Overall, the ability to integrate multiple components, reduce losses and parasitic, and enable easy coupling with other transmission line technologies are some of the key advantages of SIW technology. These advantages contribute to improved system performance, design simplicity, and miniaturization, positioning SIW as a highly favourable solution for a diverse range of high-frequency applications. Microstrip lines and coplanar waveguides can be easily coupled to SIW circuits because they are all built on the same substrate.

1.1 SIW and SIW Geometry

The SIW setup involves using a dielectric substrate with metallic layers applied to both its upper and lower surfaces. It utilizes a pair of closely spaced cylindrical holes, which are also metallized, to establish electrical connectivity between the upper and lower metal layers. These cylindrical holes, known as metal vias or posts, are responsible for forming the waveguide's side walls. In certain cases, metalized slots can be used as an alternative to vias or posts. Fig. 1.2 illustrates the geometric layout of the SIW.

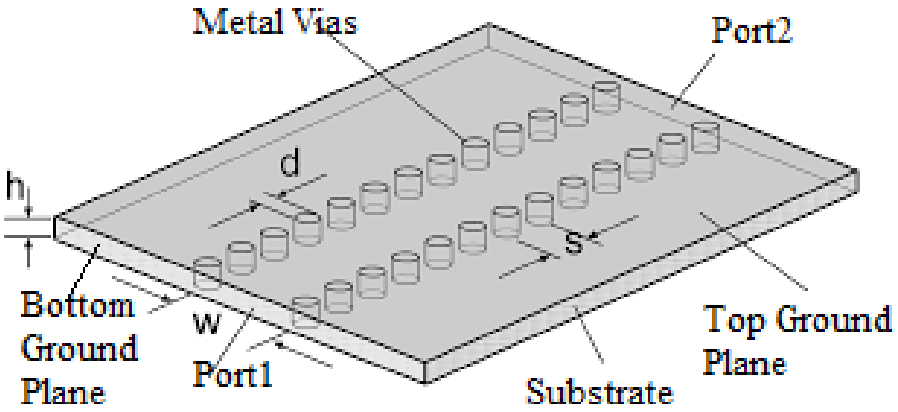

Figure 1.2 Geometrical layout of SIW [8]

Dielectric substrate material used in microstrip and coplanar waveguides can also be utilized for SIW interconnects and components. Compared to metallic RWG, the dielectric substrate's thickness is typically smaller. The following three factors dictate the physical configuration, these are waveguide width w, hole diameter d, and hole spacing s. References [6, 8] provide explanations that establish a connection between the width of the SIW and its fundamental mode as well as the frequency band in which it operates. This relationship arises due to the fact that the SIW serves as a planar alternative to the metallic RWG.

1.2 SIW Operating Principles

The SIW primarily facilitates the propagation of the dominant TE mode TE_{10} in wave propagation phenomena, which shares resemblances with a metallic RWG. However, unlike the metallic RWG, the SIW's upper and lower ground planes exhibit similar behavior in terms of surface current. The metallic vias in the SIW allow for the smooth flow of surface current along the sides, without being perturbed by gaps between the vias. SIW components are characterized as *H*-plane waveguide structures, based on their geometry and mode pattern. An essential and distinguishing feature of the SIW is its perpendicular orientation of the $\boldsymbol{E}$-field concerning the broader side, resulting in a constant field strength without vertical variations. The wave propagation properties of SIW components are largely unaffected by the substrate thickness (h), except for conductor losses. The restricted impact on wave propagation becomes apparent when analyzing the $\boldsymbol{E}$-field arrangement of the dominant mode, as depicted in Fig.1.3.

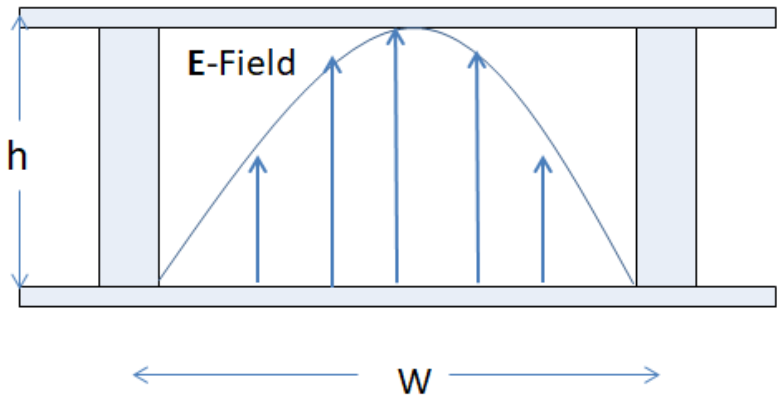

Figure 1.3 $\boldsymbol{E}$-field arrangement of the dominant mode TE_{10}

1.3 Different SIW Configurations

Compared to conventional printed transmission lines, SIW structures possess two significant disadvantages: a narrower bandwidth and larger volume. SIW structures have a specific range of frequencies they can work with. This range starts at the lowest cutoff frequency f_0 and goes up to twice that frequency $2f_0$ for the next mode. In simple terms, SIWs can handle frequencies that are about double the width of the lowest cutoff frequency. This limited bandwidth arises from the presence of cutoff frequencies for higher modes within the waveguide. In addition to the bandwidth limitation, SIW structures tend to have larger dimensions or occupy more space compared to traditional planar transmission lines. Furthermore, SIW structures' tendency to possess larger dimensions or occupy more space compared to traditional planar transmission lines can present a limitation in applications where space is restricted or miniaturization is necessary. Overall, the narrower bandwidth and larger physical size are notable aspects that differentiate SIW structures from conventional printed transmission lines [9, 10].

Typically, a SIW's width is greater than a microstrip line's width. The breadth of a SIW needs to be compared to ensure a fair comparison. When there is a minimum spacing between two consecutive microstrip lines in order to prevent cross-coupling, the size difference appears to be considerably less noticeable. In contrast, SIW structures take advantage of the reduction in size achieved through dielectric loading.

In response to the limitations in bandwidth and compactness, researchers have developed various configurations of SIW. Various configurations and topologies of SIW have been developed with the aim of addressing these challenges. This section will outline the creation of several SIW topologies that have been specifically designed to address these limitations.

1.3.1 Substrate Integrated Folded Waveguide (SIFW)

The SIFW incorporates the principle of folded RWG, which was first presented in [11], and it allows for a reduction in waveguide width by using a dual-layer substrate. Fig. 1.4 shows front view of the SIFW.

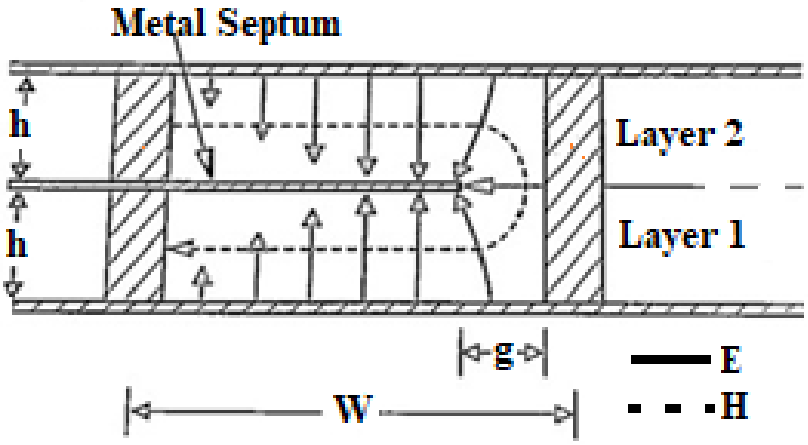

Figure 1.4 Front view of SIFW [10]

The electric field in the gap area exhibits a strong and high amplitude due to the greater non-radiating losses present in the SIFW as opposed to the SIW. Consequently, the increase in loss is less prominent for wider gaps but becomes more significant for narrower gaps. Considering that the magnetic fields in both sections are predicted to be identical yet opposing, the SIFW demonstrates reduced radiation loss from its left sidewall, as illustrated in Fig. 1.4 [12]. In addition to their compact design, SIFW configurations offer several benefits. They provide manufacturing simplicity by eliminating the need for internal vias and maintain comparable electromagnetic shielding capabilities to unfolded counterpart. The formulation of the SIFW can be found in [13].

1.3.2 Half Mode Substrate Integrated Waveguide (HMSIW)

The HMSIW is an innovative waveguide structure that deviates from the traditional SIW design by incorporating a reduced width. The HMSIW is derived by cutting the SIW either transversely or longitudinally. Fig. 1.5 depicts the geometrical layout of the HMSIW [14, 15].

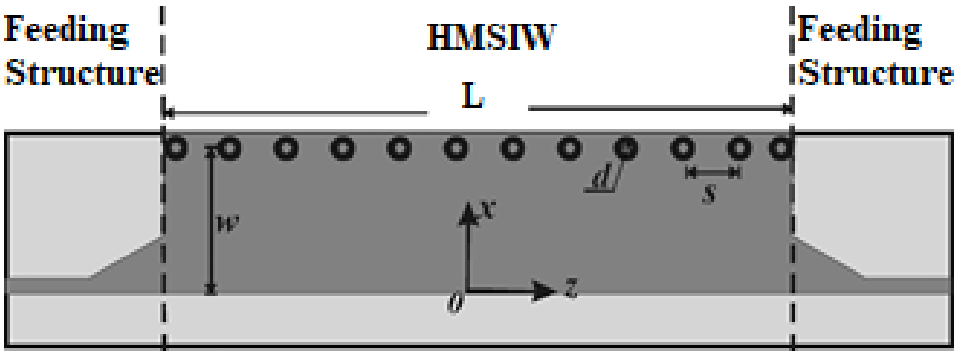

Figure 1.5 Geometrical configuration of HMSIW with feeding structure [14]

The HMSIW offers a significant advantage in terms of its simplicity, enabling a reduction in size by approximately half compared to the SIW. Despite this size reduction, the fabrication complexity is comparable to that of conventional SIW. It is important to highlight that the outer edge of the HMSIW exhibits slot-like behaviour, but it can only operate within a constrained frequency range above the first fundamental frequency. During this range, the field distribution becomes uniform, leading to significant radiation loss. With the exception of this specific frequency range, the losses experienced in the HMSIW are similar to those encountered in the conventional SIW. Fig. 1.6 illustrates the *E*-field line within the HMSIW. To achieve further size reduction, the Folded HMSIW (FHMSIW) was proposed by combining the SIFW and HMSIW approaches [16].

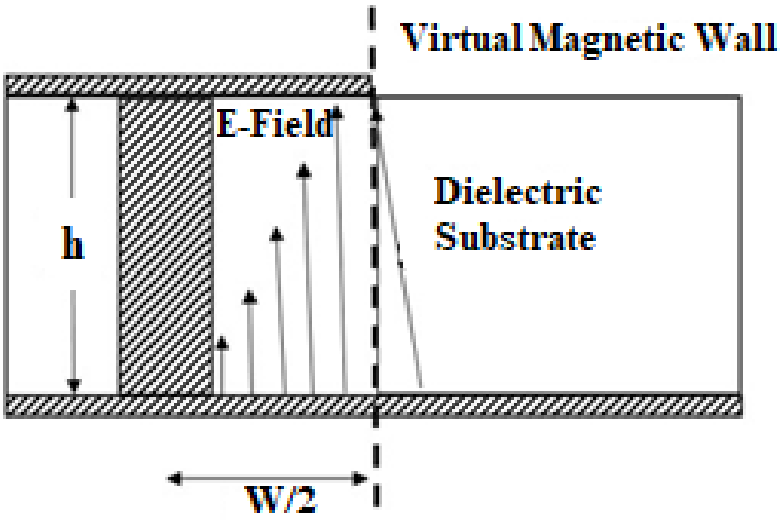

Figure 1.6 ***E***-field line in HMSIW

The fundamental principle behind the HMSIW revolves around the concept that the middle axis along the length of the SIW serves as an efficient magnetic boundary for the fundamental mode. When the HMSIW is cut into two portions along the longitudinal, the exposed portion of the remaining half portion acts like a perfect magnetic conductor, often referred to as a magnetic wall. This magnetic wall effect occurs when the width of the remaining structure is much larger compared to its height, resulting in a dominant magnetic current flow along the SIW. As a consequence, removing one half portion of the SIW while reducing the width by half preserves the same field distribution for the fundamental mode.

1.3.3 Substrate Integrated Slab Waveguide (SISW)

The SISW is a planar waveguide structure that guides and confines electromagnetic waves within a dielectric slab, typically made of a high-permittivity material. The dielectric substrate, coated with metallized conducting planes on both sides, provides support and confinement for wave propagation. In the lateral sections of the SISW's substrate, air holes are incorporated, effectively reducing the dielectric constant. This design contributes to the waveguide's overall performance and characteristics. However, the dielectric constant ε_r remains unaltered in the central region of the waveguide where no air holes are present. The electric field within the central portion of the SISW reaches its maximum value when it encounters the original dielectric constant ε_r.The operating frequency range in SISW is increased compared to SIW due to the above mentioned reasons. Consequently, the cut-off frequency in the SISW is significantly influenced [17, 18]. Figures 1.7(a) and 1.7(b) depict the top view and side view of the SISW, respectively. The dominant mode in the SISW bears resemblance to the TE_{10} mode observed in traditional dielectric- filled rectangular waveguides and SIWs.

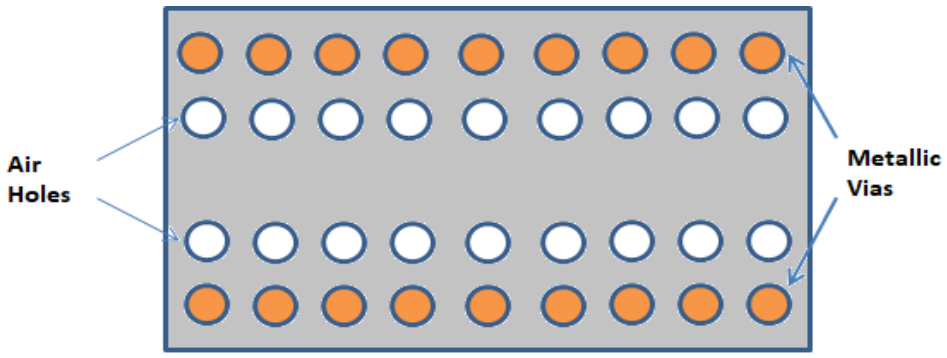

(a)

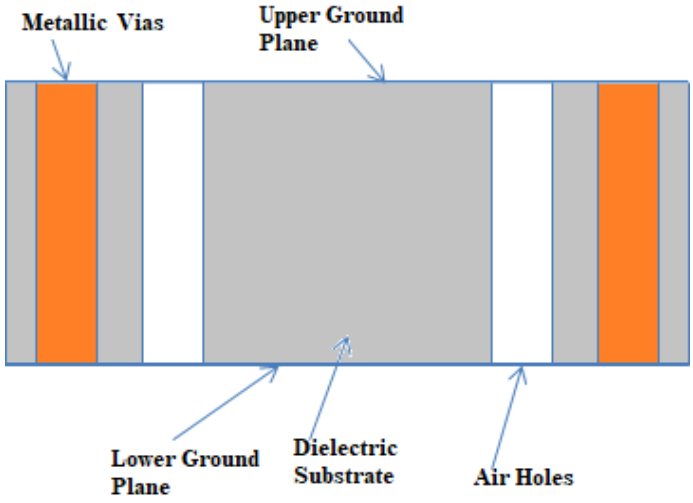

(b)

Figure 1.7 SISW (a) in Top view (b) Lateral view

1.3.4 Substrate Integrated Ridge Waveguide (SIRW)

The SIRW is an innovative waveguide configuration that provides distinctive advantages in high-frequency communication systems, radar system feeding lines, satellite communication feed lines, and various wireless technologies. It serves as a highly effective transmission medium for these applications, offering superior performance and efficiency. It is characterized by a ridge embedded within a substrate, creating a waveguide channel with unique propagation properties. The ridge acts as a guiding structure, confining the electromagnetic waves and allowing for efficient transmission along its length. A central ridge is formed within the SIW by a series of metal posts that have a reduced height. This

integration results in a compact and cost-effective design, making it suitable for miniaturized systems and integrated circuits. The SIRW exhibits low radiation losses, high power handling capabilities, and excellent impedance matching, characterizing it as a compelling option for high-frequency signal transmission in various applications such as mm-wave, radar systems, high-frequency microwave circuits, and other wireless systems. Fig. 1.8 provides an isometric view of the SIRW to illustrate this configuration.

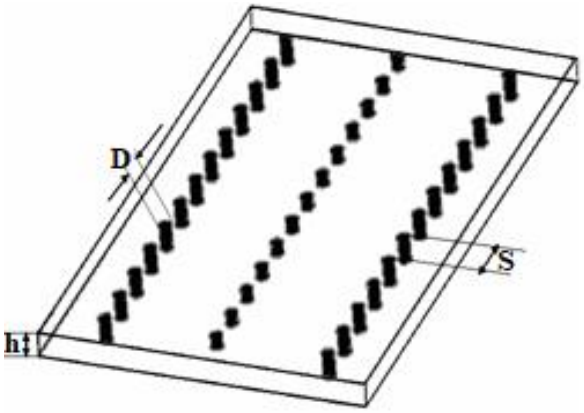

Figure 1.8 Isometric view of the SIRW [20]

In the SIRW configuration, the presence of central metal rows and large-diameter vias can create a band gap effect, which hinders efficient wave propagation. However, this issue has been addressed in the SIRW design by incorporating a modification that effectively resolves the band-gap problem. This modification allows for improved wave propagation, even when using ridge posts with larger diameters [21, 22].

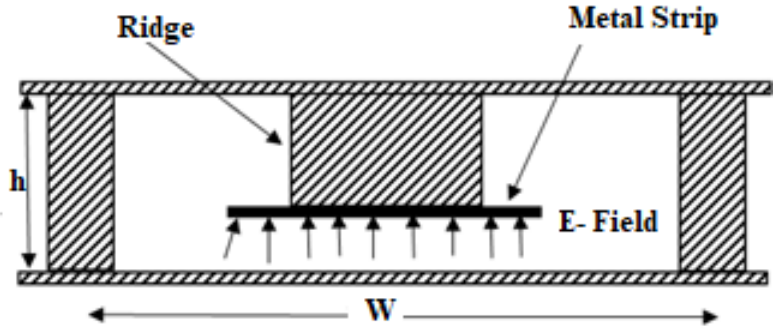

Figure 1.9. Front view of SIRW with metal strip

The integration of the SIRW and SISW principles offers the opportunity for enhanced waveguide performance. One method to accomplish this is by integrating air slots in the sides of the ridge in the SIW structure. By combining these two technologies together, the second cut-off frequency shifts to a higher frequency, thereby increasing the single-mode bandwidth.

1.4 SIW Based Components and Antennas

The field of SIW technology has experienced a notable growth in the incorporation of a diverse set of passive and active components. By utilizing similar configurations and design principles found in traditional metallic waveguides, SIW technology has seen a rapid expansion of various passive and active elements. These innovative SIW components, including filters and antennas, offer distinct advantages such as compact size, affordability, and design adaptability when compared to conventional metallic waveguides. Utilizing smaller dimensions, cost-effectiveness, and versatility.

The advantage of design flexibility in SIW comes from the ability to freely position metallic vias within the structures. These structures can be stacked or arranged into multiple layers, enabling compactness through easy width reduction. Additionally, SIW allows for the integration of planar transmission lines, planar antennas, and other technologies onto a single substrate, simplifying the fabrication of multiple technologies simultaneously. Unlike conventional metallic waveguides, the incorporation of active devices poses challenges. However, integrating them into SIW is a straightforward process. As a result, mm-wave and microwave active and passive devices are easily implementable using SIW technology. Therefore, SIW technology offers a diverse range of advantages and opportunities for the development of advanced components and systems.

1.4.1 Passive Microwave Devices

SIW technology enables the implementation of various passive devices, including filters. The performance characteristics of SIW filters lie between those of metallic waveguide filters and printed transmission line filters. SIW filters exhibit superior performance compared to printed transmission line filters, particularly at millimeter wave frequencies. In addition, SIW

filters are cost-effective, compact in size, and lightweight, making them advantageous over conventional metallic waveguide filters.

- **Filters:**

Several topologies of SIW filters are available, each achieved by incorporating metal posts into a straight SIW structure to create cavities. The simplest configuration involves a single metal post placed at the center or offset within the SIW, which acts as an inductive post. For more complex SIW filters, multiple metal posts are used to form cavities, either centered or offset within the straight SIW. These filter topologies are commonly referred to as inline SIW filters [24]. Figs 1.10 (a) and (b) illustrate the centered and offset SIW filter configurations with multiple metal posts, respectively.

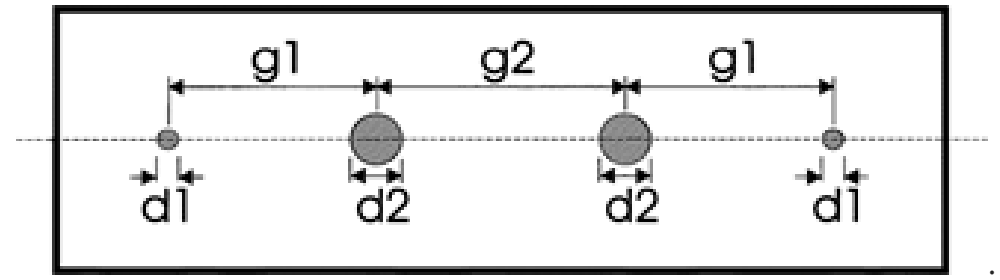

(a)

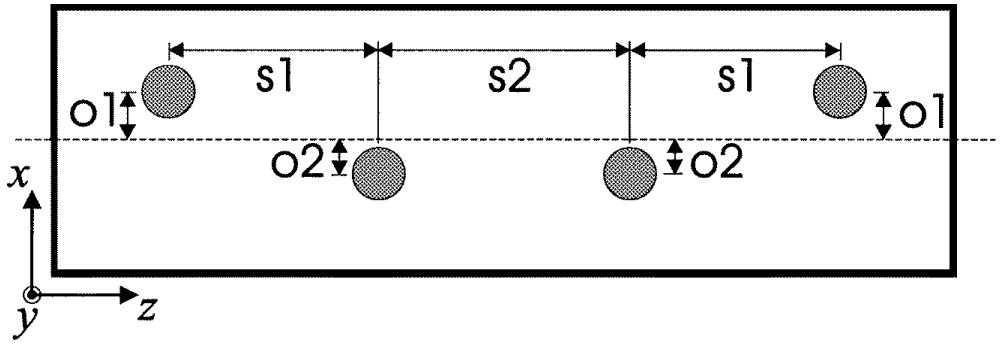

(b)

Figure 1.10 Multi posts SIW filter (a) Centered (b) Off-Set [24]

In SIW technology, the iris window cavities are formed using a pair of symmetrical metallic posts, similar to conventional metallic rectangular waveguides. This allows for the construction of inline SIW filters incorporating iris cavities. In these cases, the size of the

metal posts is maintained to be similar or identical to the size of the metallic vias within the side walls. Figure 1.11 depicts an example of an SIW iris window filter.

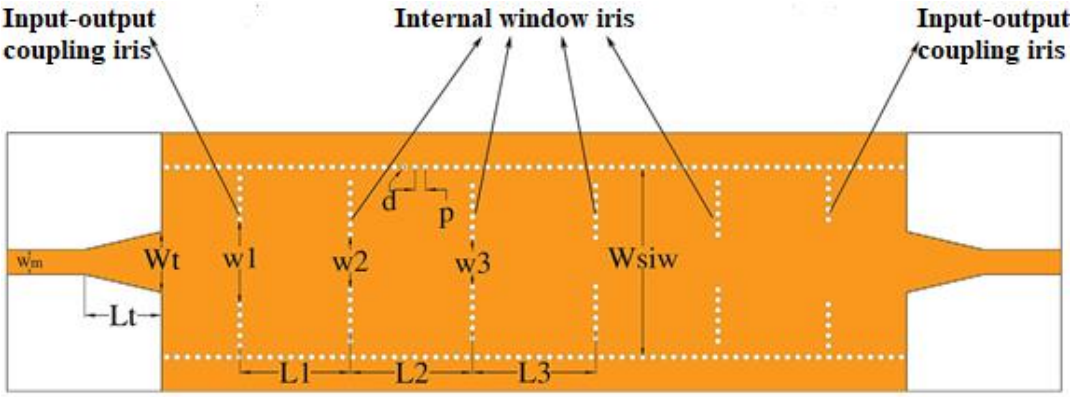

Figure 1.11 SIW iris window filter [25]

The filter characteristics in SIW can be obtained similar to those of conventional metallic waveguides due to the periodic variation of the physical as well as electrical parameters of the SIW. Fig 1.12 shows the SIW periodic filter [26].

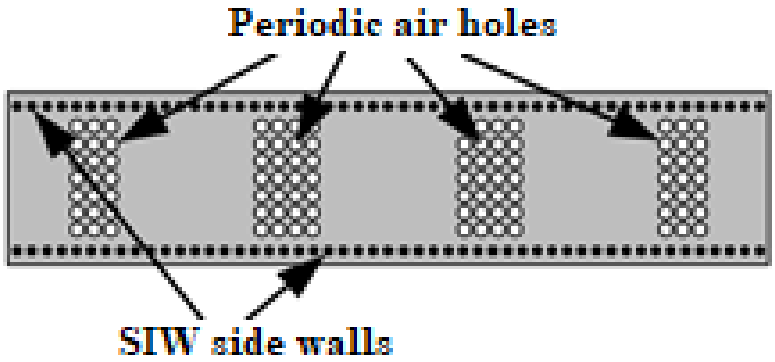

Figure 1.12 SIW periodic filter [26]

- **Directional Couplers**

SIW technology offers a convenient approach to design directional couplers, which are among the various passive microwave devices within its scope. The conventional metallic waveguide consists of two waveguides in stacked positions with holes in the common wall. In SIW technology, there is no requirement for stacking the dielectric, yet a SIW directional

coupler can be obtained simply by removing some of the metallic vias in the common wall of parallel SIW. Fig.1.13 show the isometric view of the SIW based directional coupler [27].

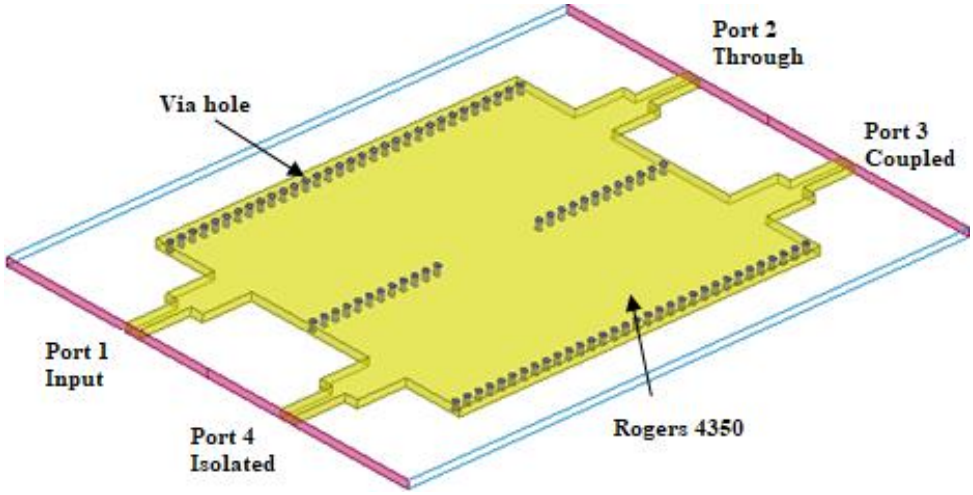

Figure 1.13 Isometric view of SIW based directional coupler [27]

The extent of electromagnetic energy coupling depends on the size of the opening formed when the vias are removed from the shared walls of the two parallel substrate integrated waveguides (SIWs). Weaker coupling occurs when fewer vias are eliminated, while stronger coupling is achieved by removing more vias. A compact cruciform structure enables the creation of a 3-dB directional coupler on a single substrate. This design, known for its simplicity and compactness, has successfully attained an 18% bandwidth [28]. Utilizing SIW technology facilitates the convenient fabrication of various passive microwave devices, including circulators, isolators, phase shifters and various tees.

1.4.2 Active Microwave Devices

Different types of active microwave devices, such as microwave mixers, microwave oscillators, microwave amplifiers, etc., can be easily designed using SIW technology. Another major advantage that is not usable for conventional metallic waveguides is that active devices can be easily mounted along with the SIW components. In the case of conventional metallic devices, active devices need interconnecting devices and joints. The SIW components can be easily connected with micro-strip lines, coplanar lines, etc. So a

complete system can be easily integrated with the SIW devices as compared to metallic waveguides.

- **Microwave Mixer**

Incorporating SIW technology, a microwave mixer is created by integrating a 3-dB SIW hybrid coupler with an active device. The hybrid coupler utilizes two diodes connected in reverse, and both the coupler and diodes are fabricated on a common substrate. To prevent the local oscillator (LO) frequency leakage, a $\frac{\lambda}{4}$ open-circuited stub is inserted between the two diodes in the hybrid coupler design. The mixer's configuration, as illustrated in Fig. 1.14, employs a stepped impedance low-pass filter to effectively separate the radio frequency (RF) and LO signals at the intermediate frequency (IF) output. The microwave oscillator designed by the SIW technology is good choice as compared to other planar lines because the resonant cavities with high quality factor can be easily designed in the SIW technology [29].

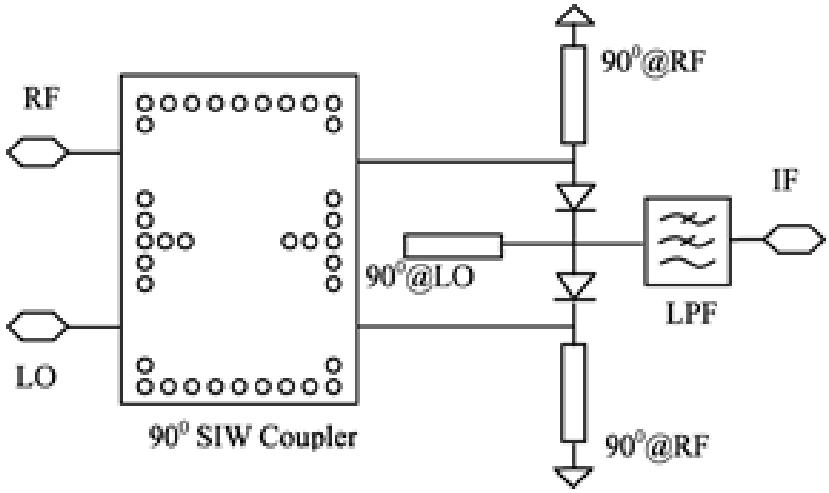

Figure 1.14 SIW mixer [29]

- **Microwave Oscillator**

SIW oscillators utilize two distinct configurations. One of the arrangements involves using the SIW cavity as a component for tuning the frequency. An SIW cavity is embedded with an amplifier circuit known as a feedback oscillator. In this arrangement the SIW cavity function like a frequency selective device. Another second configuration is referred to as a reflection oscillator [30]. A special technique is used to connect the two reflection-type

oscillators in the push-pull oscillator configuration. The output of these oscillators is combined using a Wilkinson power combiner. This component ensures that the oscillations from the two oscillators occur out of phase and at synchronized frequencies. As a result, at its initial fundamental frequency, the output signals nullify each other, while at the 2nd harmonic, they merge coherently [31, 32]. For a visual representation of the different SIW oscillator topologies, please refer to Fig.1.15.

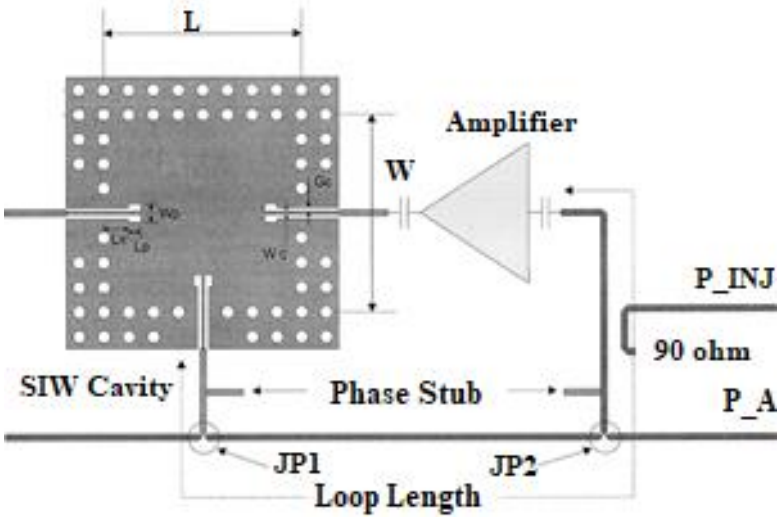

(a)

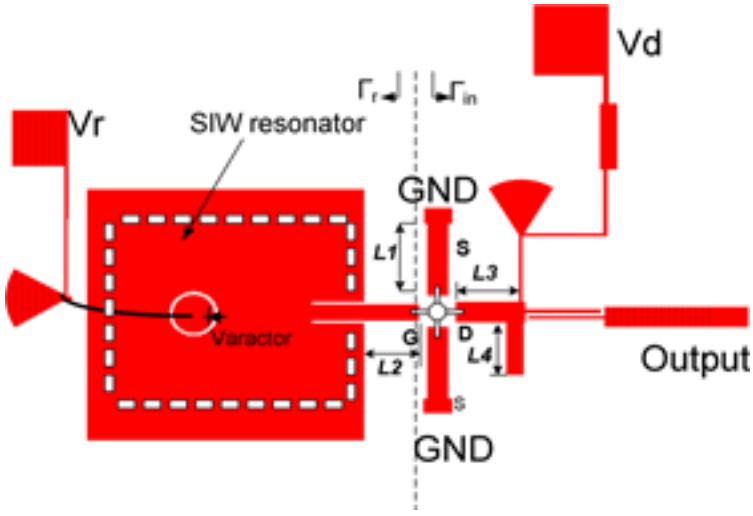

(b)

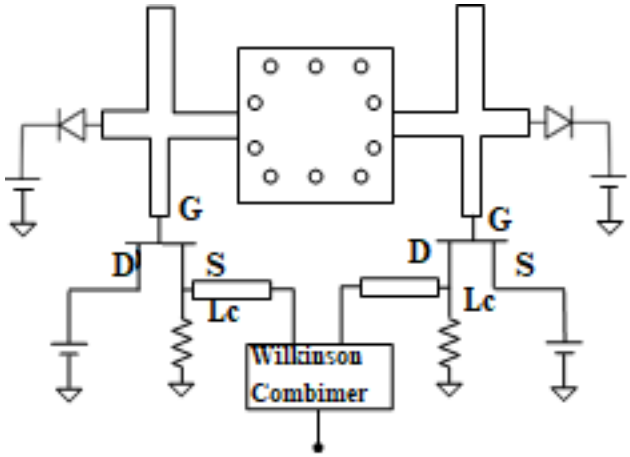

(c)

Figure 1.15 SIW Oscillator (a) Feedback type [30] (b) Reflection Type [31] (c) Push Pull reflection type [32]

- **Microwave Amplifier**

Microwave amplifiers can be designed using SIW technology, offering an alternative class of devices. The design of the SIW-based amplifier embraces a novel approach by employing SIW-based components for the matching networks at the input port as wells as at the output ports, deviating from the traditional use of microstrip elements. Furthermore, the proposed amplifier integrates printed inter digital capacitors within the input and output circuits, offering excellent DC-blocking characteristics. To visualize this innovative microwave amplifier that utilizes SIW technology, please refer to Figure 1.16 [33].

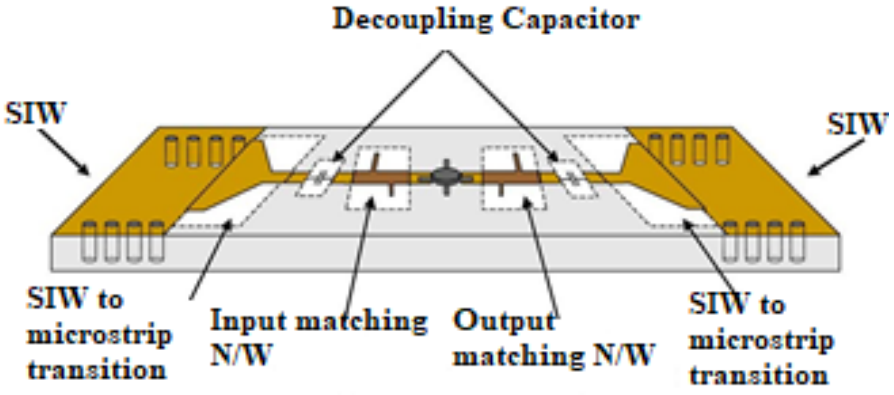

Figure 1.16 Microwave amplifier based on SIW [33]

1.5 SIW Analysis Techniques

Several modelling techniques have been developed and utilized specifically for analyzing SIW designs, which include both simple interconnects and complex components. When dealing with straight interconnects, the primary focus is on determining the field configuration of the dominant mode and gaining insights into the behaviour of subsequent propagating modes at different frequencies. Additionally, information about the phase and attenuation constants of higher modes at different frequencies is also sought. Analyzing SIW components requires a comprehensive examination of scattering parameters, including the scattering matrix referenced to the component's ports. For SIW antennas, it is essential to study their radiation characteristics, along with their frequency response. This evaluation typically involves considering the scattering matrix referenced to the component's ports. By using these modelling techniques, researchers can gain valuable knowledge about how SIW designs, including both interconnects and complex components, behave and perform. This understanding helps in optimizing their performance and improving their overall effectiveness.

1.5.1. Rectangular Waveguide Equivalent

Simulation techniques for SIW structures frequently rely on their resemblance to rectangular waveguides. By taking advantage of the similar dispersion properties shared by SIW modes and modes in traditional RWG, an equivalent RWG having an appropriate width can adequately represent the SIW structure with a comparable performance.

By establishing analytical correlations, it becomes feasible to link the widths of the SIW and the equivalent RWG, creating a meaningful connection between these two structures. The formula for estimating the SIW width using the physical parameter that characterises the SIW and the equivalent RWG, as given in the equation is as follows: [34, 49].

$$W = W_{ER} + \frac{d^2}{0.95s} \tag{1.1}$$

Where W = SIW' width, W_{ER} equivalent RWG's width, d = metallic vias's diameter and s = vias's spacing.

This equation provides a level of accuracy within 5% and remains valid when the spacing among the vias (s) is greater than 4 times the metallic vias diameters (d). The equation's reliability allows for efficient preliminary dimensioning and design modifications in the implementation of SIW technology for various applications. It can be used for tasks such as the initial sizing of SIW interconnects and simplifying SIW component geometries by considering a solid wall instead of series of vias. To incorporate an impact of $\frac{d}{W}$, equation (1.1) was suggested to be improved in [6]. Empirical factors were used to obtain the following equation:

$$W + 0.1\frac{d^2}{W} = W_{ER} + 1.08\frac{d^2}{s} \tag{1.2}$$

In [13], another relation was obtained by applying a semi-analytical method. The relation between the W and W_{ER} is given as follows:

$$W = \frac{2W_{ER}}{\pi}\cot^{-1}\left(\frac{\pi s}{4W_{ER}}\ln\frac{s}{2d}\right) \tag{1.3}$$

Where symbols have their usual meaning

1.5.2 Full -Wave Electromagnetic Modelling (FWEM) of SIW

FWEM is used to provide a more precise characterization of straight SIW. The full-wave analysis of straight SIW tries to find the phase and attenuation constants against frequency curves, along with the SIW mode field pattern. The analysis methodologies used for modelling straight SIW are classified into three major groups:

- **Analysis providing eigenvalues**

The SIW structure consists of rows of metallic vias that form a repeating periodic pattern along its length. To understand its periodic properties, we focus on the unit cell shown in Fig. 1.17 [34]. We conduct a two-port analysis to analyze the behaviour of this unit cell.

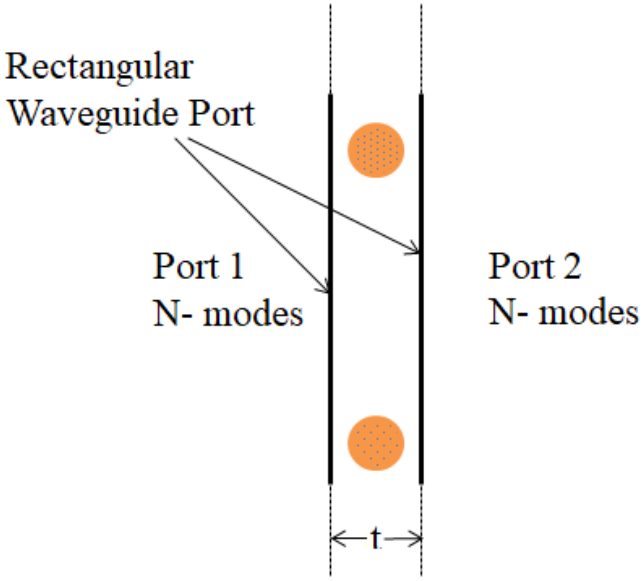

Figure 1.17 Geometrical configuration of unit cell

The ports specified are rectangular waveguide ports that are wider than the SIW width. The ports are positioned along the extended edges of the unit cell. Each port has a predetermined set of N rectangular waveguide modes because SIW exhibits an *H*-plane characteristic due to its structural configuration. The ports only take into account the TE_{n0} modes of the rectangular waveguide [10]. Initially, the transmission matrix ABCD is found out using the electromagnetic simulation, and then it is converted into an impedance or transmission matrix. The relations among the ports voltages and ABCD transmission parameters are as follows:

$$\begin{bmatrix} \frac{V_1}{I_1} \end{bmatrix} = \begin{bmatrix} A & B \\ C & D \end{bmatrix} \begin{bmatrix} \frac{V_2}{-I_2} \end{bmatrix} \tag{1.4}$$

Where, $V_{1,}, V_{2,}$ are the voltages at port 1 and $I_{1,}\, I_2$ are the currents at port 2, respectively. Ultimately, the Floquet-Bloch theorem is employed to study the periodic SIW using this equation.

$$\begin{bmatrix} \frac{V_1}{I_1} \end{bmatrix} = e^{\gamma t} \begin{bmatrix} \frac{V_2}{-I_2} \end{bmatrix} \tag{1.5}$$

Where t denotes the thickness and γ denotes wave propagation constant, of the unit cell. Now from the (1.4) and (1.5), the equation obtained as

$$\begin{bmatrix} A & B \\ C & D \end{bmatrix} = e^{\gamma t} \tag{1.6}$$

The solution of the equation (1.6) at different frequencies gives the eigenvalues or the propagation constant-frequency curve (dispersion curve) of the SIW [6].

- **Method of Moment**

The uniformity of the structural geometry and field amplitude along the Y-axis allows for a simplified 2D analysis. Additionally, the periodicity of the SIW structure facilitates the utilization of suitable periodic boundary conditions within a solitary unit cell. By taking symmetries, specifically a PMC (Perfect Magnetic Conductor) on the symmetry plane for odd modes and a PEC (Perfect Electric Conductor) for even modes, one can effectively determine the different types of modes present in the SIW. Fig. 1.18 illustrates the representation of the periodic model utilized in this analysis [2].

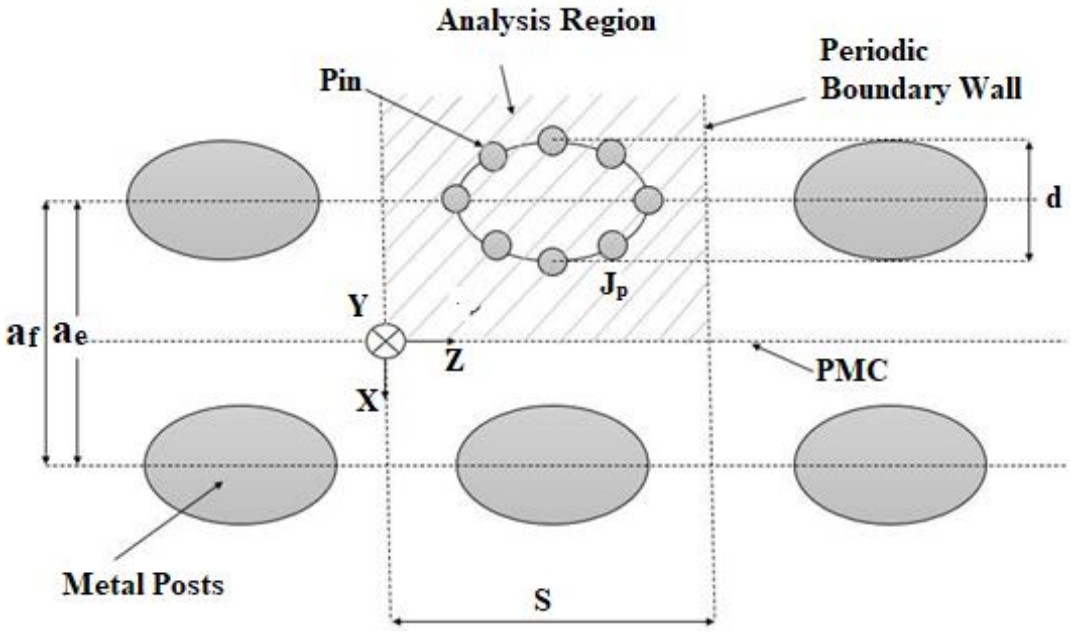

Figure 1.18. Periodic model of SIW [2]

The analysis focuses on a special structure composed of a metallic through within a rectangular region. This structure is bounded on two sides on a regular basis, while the third side has a symmetry boundary condition and the fourth side has a radiation boundary condition. The integral equation attempts to solve for an unknown variable, surface current density J_p along the Y-axis. It specifies that the dyadic Green's function G has been utilised for the computation of the variable mentioned, and its representation can be found in the integral equation (1.7), this process involves transforming the electric field created by the surface current density J_p into a Green's integral. Subsequently, a Green's integral is applied to impose the electric field boundary condition on the metal post's surface, leading to the formulation of the integral equation in connection with the specific conditions prevailing at the boundary [2, 35].

$$\oiint G\,(r, r').J_p(r')ds' = 0 \tag{1.7}$$

For the TE to z- mode, the dyadic function is expanded, then the wave number K_{zn} defined by the Floquet theorem [2].

$$K_{zn} = K_{zd} + \frac{2\pi n}{s} \tag{1.8}$$

Where n is an integer no. and K_{zd} represents the wave no. along the Z- axis.

The solution of (1.7) by the Galerkin's method of moments gives the non-trivial solution of the current density J_p in (1.7) [2].

$$\text{Det}[Z_{ij}] = 0 \tag{1.9}$$

The Z in the determinant of (1.9) is defined as [2].

$$Z_{ij} = \iint J_{pi}(r)\,.\,G(r, r').J_{pj}(r')dsds' \tag{1.10}$$

The solution of (1.10) provides the complex wave numberk_{zi}. The attenuation constant α_i and phase constant β_i is given by

$$\alpha_i = Re[k_{zi}] \tag{1.11}$$

$$\beta_i = Im[k_{zi}] \tag{1.12}$$

1.6 SIW Transition with Printed Transmission Line

PCB or LTCC technology is commonly used for fabricating printed transmission lines. Similarly, SIW fabrication also utilizes a comparable technology, enabling the convenient design and integration of both planar transmission lines and SIW on a monolithic substrate. However, to achieve proper impedance matching and feeding from these printed transmission lines to SIW, an impedance matching device is necessary. For interconnecting these components, the upper and lower conducting planes are connected together. These interconnections are illustrated in Fig. 1.19 [36]. Furthermore, the combination of PCB or LTCC technology with SIW provides benefits such as compact size and enhanced performance, making it a valuable and popular option for contemporary circuit designs.

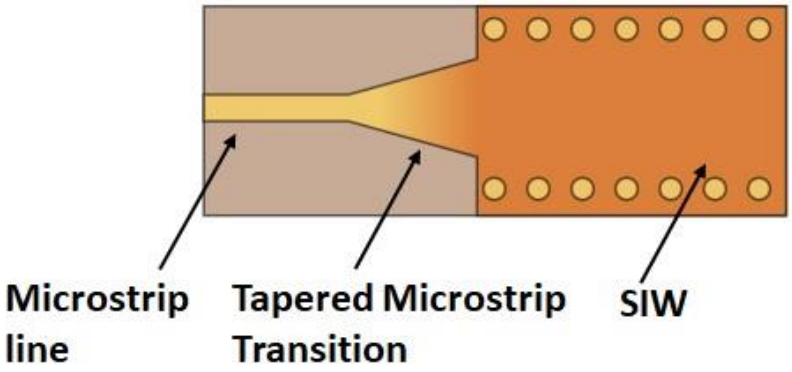

Figure 1.19 Microstrip to SIW transition

When wide bandwidth is needed, CPW (Coplanar Waveguide) feed lines are favoured over microstrip lines. This preference extends to SIW transitions as well. Specifically, when the substrate thickness is substantial, the CPW transition is preferred over the microstrip line. Fig. 1.20 illustrates the transition from CPW to SIW [37].

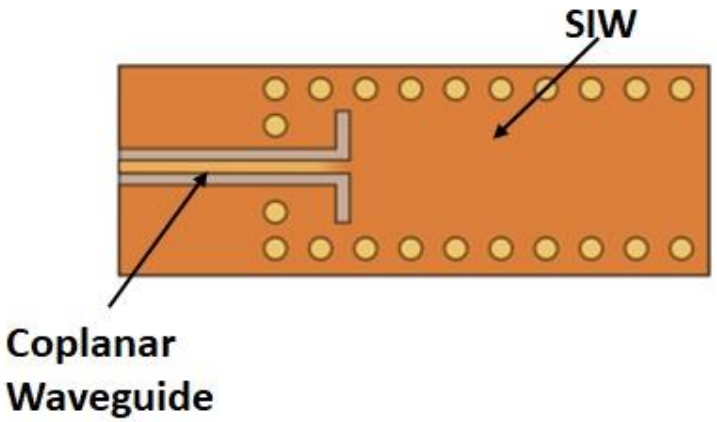

Figure 1.20 CPW to SIW transition

1.7 Losses in SIW

Within the SIW, three distinct types of losses can be identified: dielectric, conductor, and radiation losses. Interestingly, conductor and dielectric losses in the SIW share similarities with losses observed in conventional RWG filled with dielectric material. However, radiation loss in the SIW sets it apart from traditional waveguides. This radiation loss occurs due to the absence of complete electromagnetic shielding in SIW as compared to conventional RWG, leading to energy leakage through radiation. In contrast, the SIW's distinctive structure provides comprehensive electromagnetic shielding, effectively preventing radiation losses. SIW offers significantly lower propagation losses compared to standard microstrip and coplanar waveguides, enabling enhanced signal integrity and improved system performance. The three types of losses are as follows.

- **Conductor Loss (L_c) :**

The main reason for the conductor loss is the limited conductivity of the metal traces used to create the guiding structure inside the SIW. As the electromagnetic waves travel along the metal traces, a portion of the energy is dissipated as heat due to the intrinsic resistance of the conductive material. The comprehensive investigation of conductor loss in SIW in the fundamental mode of propagation can be found in references [9, 10]. In SIW, the most significant factor impacting conductor loss is the thickness of the substrate. Modifying the

substrate's thickness leads to a noticeable impact on conductor loss within the waveguide. As the dielectric substrate's thickness changes, it affects the current distribution on both the lower and upper ground planes, consequently impacting conductor loss and power dissipation in the SIW.

$$L_c = \frac{\sqrt{\pi f \varepsilon}}{h\sqrt{\sigma}} \frac{1+2\left(\frac{f_c}{f}\right)^2 \frac{h}{W_{ER}}}{\sqrt{1-\left(\frac{f_c}{f}\right)^2}} \tag{1.13}$$

Where f_c denotes the frequency of first fundamental mode. h represents height of the dielectric, σ represents the conductivity of metal, ε corresponds to relative permittivity and W_{ER} represents the width of equivalent RWG.

- **Dielectric Loss (L_d):**

In the dielectric material, the important parameters responsible for dielectric loss are the loss tangent and relative dielectric constant. These properties determine the extent of dielectric loss in the SIW.

$$L_d = \frac{\pi f \sqrt{\varepsilon_r}}{c\sqrt{1-\left(\frac{f_c}{f}\right)^2}} \tan\delta \tag{1.14}$$

The symbol c represents the velocity of EM wave in vacuum, ε_r is the relative dielectric constant, and $\tan\delta$ represents the loss tangent. It is important that this loss varies linearly with the frequency at which the electromagnetic wave propagates.

- **Radiation Loss ($L_{R)}$:**

The radiation loss occurs in the SIW, but it does not occur in the conventional metallic waveguide. The gap that exists between metallic vias inside the SIW structure is responsible for this phenomenon. If the distance among the vias follows $\frac{s}{d} < 2.5$, then the leakage is negligible, and for the practical purposes $\frac{s}{d} = 2$ can be considered [9, 10].

1.8 Motivation and Objective of the Thesis

The integration of various millimeter wave technologies onto a single substrate is significantly contributing to wireless communication network progress. The demand for high-performance microwave components capable of operating across multiple frequencies is increasing in modern wireless communication systems. Particularly, microwave filters and antennas are essential components needed to meet these demands. The development of microwave filters is expected to yield smaller sizes, increased capacities of power handling, lower costs, higher quality factors (Q), and easier integration with planar circuits.

Multiband bandpass filters find extensive utilization in contemporary communication systems like mobile phones, satellites, and radar communication systems. These filters can operate over a wide frequency range while occupying minimal space. To address the need for advanced wireless systems with compact multiband bandpass filters and antennas, it is crucial to explore technologies that offer benefits such as small form factors, low fabrication costs, and seamless integration with other active and passive devices.

SIW technology offers a promising solution to meet these requirements. Through the combination of metallic rectangular waveguides (RWG) and printed transmission lines, SIW technology effectively addresses the design criteria, as demonstrated in earlier sections. By utilising the capabilities of SIW, it is possible to develop advanced wireless systems with multiband bandpass filters and antennas that occupy minimal space, easily integrate with other components and offer cost-effective fabrication. Considering the aforementioned motivations, the following objective are defined for the research:

- To design, simulate and experimental verification of different SIW filter and components.
- To study and designing of leaky wave antenna.
- To study half mode SIW filters.
- To design different types of transitions of SIW filters with other planar transmission lines.
- To design of tuneable and multi-band filters using SIW.

- To design and simulate SIW folded waveguide.

1.9 Organization of the Thesis

The thesis has a structured arrangement comprising eight chapters, which are outlined as follows.

Chapter 1 The initial chapter provides an introduction to the fundamental geometry of the SIW. Various types of the SIW, including HMSIW, SIFW, SIRW, and more, are discussed. The chapter covers different analysis techniques employed for the SIW. Additionally, it explores the transition devices between the SIW and various printed transmission lines. Furthermore, this chapter also presents the motivation, objectives, and outline of the thesis.

Chapter 2 The second chapter is dedicated to a comprehensive literature survey. While some of the literature surveyed has been cited in the first chapter, this chapter further discusses the remaining relevant literature. It provides an extensive review of the existing research and studies related to the subject matter.

Chapter 3 In the third chapter, the focus is on the design and analysis of the sinusoidally modulated SIW. The chapter begins with the introduction of a newly developed curvilinear coordinate system. Next, the field components are derived specifically for the sinusoidally modulated SIW design. Additionally, within the chapter, the designed SIW is analyzed for the fundamental mode, investigating the imaginary propagation constant against frequency for two distinct modulation indices. Given the periodic nature of the designed SIW, it exhibits a multi-band pass filter behavior that holds potential for future millimeter-wave systems.

Chapter 4 The fourth chapter focuses on the design and analysis of a step-sized SIW using mode matching techniques (MMT). The computational time and memory requirements of MMT are compared with these parameters by commercial simulators like HFSS and CST-MWS. Moreover, a comparison is made between the scattering parameters acquired via MMT and the simulated S-parameters from HFSS and CST-MWS, along with the measured data. The mode-matching technique proves to be a valuable tool for analyzing periodic structures and waveguides with varying cross-sections. This analysis necessitates the use of a generalized scattering matrix, which establishes a connection between the outgoing and incoming modes. The chapter also explores the filter properties of the designed step-sized SIW, taking into consideration its periodic nature.

Chapter 5 The fifth chapter presents the design and analysis of a sinusoidally modulated SIFW (SMSIFW). The SMSIFW is half the width as compared to the sinusoidally modulated SIW (SMSIW). So the folded SIW is more compact than its unfolded counterpart. The dispersion curves of the SMSIFW are derived for the modulation index of 0.25 and compared with the SMSIW. It is found that dispersion curves are almost equal in SMSIFW and SMSIW. As the designed SMSIFW is periodic, it shows the multi-band filter property. The designed SMSIFW can be used as a multiband filter in future millimeter wave systems.

Chapter 6 This chapter introduces a novel antenna design that has been specially optimized for self-diplexing applications. The antenna, based on SIW technology, integrates a slot in the upper conducting plane and a cavity backing, facilitating resonance at two distinct frequencies and enhancing isolation between them. The antenna achieves impressive gain of 4.8 dBi and 6.4 dBi at 6.5 GHz and 7 GHz, respectively. With its dual-frequency capability, the system offers excellent isolation, allowing simultaneous transmission and reception at different frequencies. This design leverages leaky wave self-diplexing capabilities through dual feed and integration of a slot in the upper conducting plane.

Chapter 7 reveals the design of three distinct HMSIW components: an HMSIW, an HMSIW band-pass filter, and an HMSIW leaky wave antenna. To comprehend their unique traits, we compare the propagation charteristics of the full mode SIW and HMSIW. The designed HMSIW exhibits a remarkable feature: through the integration of a defected ground structure in the lower ground plane, it transforms into an HMSIW band-pass filter. This manipulation allows convenient tuning of the filter's center frequency, enhancing its adaptability and flexibility. Furthermore, the chapter explores the development of a half-mode SIW leaky wave antenna, achieved by integrating parallel slots in the upper ground plane. This innovative technique yields an antenna with exceptional performance for C-band wireless applications.

Chapter 8 The eighth and final chapter of this thesis functions as the conclusive section, encapsulating the essential discoveries, results, and contributions of the conducted research. Moreover, it outlines potential avenues for future exploration and study within the field, presenting directions for further investigation and advancement.

CHAPTER 2

Literature Survey

In order to accomplish the objectives outlined in the introduction chapter, a thorough assessment of the literature is done and reported in this chapter. The literature briefly discusses the analysis of the rectangular waveguide and SIW. Several band-pass filters, especially with periodic geometries, have been discussed to get the desired response while taking the size/complexity trade-off into account. This survey also focuses on SIW-based antennas. Some of the reviewed literature is also cited in Chapter 1. The surveyed literature with a research gap is as follows:

F. Grine et al. [38] proposed a SIW and a periodically drilled SIW with air vias were designed. The periodic arrangement of air holes in the SIW design reduces the effective permittivity and enhances the quality factor. When combined with the cavities, the designed periodic SIW functions as a low loss filter with a high bandwidth. Fig. 2.1 illustrates the designed SIW filter with its dispersion curves and S parameters.

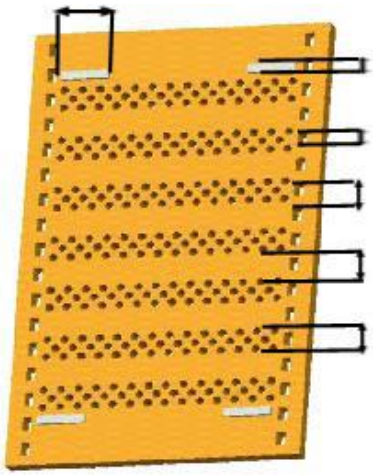

(a)

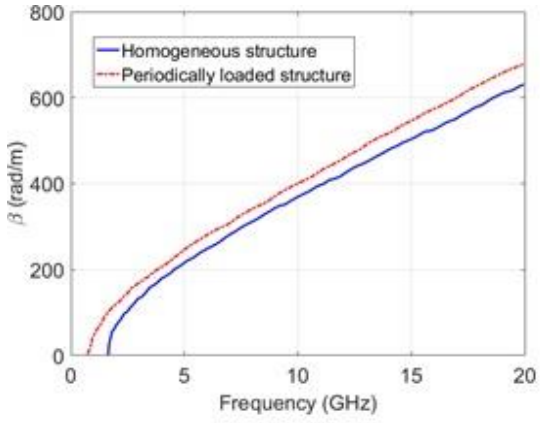

(b)

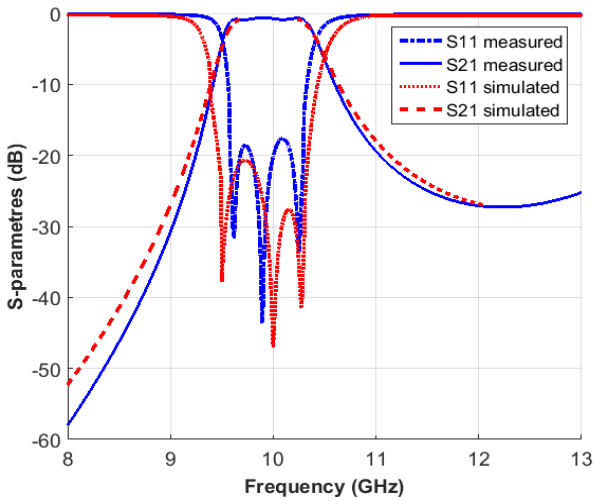

(c)

Figure 2.1 (a) SIW filter (b) Dispersion Curve (c) S-parameters of the filter [38]

Research Gap: There exists a significant difference in the cutoff frequency between the loaded and unloaded SIW, and the radiation from the air holes can be substantial. These parameters present opportunities for optimization.

A. K. Mallick et al. [39] analyze the electromagnetic wave propagation in a rectangular wave guide, whose width varies sinusoidally in the wave propagation direction. The Helmholtz wave equation is effectively addressed by imposing the appropriate boundary condition. By doing so, we can deduce the propagation constant as well as the field components of the RWG. To analyze the RWG thoroughly, they employ various methods, including numerical analysis, Hill's equation, and the circuit theory approach.

Research Gap: The analysis can be conducted in SIW considering the design limitations. Additionally, the filter criteria can be explored further due to the periodicity of the structure.

L. Huang et al. [40] designed a SIW wideband high selectivity band pass filter with wide bandwidth. To achieve periodicity in the structure, the upper ground plane of the SIW incorporates etched electronic band gap (EBG) structures. By adjusting the EBG parameters, undesirable harmonics in the upper stop-band are reduced. The complementary split-ring

resonators are also incorporated near the two feed lines. Fig. 2.2 displays the SIW filter with the corresponding *S*-parameters, as proposed in the study.

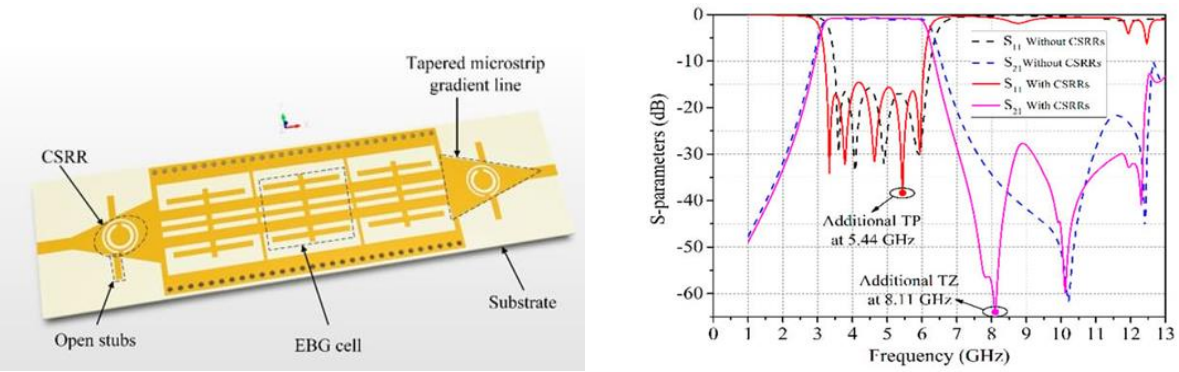

(a) (b)

Figure 2.2 (a) Designed SIW filter (b) S-parameters [40]

Research Gap: The incorporation of various EBG structures presents an opportunity for further investigation, and the bandwidth can also be controlled effectively using either EBG or CSRR

Y. Cassivi et al. [41] Y. Cassivi et al. [41] introduced the BI-RME (Boundary Integral Resonant Mode Expansion) method, augmented with Floquet's theorem, as a numerical technique to analyze and calculate dispersion parameters in waveguides, including the substrate integrated rectangular waveguide. This method involves modifying the field representation within the waveguide using a superposition of resonant modes, enabling the determination of dispersion characteristics. Fig. 2.3 illustrates the dispersion characteristics of the proposed waveguide design, showcasing the correlation between the propagation constant and the guided wave frequency. This approach offers promising opportunities to gain deeper insights into wave propagation behavior, potentially advancing waveguide technology.

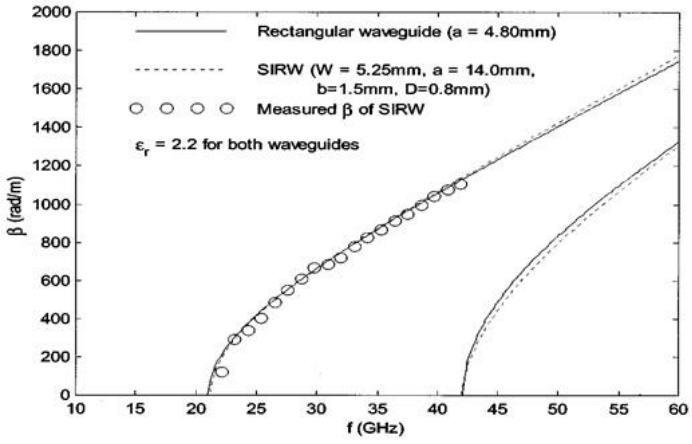

Figure 2.3 Dispersion curve of proposed waveguide [41]

Research gap: An alternative, simpler analysis such as Hill's equation-based or numerical analysis-based can be made, and a dispersion curve can be plotted.

D. Deslandes et al. [42] investigate an innovative transitional element that bridges a substrate-integrated rectangular waveguide with a microstrip line. Their newly devised planar structure incorporates both components on the same dielectric and establishes a straightforward connection using a simple taper. Fig. 2.4 likely illustrates the proposed transition, depicting the insertion loss and reflection loss characteristics. The authors aim to streamline the mounting system typically required for such transitions by simplifying the overall setup. This innovative approach exhibits promising potential in terms of ease of manufacturing, cost-effectiveness, and potentially improved performance.

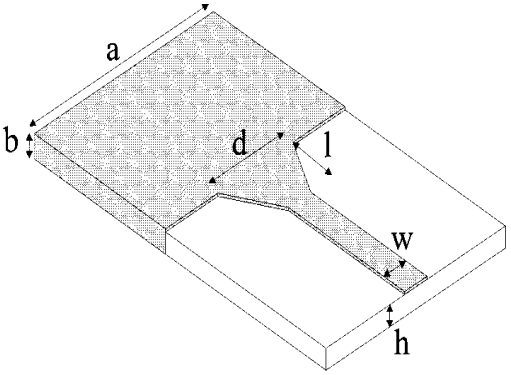

(a)

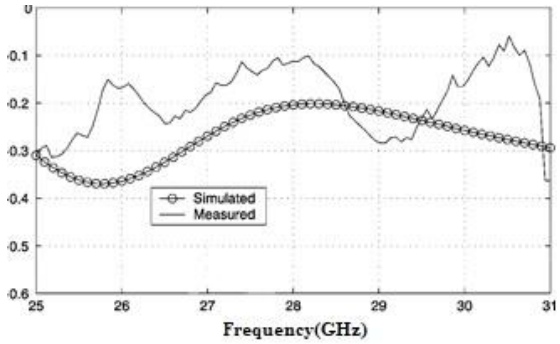

(b)

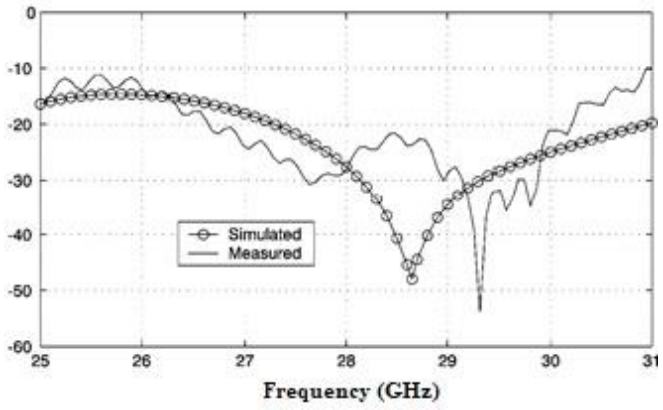

(c)

Figure 2.4 (a) Microstrip line to waveguide transition (b) Insertion loss (c) Return loss [42]

P. Moon et al. [43] gives a good methods of separation of variables because certain coordinates systems allows the separation of variables and also defines the Lames coefficients for different orthogonal coordinates systems.

T. Witaker et al. [44] present various physical problem analysis methods as well as a simple method for solving equations with periodic coefficients using Mathieu's functions, Hill's equations, Stackel's determinants and Hill's equations.

A Iqbal et al. [45] likely provide a comprehensive summary of the advancements and trends in SIW filter technology. The paper may discuss topics such as filter design techniques, fabrication processes, performance optimization, and applications of SIW filters in communication systems and other relevant areas. In the SIW structure, two parallel copper plates serve as the main guiding structure. These plates are typically embedded in a dielectric substrate, which provides mechanical support and insulation. SIW is a good option for components for mm-Wave and RF systems because of its small size, flexibility, and low cost. The complete paper provides an overview of SIW technology, explores filters based on SIW, and conducts comparative analyses of various literature sources.

Z Kordiboroujeni et al. [46] introduce an analytical formulation for determining the width of the SIW, allowing direct and efficient calculations for a specific frequency. This equation eliminates the need for iterative procedures or complex polynomial solutions. A key

objective of this formula is to reduce reflections at the interface between the SIW and an equivalent-width all-dielectric waveguide. The derivation employs a MMT to ensure precise and accurate results. Fig. 2.5 offers an isometric view of the proposed SIW configuration.

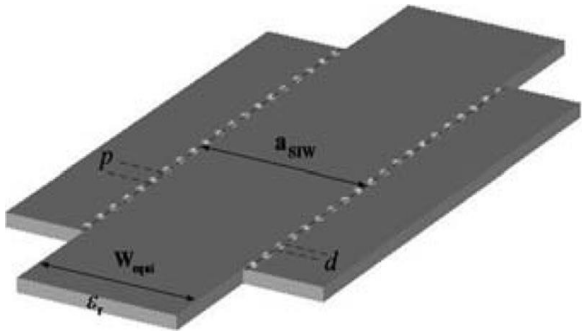

Figure 2.5 Isometric view of the proposed SIW [46]

Research Gap: The paper lacks the plotting of dispersion curves for the SIW, and there is also a need for a thorough analysis of the mode matching techniques at the interfaces.

Z. Kordiboroujeni et al. [47] investigated the development and investigation of a Ku-band SIW T-junction diplexer. The researchers utilized the MMT technique for the analysis and design process. The diplexer was specifically engineered to deal with two distinct frequencies: 14.55 GHz and 15.85 GHz, offering narrow bandwidths of 4.12% and 3.79%, respectively. To validate their findings, the study compared the analysis results with simulations from widely-used commercial field solvers like CST and HFSS. To visually represent the SIW diplexer and its characteristics, Fig. 2.6 was included in the research.

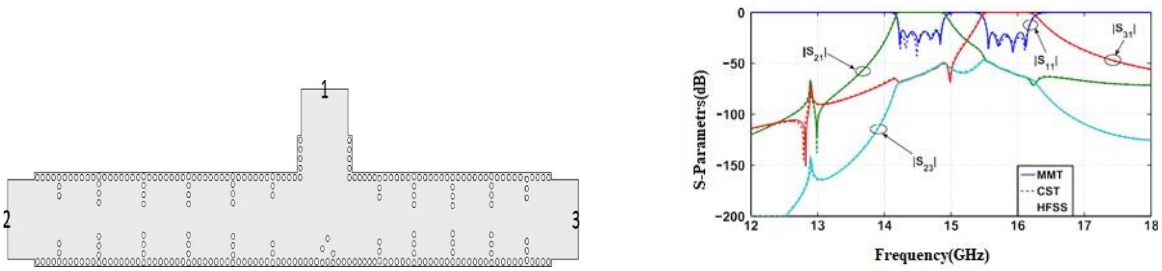

(a) (b)

Figure 2.6 (a) SIW diplexer (b) S-parameters [47]

Research Gap: The mode matching analysis can be applied for making a step periodic SIW and the filter characteristics can be investigated.

J. Bornemann et al. [48] discuss a method for describing a specific class of waveguide discontinuities using field theory. To address discrepancies when resonant effects occur, the researchers propose a modified TE wave approach combined with the MMT. However, when resonant effects are present, the application of the traditional TE MMT for waveguide discontinuity analysis encounters difficulties. In order to overcome these discrepancies, the authors suggest a generalized analysis that involves a linear combination of TE and TM modes. Fig. 2.7 depicts a waveguide discontinuity.

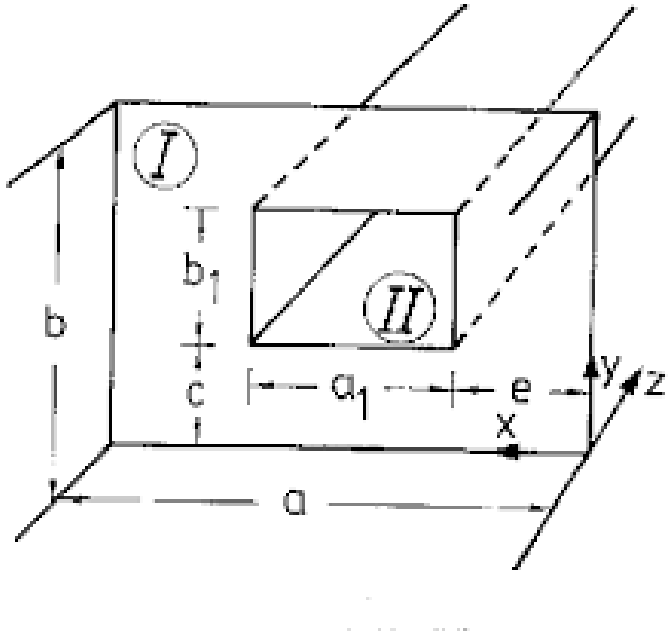

Figure 2.7 Waveguide discontinuities [48]

Research Gap: The discontinuities in the SIW can be easily made, and mode matching techniques can be used to obtain scattering (S) parameters.

D Deslandes et al. [49] propose a comprehensive analysis method for calculating the complex propagation constants in SIW. The approach combines the surface impedance concept, the moment method, and a transverse resonance method. The results acquired using this technique are then represented visually using a parametric curves and graphs,

illuminating the periodic SIW's leakage and wave guiding characteristics. Some SIW designs rules are represented as: $s > d, \frac{s}{\lambda_C} < 0.25$ and $\frac{s}{d} < 2$. The different SIW regions are defined in Fig. 2.8. Where, s is the spacing among the vias, d represents the diameter of each vias and λ_c represents cut off wavelength.

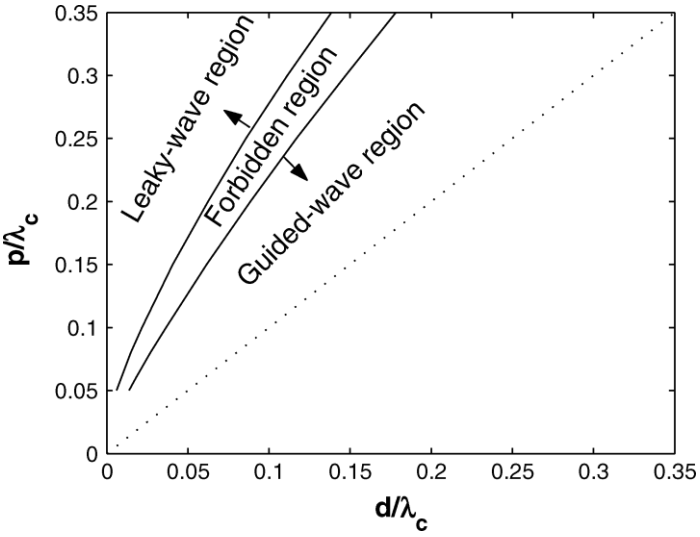

Figure 2.8 Different regions of SIW [49]

Research Gap: The scattering parameters (S-parameters) can be obtained from the periodic structure, and filter characteristics can be obtained.

A. V. Labay et al. [50] examines the computation of waveguide multiport junctions with discontinuity distortion. The researchers introduce a novel approach using a generalized modal scattering matrix to determine the scattering matrix of the junction. In contrast to conventional techniques that rely on three-plane MMT and similar methodologies, which solely address the dominant mode, this novel approach allows for the examination of structures influenced by the junction's discontinuity distortion. Fig. 2.9 in their research illustrates a rectangular waveguide T junction featuring the mentioned discontinuity junction.

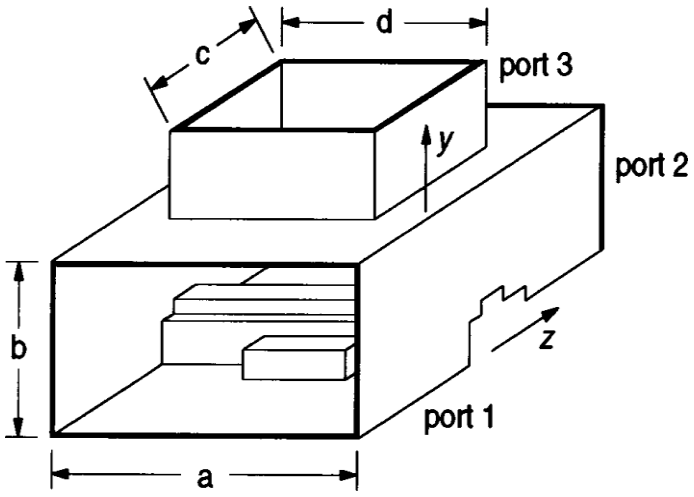

(a)

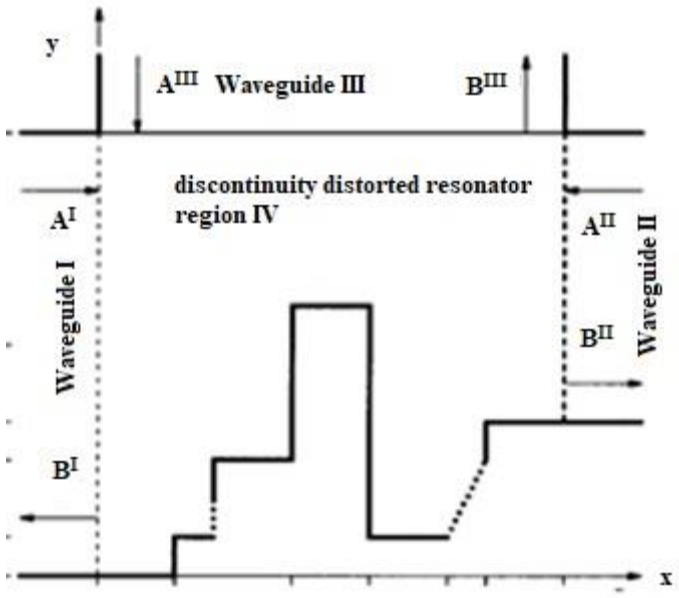

(b)

Figure 2.9 (a) T-junction with rectangular waveguide (b) Discontinuity division [50]

S. Nandi et al. [51] present a cavity-backed SIW antenna fed by two different microstrip feed lines. The cavity's upper metallic plane incorporates a pair of transverse slots with varying lengths that radiate at two distinct resonant frequencies. Between two ports, a high level of isolation (greater than 27.9 dB) is attained, which results in the antenna's self-

diplexing property. At 8.26 GHz and 10.46 GHz, the suggested antenna provides gains of 3.56 and 5.24 dBi, respectively. Fig. 2.10 shows the proposed SIW based antenna and its S-parameters.

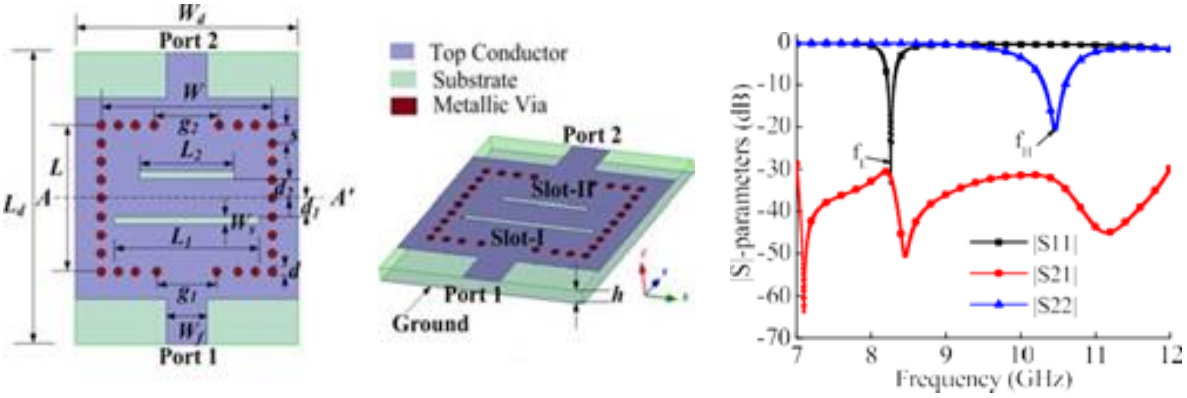

(a) (b)

Figure 2.10 (a) Proposed SIW antenna (b) *S*-parameters curve [51]

Research Gap: There exists a potential for enhancing the S parameters through the implementation of inset feeds, with the added benefit of offsetting them from each other. Additionally, there is room for further improvement in the antenna's gain. To achieve this, a reduction in the number of slots can be explored for the two resonating frequencies.

D. K. Park et al. [52] concentrate on developing a microstrip patch antenna that is compact in size and operates at two different frequencies, while also ensuring orthogonal polarization and significant isolation between its feeding lines. The primary aim of this design is to achieve effective isolation in both the uplink and downlink frequencies. To enhance the isolation in the feeding lines of the antenna, the researchers employ a specific patch conductor configuration on a high dielectric constant material.

Research Gap: The research gap lies in investigating whether the isolation enhancement concept used in microstrip patch antennas can be effectively applied to SIW antennas. Ultimately, SIW antennas provide even higher isolation between their feeding lines, and the potential impact of incorporating a cavity on the antenna's gain requires further exploration

S. Mukherjee et al. [53] introduced an innovative approach for constructing a self-diplexing planar slot antenna, leveraging the principles of SIW effectively**.** The antenna design incorporates a SIW cavity with a slot shaped like a bow tie, being driven by two distinct feed lines. Through careful optimization of the antenna's dimensions, they achieved resonance at two separate X band frequencies (8-12 GHz) while achieving exceptional isolation of over 25 dB. The thoroughly optimized design effectively incorporates the self-diplexing phenomenon, resulting in significant performance enhancements for the antenna. The authors provided detailed illustrations of the proposed SIW antenna's structure and the frequency-dependent S parameters in Fig. 2.11**.**

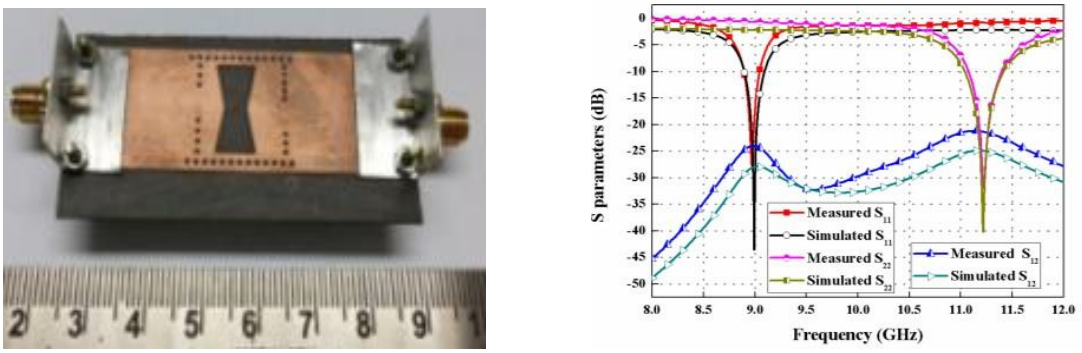

(a) (b)

Figure 2.11 (a) SIW antenna (b) S_{11} vs. frequency curve [53]

Research Gap: There is potential to further enhance the isolation between the feed lines through the application of different frequency bands. Additionally, the antenna's gain is currently low and offers room for further improvement.

G. Q. Luo et al. [54] present a present a novel cavity-backed planar slot antenna that combines SIW and grounded coplanar waveguide (GCPW) on a single substrate. The antenna attains a bandwidth of 1.7% and a total gain of 5.4 dBi. For a visual representation, Fig. 2.12 illustrates the proposed SIW antenna with its S_{11} vs. frequency curve.

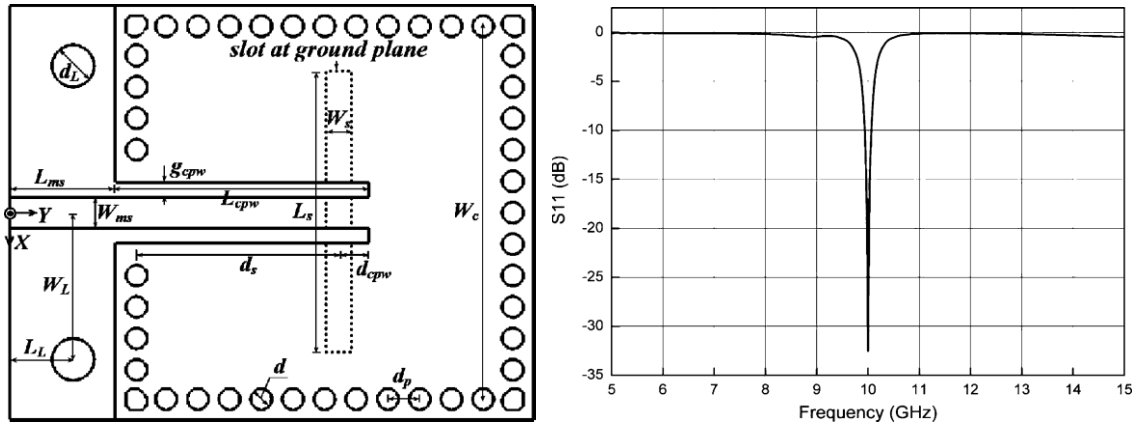

(a) (b)

Figure 2.12 (a) SIW cavity backed antenna (b) S_{11} vs. frequency curve [54]

S. Mukherjee et al. [55] introduced a SIW cavity-supported slot antenna specially designed for X band applications. To enhance the antenna's bandwidth, they implement an innovative offset microstrip line feeding approach, along with a transition from microstrip to coplanar waveguide. These techniques enable concurrent generation of the TE_{120} mode inside the cavity, leading to improved impedance matching with the slot antenna. For a visual representation of their proposed SIW antenna and its performance, Fig 2.13 displays the SIW antenna and its S_{11} vs. frequency curve.

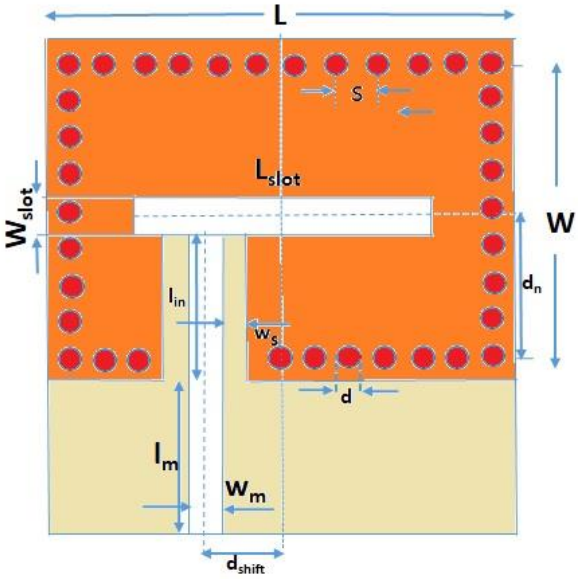

(a)

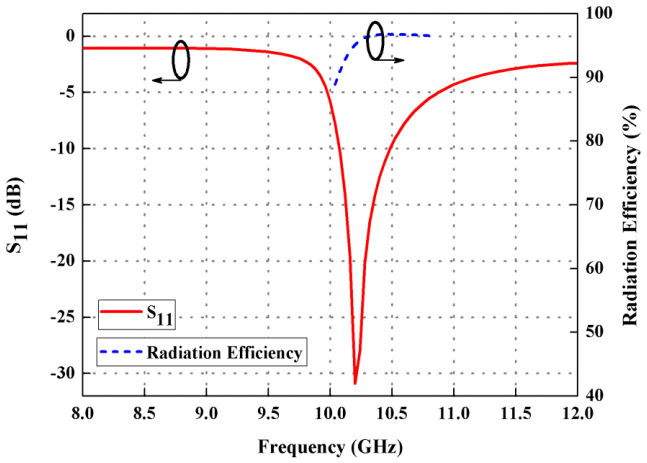

(b)

Figure 2.13 (a) Designed SIW antenna (b) S_{11} vs frequency curve [55]

Research Gap: The antenna is radiating at a single frequency, the upper ground plane is divided into different regions, and the feeding is done separately, the antenna can work at multiple frequencies, considering the isolation among the feeds.

G. Q. Luo et al. [56] introduced a pioneering approach with the goal of substantially increasing the bandwidth in a SIW-based antenna. The focal point of their method was the concurrent excitation of a pair of hybrid modes within the SIW-backed cavity. Fig. 2.14 shows the proposed antenna and its $|S_{11}|$ curve.

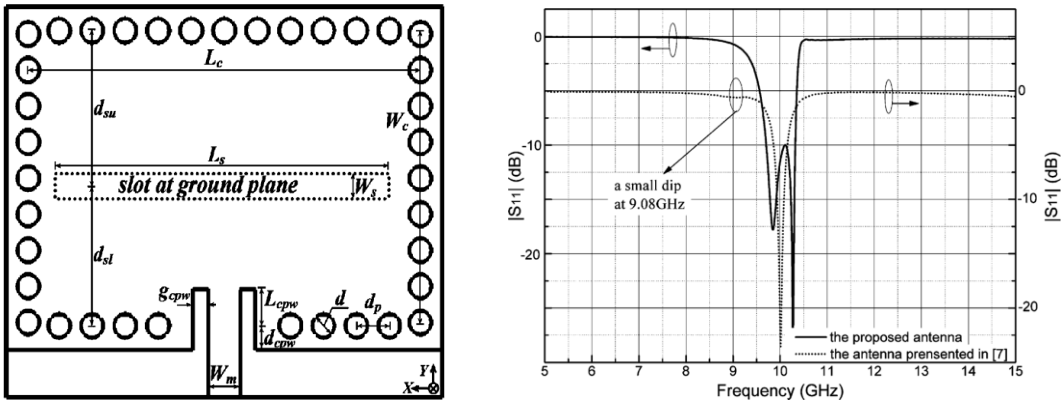

(a) (b)

Figure 2.14 (a) Proposed SIW antenna (b) S_{11} vs. frequency curve [56]

Research Gap: The existing configuration of the proposed antenna shows resonance at only one frequency, resulting in a relatively low total gain. However, introducing a slot in the upper ground plane and using dual feeds can transform it into a dual-resonating antenna, potentially improving its overall performance and versatility.

W. Che et al. [57], proposed the folded substrate integrated waveguide (FSIW) concept, featuring about 50% width of the SIW. Their analysis covered the FSIW's propagation behavior, including the optimal central metal vane gap (g). Interestingly, FSIW demonstrated propagation similarities to the conventional SIW, as shown in Fig. 2.15.

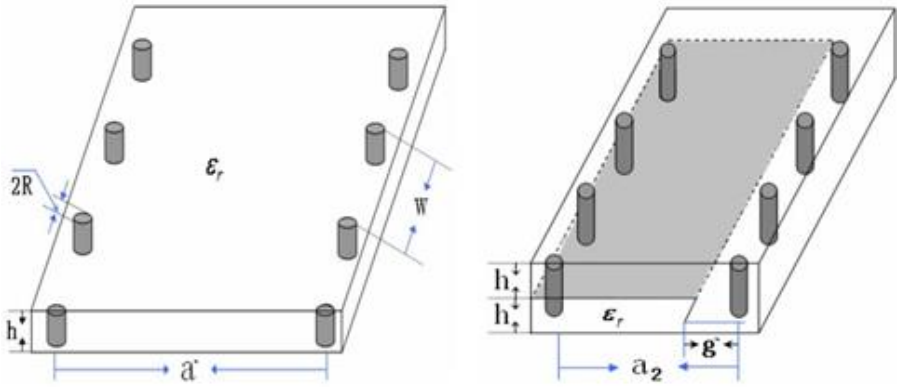

(a) (b)

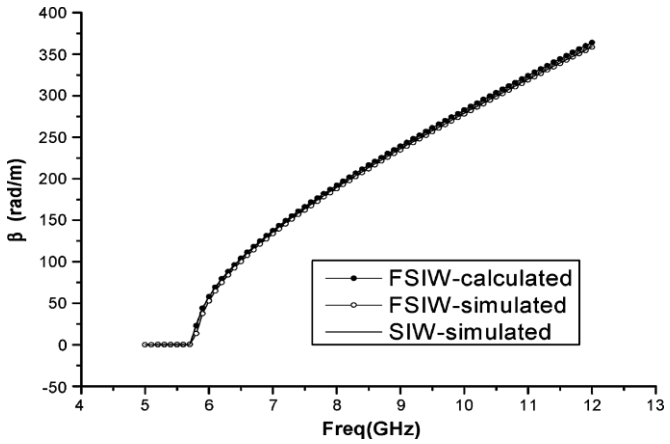

(c)

Figure 2.15 Configurations of (a) SIW and (b) FSIW (c) Comparison curve of propagation constants [57]

Research Gap: The analysis of the FSIW can be made by different methods; the FSIW can be divided into three regions, and the boundary condition can be applied for finding the propagation constant.

N. Trong et al. [58] have developed a numerical solution to analyze the propagation behavior of folded substrate-integrated waveguides (FSIW). They utilized a variational method to efficiently solve the stationary equation for each form of FSIW. Fig.2.16 in their work likely illustrates the configuration of the two types of folded SIW and provides a comparison of their dispersion curves.

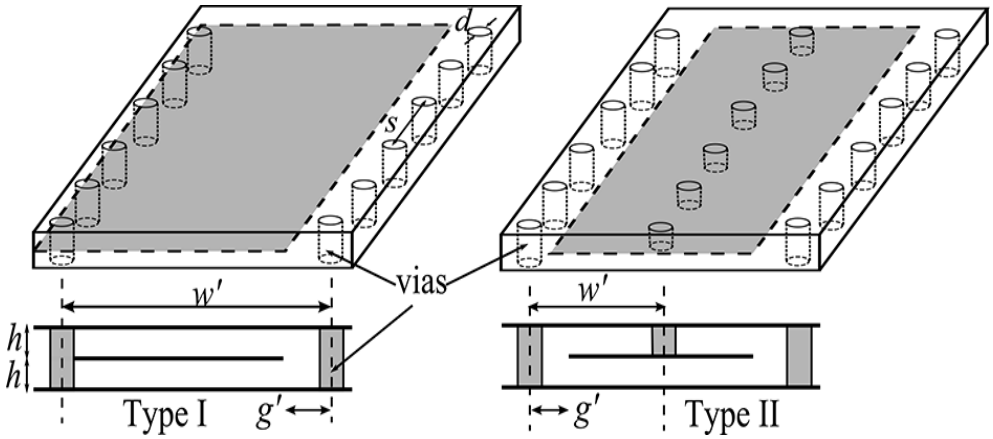

(a) (b)

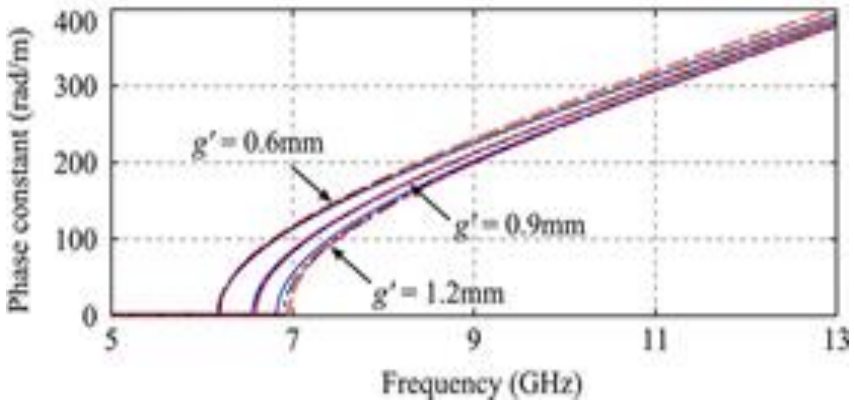

(c)

Figure 2.16 Configurations of (a) FSIW and (b) FSIW with central vias (c) Comparison curve of propagation constants

Research Gap: The numerical variational method can be applied to different shapes of folded SIW, such as sinusoidally modulated FSIW, to find the dispersion characteristics of folded SIW [58]

X Guo et al. [59] introduces a synthesis method for designing multiband band-pass filters using multimode resonator theory in SIW technology. The authors propose a compact topology that allows the filters to generate multiple filtering pass bands without increasing in size. Fig. 2.17 shows the proposed SIW filter with S-parameters.

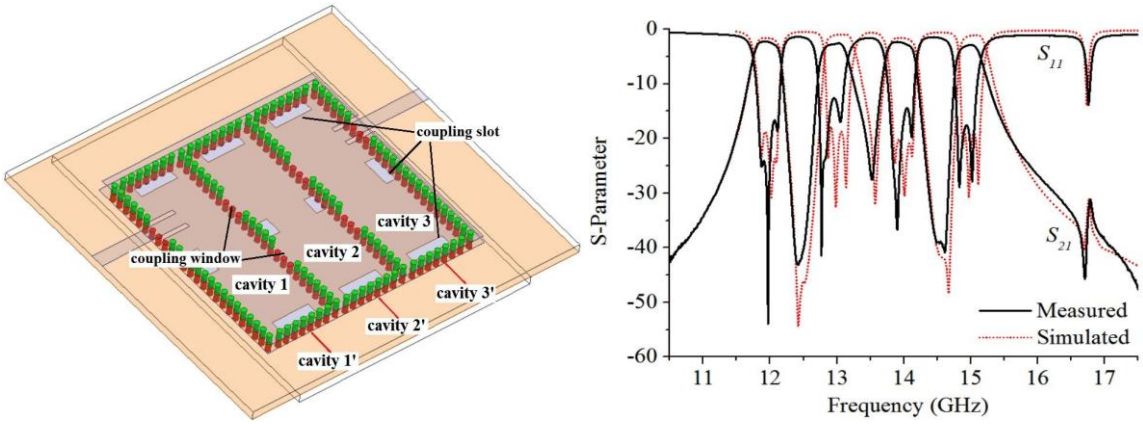

(a) (b)

Figure 2.17 (a) SIW filter (b) S-parameters

Research Gap: The multiband filter can be realized by using a periodic structure with reduced insertion loss. The selectivity of the filter can be improved.

S. Kumari et al. [60] introduce the FSIW filter, which is designed to be suitable for the Wi-Fi 6E system. Longitudinal as well as transverse slots have been employed to modify the impedance and fine-tune the resonant frequencies, meeting the desired specifications. The resulting structure exhibits low insertion loss.

Research Gap: The filter characteristics is obtained by making slot in the central metal vane, the slot can be different shapes, or central metal vane could be periodic structure, to obtained different filter characteristics.

Martínez et al. [61] present two distinct designs of band-pass filters for S-band applications, utilizing SIW technology. In the first design, the SIW substrate incorporates rectangular perforations placed periodically. The cutoff frequency of the first Floquet mode in the periodic structure determines the lower cutoff frequency. In the second design, the first band gap of the same structure governs both the rejection band and the upper cutoff frequency, a periodic array of square CSRR is etched onto the SIW's surface to achieve the desired band-pass filter characteristics.

Research Gap: The periodic structure can be changed with different structure, insertion loss can be improved further.

Q. Lai et al. [62] present a HMSIW, provide the dispersion characteristics of the proposed HMSIW and compare them with those of the full-mode SIW. The HMSIW exhibits dispersion characteristics similar to the full-mode SIW while occupying approximately half the size.

Research Gap: The proposed HMSIW undergoes a transformation into a band-pass filter by implementing a defecting ground structure, and its conversion into a leaky wave antenna by incorporating slots in the lower ground plane remain unexplored areas of investigation. Understanding and realizing these transformations could lead to significant advancements in the functionality and versatility of the HMSIW structure.

J. Xu et al. [63] presented a leaky wave antenna based on HMSIW, highlighting its small size, broad frequency coverage, and radiation pattern with uniformity in all directions. These features render it highly relevant for millimeter-wave systems that prioritize space efficiency, a broad operating range, and uniform signal coverage as essential requirements. The antenna's performance and characteristics hold significant promise for advancing communication and sensing applications in millimeter-wave technology.

Research Gap: The dispersion curves of HMSIW can be generated and compared with those of SIW. The propagation constant is a crucial parameter supporting the leaky wave radiation of HMSIW.

CHAPTER 3

Design and Analysis of Sinusoidally Modulated Substrate Integrated Waveguide and Filter

In this chapter, we embark on a thorough investigation into the design and analysis of a substrate integrated waveguide (SIW) that showcases the distinctive feature of varying widths along the direction of electromagnetic wave propagation within the substrate. This design concept introduces a novel approach to waveguide engineering, allowing for enhanced control over the propagation characteristics of electromagnetic waves. By carefully manipulating the width profile along the axial direction, we can achieve tailored electromagnetic behaviour, enabling the realization of advanced functionalities and improved performance in various microwave and millimeter-wave applications. Specifically, we derive expressions for the modal field components corresponding to the transverse electric (TE) mode, enabling a thorough understanding of the waveguide's behaviour. By implementing a sinusoidally modulation in the width of the waveguide, we examine several noteworthy properties of the resulting periodic structure. The propagation constant (phase constant) exhibits frequency-dependent characteristics, while the electric field experiences axial variations associated with the lowest order mode of propagation. Additionally, the waveguide exhibits inherent filtering properties. To validate our findings, we compare the analytical results with simulation outcomes and measured data, revealing a high degree of agreement. By providing valuable insights into the behaviour and potential applications of the designed substrate integrated waveguide, our study contributes to the advancement of integrated waveguide technology.

3.1 Introduction

The growing need for communication systems has stimulated the advancement of specialized filters designed to provide low insertion loss, ease of manufacturing, and compatibility with RF circuits. In this chapter, a novel approach using a sinusoidally varying width SIW is proposed to address these requirements. The SIW design exhibits the behaviour of a

multiband pass filter, making it exceptionally well-suited for upcoming microwave and mm-wave circuits. Within recent communication systems, selective filters play a pivotal role by enabling the transmission and reception of targeted frequency bands while efficiently mitigating undesired signals.

Achieving low insertion loss and streamlining manufacturing processes are pivotal factors in filter design. Furthermore, integrating filters into RF circuits enhances overall system efficiency and compactness.

Recent studies have focused on exploring electromagnetic properties in periodic structures, with particular attention in periodically loaded transmission lines and unidirectional high frequency microwave devices [38, 39]. Periodicity can be achieved by either modifying the electrical properties of the transmission line or by employing a hollow RWG filled with a dielectric substance featuring varying relative permittivity. Such structures exhibit unique wave characteristics. Additionally, research has delved into other periodic structures, DGS and EBG [40, 64, 65].

SIWs have become a subject of significant interest in microwave and mm-wave circuits, especially with a focus on filters. [66]. Numerous benefits of SIW technology include cheap cost, low attenuation, high quality factor, excellent power handling capability, and seamless integration [4, 41, 67-72]. The structure involves a RWG filled with dielectric substrate, with metallic cladding serving as the upper and lower walls, and side walls is in the form of metallic vias. This seamless integration of the different components such as passive components, and active components along with the SIW enhances the performance and efficiency of wireless systems [72, 73]. Indeed, the combination of SIWs with periodic structures enables the creation of compact wideband filters. This is accomplished by utilizing the first fundamental frequency characteristics of SIWs and the band-stop behaviour of periodic structures. The synergy between these elements contributes to the efficient filtering of signals in a broad range of frequencies.

The chapter begins by analyzing the SIW and employing coordinate transformations to attain separability of the field equations. In this chapter, we focussed into the establishment of orthogonality conditions for transformed coordinates and thoroughly explore the separability of Helmholtz's wave equations within the curvilinear coordinate system. By doing so, we aim

to gain a comprehensive understanding of the intricacies involved in this process and its implications for various applications. The resulting separated form of the wave equation relies solely on metric coefficients. Using a straightforward separable transformation, we convert the wave equation into Hill's equation. Following that, we employ an analytical approach to evaluate the propagation constant and compare it with HFSS simulation and experimental results. Lastly, we derive the electric and magnetic fields for the transverse mode of wave propagation in the proposed sinusoidally modulated SIW. This thorough analysis sheds light on the system's behaviour and performance, offering valuable insights for future advancements and practical applications.

3.2 Transformation of Coordinates System

The designed sinusoidally SIW is visually represented in Fig. 3.1, illustrating its structure and layout within a Cartesian coordinate system. This figure serves to provide a diagrammatic interpretation of the waveguide. The coordinate system used in the diagram defines the three-dimensional space with coordinates (x, y, z). The orientation of these coordinates is specifically chosen so that Y axis coincide with longitudinal axis of the SIW. Additionally, point 'O', which serves as the reference point in both coordinate systems, is assigned as the centre of the modulated SIW in the transverse cross-sectional plane.

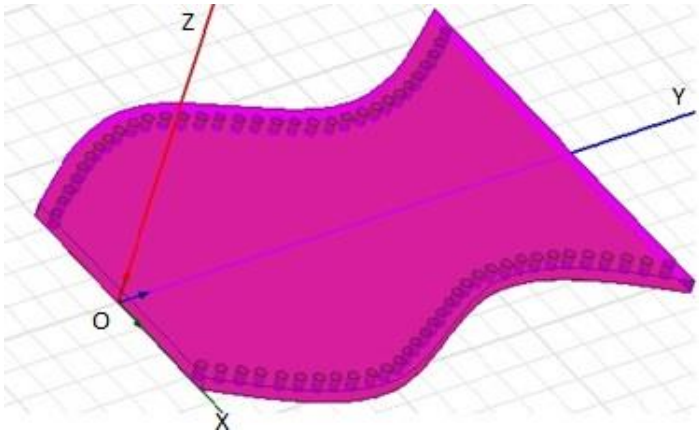

Figure 3.1 shows the coordinate axes and a 3D diagrammatic perspective of the SIW

The waveguide undergoes its primary modulation, meaning that the most significant changes occur, in the XY plane. This modulation sets it apart from a standard uniform-width substrate integrated waveguide where the modulation is absent. In contrast, in the YZ plane, the

structure of the waveguide's walls experiences variations along the x-coordinate due to the modulation. This change in structure reflects the altered design of the waveguide to accommodate the modulation. Furthermore, the width of the waveguide exhibits a continuous variation along the Y-axis. As we move along the Y-axis, the width of the waveguide changes, creating a profile that deviates from a constant value. This continuous variation enables the waveguide to fulfil its intended purpose within the overall system.

To effectively describe the unique characteristics of the SIW, an alternative curvilinear orthogonal coordinate system (u_1, u_2, u_3) is introduced. Coordinate system is designed in a specific manner to ensure that the modulated walls in SIW align with particular planar surfaces that are defined by the coordinates. By employing this alternative coordinate system, we can accurately represent and analyze the behaviour of the SIW in relation to its modulation. Within this coordinate system, the coordinate u_1 denotes the direction of the modulated wave. It maintains a constant average value, represented as $\bar{u}_1$, which captures the overall trend of the modulation. By incorporating this coordinate, we can map the x-coordinate of the SIW's side wall, which varies in accordance with the modulation pattern and the chosen coordinate system.

$$\bar{x} = \bar{u}_1[1 + \mu f(2\pi y/p)] \tag{3.1}$$

Where variable μ represents the depth of the waveform modulation and its value falls within the range of 0 to 1, and $f\left(\frac{2\pi y}{p}\right)$ is a periodic function with a period of p, $\bar{u}_1 \geq 0$ and $\left|f\left(\frac{2\pi y}{p}\right)\right| \leq 1$. It is essential to note that the u_2 axis deviates from the Y-axis and is perturbed away from y. Moreover, the coordinate u_3 follows a linearly functional relationship with z coordinates. As a result, the new coordinate system is precisely defined as [39]. Moreover, the coordinate u_3 exhibits a linear functional relationship with z coordinates. Consequently, the new coordinate system is precisely defined as [39].

$$\begin{aligned} u_1 &= \frac{x}{1+\mu f\left(\frac{2\pi y}{p}\right)} \\ u_2 &= y + \Delta(\mathrm{x},\mathrm{y}) \\ u_3 &= z \end{aligned} \tag{3.2}$$

In order to facilitate interpretation, it is essential that the designed coordinate system u_i ($i = 1,2,3$) to exhibit orthogonality and separability in certain real world situations. Achieving orthogonality requires determining the perturbation function Δ. This function, denoted as $\Delta(x, y)$, and has a lower values when there is a gradual change in the width of the SIW along the axial direction. By expanding $f\left(\frac{2\pi y}{p}\right)$ and $\Delta(x, y)$ in terms of y using Taylor's series, the higher-order terms become insignificant and can be neglected, subject to the following conditions [43].

$$\left|\left(\frac{2\pi}{p}\right)\mu f'\left(\frac{2\pi u_2}{p}\right)\Delta(x, y)\right| << 1 \tag{3.3}$$

$$x = u_1[1 + \mu f\left(\frac{2\pi y}{p}\right)]$$

$$y = u_2 - \Delta(x, y)$$

$$z = u_3 \tag{3.4}$$

The expansion of *x* coordinates by Taylor's series becomes

$$x = u_1\left[1 + \mu\left\{f\left(\frac{2\pi u_2}{p}\right) - \frac{2\pi}{p}f'\left(\frac{2\pi u_2}{p}\right)\Delta(x, y) + \cdots\right\}\right] \tag{3.5}$$

$$x \approx u_1\left[1 + \mu f\left(\frac{2\pi u_2}{p}\right)\right] - u_1\frac{2\pi}{p}f'\left(\frac{2\pi u_2}{p}\right)\Delta(x, y) \tag{3.6}$$

Where $$f'\left(\frac{2\pi u_2}{p}\right) = \frac{df\left(\frac{2\pi u_2}{p}\right)}{d\left(\frac{2\pi u_2}{p}\right)} \tag{3.7}$$

The expression becomes to

$$x \approx u_1\left[1 + \mu f\left(\frac{2\pi u_2}{p}\right)\right] \tag{3.8}$$

Provided by

$$\frac{2\pi}{p}f'\left(\frac{2\pi u_2}{p}\right)\Delta(x, y) \ll 1 + \mu f\left(\frac{2\pi u_2}{p}\right) \tag{3.9}$$

In order to satisfy the condition specified in (3.7), it is necessary to ensure its fulfilment from y to u_2. Considering that $\Delta(x, y)$ exhibits slow variation with respect to y coordinates, we can employ the Taylor's series expansion around u_2 for $\Delta(x, y)$. By disregarding higher order terms in this Taylor's series, we obtain an expression for $\Delta(x, y)$ as stated in [43].

$$\Delta(x, y) = \Delta(x, u_2) \tag{3.10}$$

Provided by

$$\left|\frac{\partial\Delta(x,u_2)}{\partial u_2}\right| << 1 \tag{3.11}$$

or

$$\left|\frac{\partial\Delta\left[u_1\left\{1+\mu f\left(\frac{2\pi u_2}{p}\right)\right\},u_2\right]}{\partial u_2}\right| \tag{3.12}$$

The fulfilment of the coordinate transformation requires the satisfaction of an additional condition, denoted as equation (3.12).

$$x = u_1[1+\mu f\left(\frac{2\pi u_2}{p}\right)]$$

$$y = u_2 - \Delta\left[u_1\left\{1+\mu f\left(\frac{2\pi u_2}{p}\right)\right\},u_2\right]$$

$$z = u_3 \tag{3.13}$$

The value of $\Delta(x, u_2)$ is carefully chosen to achieve the desired property of orthogonality in the new coordinate system u_i.

The requirement of the orthogonality shows [43].

$$\frac{\partial\Delta(x,y)}{\partial u_1}\left[1-\frac{\partial\Delta(x,u_2)}{\partial u_2}\right] = \frac{2\pi}{p}u_1\mu f'\left(\frac{2\pi u_2}{p}\right)[1+\mu f\left(\frac{2\pi u_2}{p}\right)] \tag{3.14}$$

By using the equation no (3.12) the equation reduces

$$\frac{\partial\Delta(x,u_2)}{\partial u_1}\left[1-\frac{\partial\Delta(x,u_2)}{\partial u_2}\right] = \frac{2\pi}{p}u_1\mu f'\left(\frac{2\pi u_2}{p}\right)[1+\mu f\left(\frac{2\pi u_2}{p}\right)] \tag{3.15}$$

By performing integration on this equation, the resulting expression is

$$\Delta(x,u_2) \approx \frac{2\pi}{p}\frac{1}{2}{u_1}^2\mu f'\left(\frac{2\pi u_2}{p}\right)\left[1+\mu f\left(\frac{2\pi u_2}{p}\right)\right] \tag{3.16}$$

This value of $\Delta(x, u_2)$ will make the new curvilinear system orthogonal. So as to achieve the separability of the electromagnetic wave equation the unitary vectors may be defined as $\vec{a}_i = h_i\vec{\imath}_i$.

By defining the unitary vectors as $\vec{a}_i = h_i\vec{\imath}_i$, the chosen value of $\Delta(x, u_2)$ achieves orthogonality in the new curvilinear system and facilitates the separability in wave equation.

The indices $(i = 1,2,3)$ indicate that the definition of the unitary vectors applies to each coordinate direction. The symbol h_i represents the Lame's coefficients associated with each

coordinate direction, as defined in equations (3.12) and (3.13). These coefficients play a role in characterizing the scaling factors of the unitary vectors in the curvilinear coordinate system [43].

$$h_1 = \sqrt{\left[1 + \mu f\left(\frac{2\pi u_2}{p}\right)\right]^2 + \left(\frac{\partial \Delta}{\partial u_1}\right)^2}$$

$$h_2 = \sqrt{\left[1 + \left[\frac{2\pi}{p} u_1 \mu f'\left(\frac{2\pi u_2}{p}\right)\right]^2\right]}$$

$$h_3 = 1 \tag{3.17}$$

The transformation of unitary vectors in the new curvilinear coordinate system are determined based on unit vectors in the Cartesian coordinate system as

$$\hat{\imath}_1 = \frac{\hat{\imath}_x\left[1+\mu f\left(\frac{2\pi u_2}{p}\right)\right] - \hat{\imath}_y \frac{\partial \Delta}{\partial u_1}}{\sqrt{\left[1+\mu f\left(\frac{2\pi u_2}{p}\right)\right]^2 + \left(\frac{\partial \Delta}{\partial u_1}\right)^2}}$$

$$\hat{\imath}_2 = \frac{\hat{\imath}_x\left[\frac{2\pi}{p} u_1 \mu f'\left(\frac{2\pi u_2}{p}\right)\right] + \hat{\imath}_y\left[1 - \frac{\partial \Delta}{\partial u_2}\right]}{\sqrt{1+\left[\frac{2\pi}{p} u_1 \mu f'\left(\frac{2\pi u_2}{p}\right)\right]^2}}$$

$$\hat{\imath}_3 = \hat{\imath}_z \tag{3.18}$$

Under the condition mentioned in reference [43], the wave equation in the newly introduced orthogonal coordinate system can be made separable.

$$\left[\frac{2\pi}{p} u_1 \mu f'\left(\frac{2\pi u_2}{p}\right)\right]^2 \ll 1 \tag{3.19}$$

The conditions in (3.11), (3.12), and (3.19) are all physically valid. Utilizing the condition specified in equation (3.19), equations (3.17) and (3.18) can be simplified to equations as

$$h_1 = 1 + \mu f\left(\frac{2\pi u_2}{p}\right)$$

$$h_2 \approx 1$$

$$h_3 = 1$$

And

$$\hat{\imath}_1 = \hat{\imath}_x - \hat{\imath}_y \left[\frac{2\pi}{p} u_1 \mu f'\left(\frac{2\pi u_2}{p}\right)\right]$$

$$\hat{\imath}_2 = \hat{\imath}_y + \hat{\imath}_x \left[\frac{2\pi}{p} u_1 \mu f'\left(\frac{2\pi u_2}{p}\right)\right]$$

$$\hat{\imath}_3 = \hat{\imath}_z \tag{3.20}$$

Afterwards, a novel curvilinear orthogonal coordinate system is established, incorporating all necessary constants, resulting in a wave equation that exhibits separability. The focus lies on solving the electromagnetic wave equation, with particular emphasis on waves propagating within the periodic structure depicted in Fig. 3.1. The size parameters or geometric properties of the SIW can be determined by combining equations (3.12) and (3.16). By combining these equations, valuable insights on the geometric parameters of the SIW can be obtained, enabling precise characterization and optimization.

$$\left|\left(\frac{2\pi u_1}{p}\right) \mu f''\left(\frac{2\pi u_2}{p}\right)\right| \left[1 + \mu f\left(\frac{2\pi u_2}{p}\right)\right] << 1 \tag{3.21}$$

3.3 Electromagnetic Wave Equations

In the modulated SIW, the wave propagates along the Yaxis, while the width varies in the direction of X direction, limiting the solution to the TE mode in y. Here new orthogonal coordinate system, along with unitary vectors, has been designed. However, obtaining a solution for the TE to y mode in the electromagnetic wave equation is not a straightforward process, because $\left(\nabla^2 \vec{F}_y\right) \neq \nabla^2 F_y$. Consequently, to find the solution for TE to z, we take into account the vector magnetic potential $\vec{A} = \psi^a \hat{\imath}_z$ and the vector electric potential $\vec{F} = \psi^f \hat{\imath}_z$. Here, ψ^a and ψ^f correspond to the wave functions associated with the potentials. The expression of the electric field is defined in terms of the magnetic vector potential, and the magnetic field is defined in terms of the electric vector potential, as shown in reference [74].

$$\vec{E} = -j\omega\mu\vec{A} - \nabla \times \vec{E} + \frac{1}{\sigma + j\omega\varepsilon} \nabla\left(\nabla . \vec{A}\right) \tag{3.22}$$

$$\vec{H} = \nabla \times \vec{A} - (\sigma + j\omega)\vec{F} + \frac{1}{j\omega\varepsilon} \nabla\left(\nabla . \vec{F}\right) \tag{3.23}$$

In the u_i coordinate system, the electric and magnetic fields can be derived exclusively by substituting the values of $\vec{F}$ and $\vec{A}$ into equations (3.22) and (3.23). Using this coordinate system, the components of the TE fields to z are

$$E_1 = \frac{1}{j\mu\omega h_1}\frac{\partial^2\psi^a}{\partial u_1 \partial u_3}$$

$$E_2 = \frac{1}{j\varepsilon\omega}\frac{\partial^2\psi^a}{\partial u_1 \partial u_3}$$

$$E_3 = \frac{1}{j\mu\omega}\left[\omega^2\varepsilon\mu + \frac{\partial^2}{\partial u_3^2}\right]\psi^a$$

$$H_1 = \frac{\partial\psi^a}{\partial u_2}$$

$$H_2 = -\frac{1}{h_1}\frac{\partial\psi^a}{\partial u_1}$$

$$H_3 = 0 \tag{3.24}$$

Within the u_i orthogonal coordinate system, ψ^a signifies the outcome of the scalar Helmholtz wave equation, the explicit form of which can be found in reference [43].

$$\nabla^2\psi^a + K^2\psi^a = 0 \tag{3.25}$$

$$\frac{1}{h_1 h_2 h_3}\sum_{i=1}^{3}\frac{\partial}{\partial u_i}\left(\frac{h_1 h_2 h_3}{h_i^2}\frac{\partial\psi}{\partial u_i}\right) + k^2\psi^a = 0 \tag{3.26}$$

The wave number k = $\sqrt{\omega^2\mu\varepsilon}$, where ω represents the angular frequency, μ is the magnetic permeability, and ε is the electric permittivity. The wave function is represented by ψ , and by assuming it to have the form $\psi = U_1(u_1)U_2(u_2)U_3(u_3)$, the equation can be tackled using the widely utilized method of variable separation. This method is commonly applied to handle partial differential equations of this nature. Consequently, equation (3.22) can be split into three separate partial differential equations, as outlined in reference [39].

$$\frac{d^2U_1}{du_1^2} + K_1^2U_1 = 0 \tag{3.27}$$

$$\frac{d^2U_2}{du_2^2} + \frac{1}{h_1}\frac{dh_1}{du_2}\frac{dU_2}{du_2} + \left(k^2 - \frac{K_1^2}{h_1^2}\right)U_2 = 0 \tag{3.28}$$

The separation constant, K_1 is an important factor in the wave function.

The wave function $\psi^a = \text{Cos}(K_1 u_1) U_2 Sin(K_1 u_1) U_2$

(3.29) Where, U_2 represents the solution of equation (3.26).In this study, it is assumed that the fields exhibit symmetry around $u_1 = 0$. Thus, the equation is analyzed based on this assumption and can be taken as

$$\psi^a = \text{Cos}(K_1 u_1)\, U_2 \tag{3.30}$$

The equation provides the components of the field.

$$E_1 = 0,\ E_2 = 0 \text{ and } E_3 = -j\omega\mu Cos(K_1 u_1) U_2$$

$$H_1 = Cos(K_1 u_1) \frac{dU_2}{du_2},\ H_2 = \frac{K_1}{h_1} Sin(K_1 u_1) \text{ and } H_3 = 0 \tag{3.31}$$

To determine the separation constant K_1, the boundary condition $E_3 = 0$ is applied at $u_1 = \pm \bar{u}_1$.

$$K_1 = \frac{(2n+1)\pi}{\bar{u}_1}, \text{ Where } n = 0,1,2,3,4 \ldots \ldots \ldots \tag{3.32}$$

In the Cartesian coordinate system (x, y, z) the non-zero components are

$$E_z = -j\omega\mu Cos(K_1 u_1) U_2$$

$$H_x = Cos(K_1 u_1) \frac{dU_2}{du_2} + \frac{\frac{2\pi}{p} u_1 \mu f'\left(\frac{2\pi u_2}{p}\right) K_1}{1+\mu f\left(\frac{2\pi u_2}{p}\right)} Sin(K_1 u_1) U_2$$

$$H_y = \frac{K_1 Sin(K_1 u_1) U_2}{1+\mu f\left(\frac{2\pi u_2}{p}\right)} - \frac{2\pi}{p} u_1 \mu f'\left(\frac{2\pi u_2}{p}\right) K_1\, Cos(K_1 u_1) \frac{dU_2}{du_2} \tag{3.33}$$

When considering the axis of the SIW, where $x = 0$, it follows that $u_1 = 0$ and $\Delta = 0$ In this case, the coordinate y corresponds to u_2. Consequently, in the axial direction of the SIW, the field components are computed as follows

$$E_x = E_y = H_z = 0$$

$$E_z = -j\omega\mu U_2,\ H_x = \frac{\partial U_2}{\partial y} \tag{3.34}$$

In the limiting case where μ approaches 0, the coordinate u_1 tends to x, u_2 tends to $W_{SiW}/2$, and u_3 tends to z. In this case, the given formulas transform into the equations describing the fields in a uniform waveguide.

3.4 Determination of Propagation Constant

To determine the propagation behaviour of the wave inside the proposed SIW, it is necessary to solve the differential equation provided in (3.28). The properties related to the transmission of the designed structure are determined. To streamline the analysis, subscript in equations is omitted as replacing U_2 with U and u_2 with u. The value of the hill coefficient h_1 is obtained from equation (3.20). When the SIW is subjected to sinusoidal modulation, with $f\left(\frac{2\pi u}{p}\right) = -cos\left(\frac{2\pi u}{p}\right)$ the equation (3.28) undergoes the following transformation.

$$\frac{d^2U}{du^2} + \frac{\frac{2\pi}{p}\mu Sin\left(\frac{2\pi u}{p}\right)}{1-\mu Cos\left(\frac{2\pi u}{p}\right)}\frac{dU}{du} + \left[k^2 - \frac{K_1^2}{\left\{1-\mu Cos\left(\frac{2\pi u}{p}\right)\right\}^2}\right]U = 0 \tag{3.35}$$

$$\frac{d^2U}{dz^2} + J(z)V = 0 \tag{3.36}$$

Where

$$J(z) = (P/\pi)^2\left[k^2 - \frac{K_1^2}{(1-\mu Cos2z)^2}\right] \tag{3.37}$$

The function $J(z)$ is symmetric with respect to z. A Fourier series can be used to depict its expansion, as seen below.

$$J(z) = \Theta_0 + 2\sum_{n=1}^{\infty}\Theta_{2n}Cos(2nz) \tag{3.38}$$

The coefficients Θ_n in equation (3.38) are constants that are already known. The equation remains valid for all values of z if the infinite series $\sum_{n=0}^{\infty}\Theta_n$ converges absolutely. Let's express the solution of the equation as $V = \Phi(z)e^{(\gamma Z)}$ where γ represents the characteristics exponent or propagation constant, and it is a complex number. To determine the characteristics exponents, we set the Hill's determinant $\Delta(j\gamma) = 0$, as mentioned in reference [44].

$$\Delta(j\gamma) = \begin{vmatrix} \cdots & \cdots & \cdots & \cdots & \cdots & \cdots \\ \cdots & \frac{(j\gamma+4)^2-\theta_0}{4^2-\theta_0} & \frac{-\theta_1}{4^2-\theta_0} & \frac{-\theta_2}{4^2-\theta_0} & \frac{-\theta_3}{4^2-\theta_0} & \cdots \\ \cdots & \frac{-\theta_1}{2^2-\theta_0} & \frac{(j\gamma+2)^2-\theta_0}{2^2-\theta_0} & \frac{-\theta_1}{2^2-\theta_0} & \frac{-\theta_2}{2^2-\theta_0} & \cdots \\ \cdots & \frac{-\theta_2}{0^2-\theta_0} & \frac{-\theta_1}{0^2-\theta_0} & \frac{(j\gamma)^2-\theta_0}{0^2-\theta_0} & \frac{-\theta_1}{0^2-\theta_0} & \cdots \\ \cdots & \frac{-\theta_3}{2^2-\theta_0} & \frac{-\theta_2}{2^2-\theta_0} & \frac{-\theta_1}{2^2-\theta_0} & \frac{(j\gamma-2)^2-\theta_0}{2^2-\theta_0} & \cdots \\ \cdots & \cdots & \cdots & \cdots & \cdots & \cdots \end{vmatrix} = 0 \qquad (3.39)$$

The Hill's determinant, as stated in reference [44], can be expressed by a simplified expression.

$$\Delta(j\gamma) = \Delta(0) - Sin^2\left(\tfrac{1}{2}\pi j\mu\right) Cosec^2\left(\tfrac{1}{2}\pi\sqrt{\theta_0}\right) = 0$$

Then,

$$\Delta(0) = Sin^2\left(\tfrac{1}{2}\pi j\mu\right) Cosec^2\left(\tfrac{1}{2}\pi\sqrt{\theta_0}\right)$$

$$Cosh(\pi\gamma) = 1 - 2\,\Delta(0) Sin^2\left(\tfrac{1}{2}\pi\sqrt{\theta_0}\right) \qquad (3.40)$$

Now comparison of (3.36) and (3.37) yields the even harmonics of θ

$$\theta_0 = \left(\frac{p}{\pi}\right)^2 \left[k^2 - K_1^2\left\{1 + \frac{3}{2}\mu^2 + \frac{15}{8}\mu^4 + \cdots\right\}\right]$$

$$\theta_2 = -\frac{1}{2}\left(\frac{p}{\pi}\right)^2 \left[K_1^2\left\{2\mu + 3\mu^3 + \frac{60}{16}\mu^5 + \cdots\right\}\right]$$

$$\theta_4 = -\frac{1}{2}\left(\frac{p}{\pi}\right)^2 \left[K_1^2\left\{\frac{3}{2}\mu^2 + \frac{5}{2}\mu^4 + \frac{105}{32}\mu^6 + \cdots\right\}\right]$$

……. ……. ……. ……. …… (3.41)

After performing the analysis up to θ_{26} , we can apply Cauchy's ratio test using equation (3.40) to determine certain properties or characteristics.

$$\sum_{n=1}^{\infty} \theta_{2n} = \left(\frac{p}{\pi}\right)^2 [k^2 - K_1^2(1 + 2\mu + 3\mu^2 + 4\mu^3 + 5\mu^4 + 6\mu^5 + 7\mu^6 + 8\mu^7 + \cdots)]$$

(3.42)

The characteristics exponent $\Delta(0) = 0$ is determined using equation (3.40). By reducing the infinite Hill's determinant to a finite order, we can evaluate its value. In a device without any loss, the phase constant can be determined by substituting $j\beta$ for γ in equation (3.40). The

analysis reveals the theoretical relationship between the phase constant and frequency for modulation indices of 0.146 and 0.246, as depicted in Fig. 3.3.

3.5 Design Methods and SIW Result Analysis

Fig. 3.2 provides a top view of SIWs that are designed with sinusoidally varying widths. These SIWs have a length of 30 mm and their widths change sinusoidally with different modulation indexes. The designed SIWs demonstrate comparable transmission and distribution characteristics to conventional waveguides. Through the sinusoidal variation of the SIW width, it becomes possible to selectively attenuate or allow specific frequency components of transmitted signals, thereby creating a filtering effect. This filtering effect is achieved by preferentially attenuating certain frequencies or permitting them to pass through the SIW, offering control over the signal spectrum. The sinusoidal variation in width can introduce variations in the propagation characteristics, such as the effective refractive index, group delay, or dispersion properties of the waveguide.

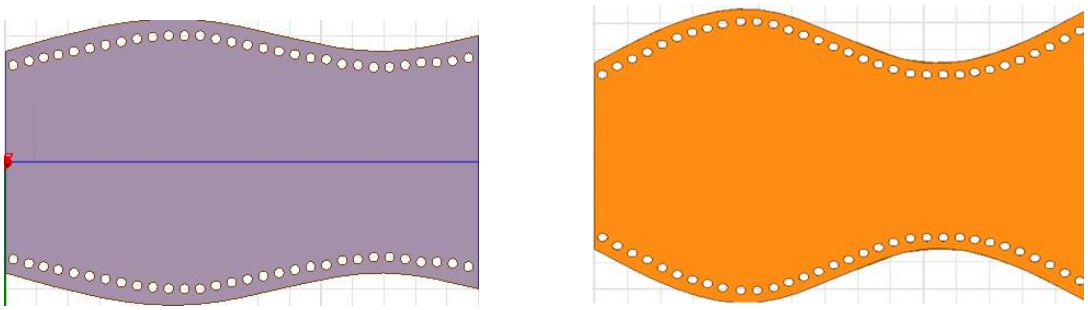

(a) (b)

Figure 3.2. (a) SIW at μ of 0.146 (b) SIW at μ of 0.246

The substrate material chosen for these designs is RO 4350B, which possesses a relative dielectric constant of 3.48. The substrate has a height of 0.762 mm. To minimize radiation between the vias, the spacing between them is set to 0.91 mm, while the vias themselves have a diameter of 0.61 mm. The design parameters are carefully adjusted to ensure negligible radiation. In this design, the wavelength (λ) of the periodic structure is 20 mm, and the total length of the SIW is 1.5 times the wavelength. The modulation index (μ) is determined by using a simple expression as used in the amplitude modulation, as follows:

$$\mu = \frac{W_{max} - W_{min}}{W_{max} + W_{min}} \tag{3.43}$$

The plot in Fig. 3.3 presents a comparative analysis of the phase constant as a function of frequency for different modulation indices, concerning the designed SIWs.

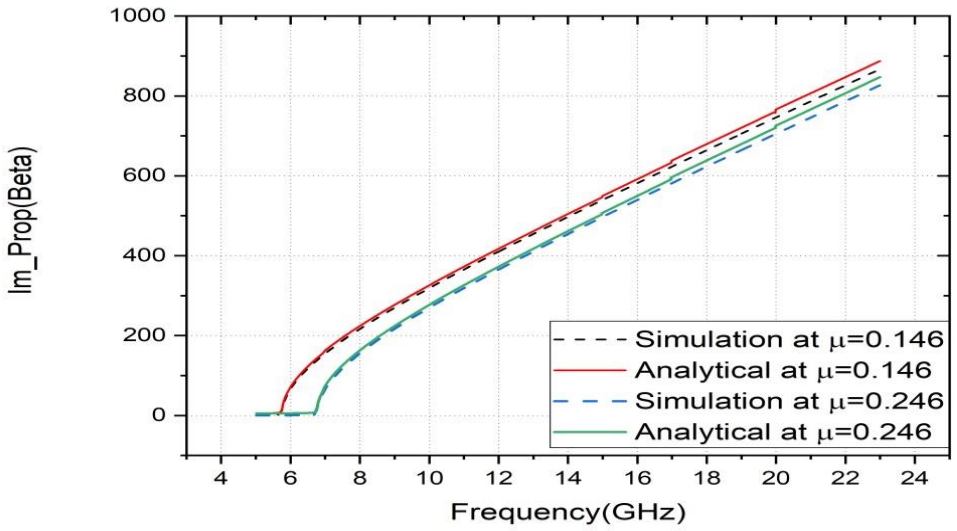

Figure 3.3 Comparision curve of phase constant vs. frequency curve

The graph above shows a comparison of the phase constant (β) versus frequency curves obtained from analysis and simulation for two different modulation indices: 0.146 and 0.246.in case of dominant TE_{10} mode. Interestingly, the curves derived from simulation and analysis exhibit a significant degree of similarity. It is evident that the phase constant undergoes changes as the modulation index of the waveguide is altered. In Fig. 3.4, the $\vec{\boldsymbol{E}}$-field of the TE_{10} mode f propagation at a modulation index of 0.246 is presented. Importantly, the electric field distribution bears a strong resemblance to that of a conventional RWG.

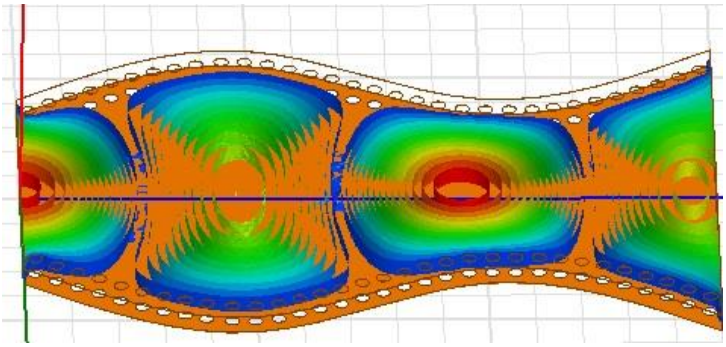

Figure 3.4 $\vec{E}$- Field for the TE_{10} mode

3.6 SIW Filter Characteristics

Due to the periodic nature of the designed SIW, it exhibits distinct pass band and stop band characteristics, making it function as a band pass filter. As with any filter design, the development of periodic SIW filters involves careful simulation, optimization, and prototyping to achieve the desired performance. The use of advanced electromagnetic simulation tools and analysis helps in the efficient design of these filters. Fig. 3.5 illustrates the $S_{11}(dB)$ and $S_{12}(dB)$ curves for the different modulation index, which represent the performance of the designed SIWs as a multiband filter. The designed SIWs demonstrate negligible insertion loss within the passband. The center frequency and bandwidth of the filter can be adjusted by modifying the modulation index.

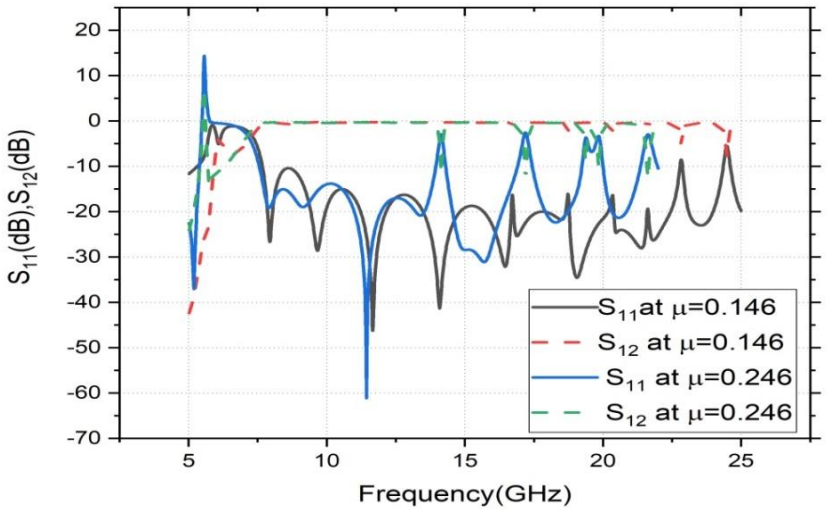

Fig. 3.5 $S_{11}(dB)$ and $S_{12}(dB)$ vs. frequency curves

A substrate integrated waveguide (SIW) with sinusoidal modulation, having a modulation index of 0.246, has been successfully fabricated using a PCB process on a 0.762 mm-thick RO 4350B dielectric substrate. The physical realization of the SIW can be observed in Fig. 3.6.

(a) (b)

Figure 3.6 Fabricated SIW (a) Top View (b) Back View

The fabricated SIW with a modulation index of 0.246 was subjected to measurements using the PNA-X Agilent N5247A microwave vector network analyzer. The measured S_{11} and S_{12} parameters were then compared to the simulated values, as illustrated in Fig. 3.7. Remarkably, the nature of the curves exhibited a striking resemblance.

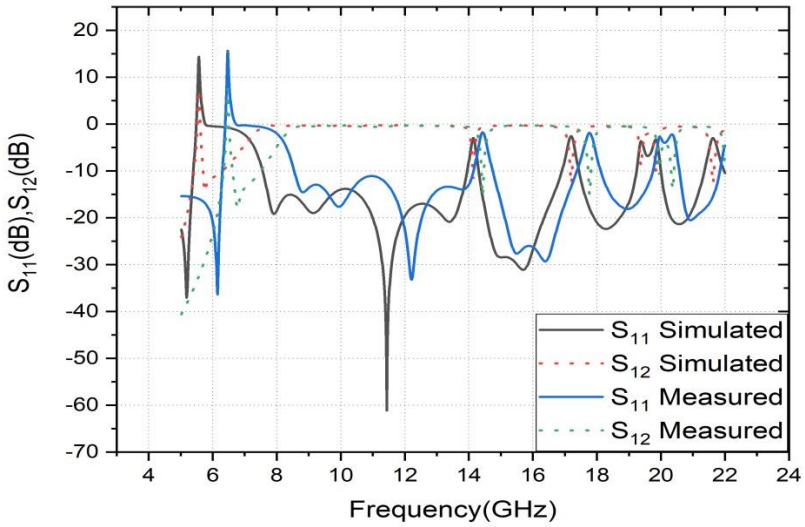

Figure 3.7 Measured vs. simulation curve

In the simulation, the first passband spanned a frequency range of approximately 7.66 GHz to 13.88 GHz, while in the experimental observation, it covered a slightly different range of approximately 8.33 GHz to 13.33 GHz Similarly, the second passband in the simulation ranged from approximately 14.3 GHz to 16.7 GHz, whereas in the experimental observation, it extended from approximately 14.8 GHz to 17.2 GHz. The third pass bands in the simulation were expected to occur between approximately 17.5 GHz to 19.1 GHz, but in the experimental observation, they were found to be in the range of approximately 18 GHz to 19.4 GHz. It is evident that there are minor variations in the frequency ranges observed between the simulation and the experimental results in all the bands.

The discrepancy between the simulated and experimental results can be linked to a variety of factors, including the finite conductivity of the metal/via, inherent fabrication errors, the influence of parasitic effects, and the impact of SMA connectors. However, it is worth noting that through the utilization of refined fabrication techniques, these limitations can be alleviated. With the implementation of enhanced fabrication methods, it becomes feasible to minimize these discrepancies and achieve a closer alignment between simulation and experimental observations.

3.7 Conclusion

In this chapter, we have presented a straightforward derivation of the equations describing the electric and magnetic fields. By assuming the fields to be invariant along the Z-axis, we effectively eliminate the need to consider the longitudinal component. To determine the imaginary propagation constant of SIW, we made use of Hill's equation, which proved to be a valuable mathematical tool in our analysis. Through these techniques, we gained a deeper understanding of the field characteristics within the waveguide structure, facilitating the exploration of its transmission properties.

We compared the analytical and simulated phase constants for a specific modulation index, highlighting the agreement between the two approaches. Additionally, we investigated the periodic nature of the designed SIW and explored its filtering properties.

Significantly, our examination of the phase constant curve has uncovered a remarkable characteristic of the sinusoidally modulated SIW, it exhibits the behaviour of a fast wave

structure as seen from propagation constant curve. This intriguing attribute makes it particularly well-suited for the development of leaky wave antennas. The insights gained from this chapter not only deepen our comprehension of the fundamental principles at play but also pave the way for exciting practical applications in antenna design. These findings hold great potential for advancing the field and exploring novel avenues in antenna technology.

CHAPTER 4

Design and Mode Matching Analysis of Stepped Substrate Integrated Waveguide and Filters

This thesis chapter introduces a novel approach to analyzing stepped substrate integrated waveguides (SIWs) and investigates their generalized scattering properties. The analysis focuses on the cascaded H-plane discontinuity within the SIW across different frequency bands. In order to solve the field equations at the four step discontinuities and get the scattering parameters (S) for each location, the study uses mode-matching techniques (MMT). To validate the reliability of the MMT approach and enable a comparative study, the investigation incorporates two widely-used commercial simulators: HFSS and computer simulation technology microwave studio (CST-MWS). Separate simulation studies are conducted using HFSS and CST-MWS, and the obtained scattering parameters through MMT are then compared with the simulated S-parameters from these software packages. Furthermore, to validate the accuracy of the MMT results, experimental verification is carried out by fabricating the SIW and analyzing its performance. The comparison of the S-parameters among MMT, HFSS, CST-MWS, and the measured data demonstrates a high level of agreement, indicating the similarity in the results obtained through MMT and the commercial simulators. This comparison serves as a validation of the accuracy and reliability of the MMT approach in predicting the scattering properties of the cascaded discontinuities within the SIW structure. Furthermore, the computational performance of MMT is evaluated by comparing its processor computation time and memory usage with those of HFSS and CST-MWS. This analysis provides insights into the computational efficiency of MMT relative to the commercial simulators. Additionally, the designed SIW structure exhibits a filter-like property due to its periodic nature, further supporting its potential applications as a frequency-selective device.

4.1 Introduction

In recent years, the field of RF and microwave components has witnessed a remarkable surge in interest and advancements. Technology continues to evolve, driving the exploration,

recommendation, investigation, and successful deployment of new applications [45]. With the rise of the millimeter wave communication era, there is a constant stream of announcements regarding new frequency bands and standards [75]. In the evolving landscape of advanced high-frequency wireless circuits, SIWs have emerged as a focal point, especially in the context of filters [66]. SIWs, are structures resembling waveguides and are fabricated by employing periodic rows of metallic vias. These vias connect the top and bottom ground planes of a dielectric substrate [76]. SIW components possess many advantages akin to traditional waveguides, including low loss, cost-effectiveness, high quality factor, high power-handling capabilities, and ease of integration. Consequently, the SIW technology has garnered substantial interest and attention [77-79]. This technology allows for the integration of active devices, passive structures, and additional components onto a single substrate, enabling the incorporation of complete wireless systems within the SIW framework [41, 80]. Extensive research has resulted in numerous SIW-based bandpass filters with enhanced performance, as documented in the literature [66, 75-80]. By combining SIWs with periodic structures, engineers have been able to develop compact wideband filters. This integration utilizes the sharp cut-off frequency characteristics of SIWs and exploits the band stop behaviour typically exhibited by periodic structures.

Achieving periodicity within the waveguide can be accomplished by modifying the electromagnetic properties of the transmission line. For instance, a empty, uniform waveguide can be filled with a dielectric material that exhibits varying relative permittivity. This alteration enables the propagation of electromagnetic waves with characteristics similar to those observed in stepped waveguides [41, 67].Various modelling techniques have been developed and employed to analyze SIWs, including both straight interconnects and complex components. While techniques such as finite element methods (FEM), methods of moments (MOM), and finite difference time domain (FDTD) offer flexibility, they often come with high computational complexity [67]. On the other hand, MMT provide faster and more accurate solutions for analyzing periodic structures and waveguides with varying cross-sections. In the case of a stepped SIW, which represents an H-plane discontinuity, MMT focuses on analyzing the electric field parallel to the transverse direction. It is important to note that the only mode supported by the SIW is the TE_{m0} mode, where ($m = 1,2,3 \ldots\ldots$). When the step discontinuity is excited by a TE_{m0} mode that differs from modes of the same

nature, both propagating and evanescent modes are generated. The evanescent mode does not propagate energy but instead stores it, giving rise to reflection issues. In cases where the discontinuities are in close proximity, higher modes can also be generated. Analyzing such types of cases requires the use of a generalized scattering matrix, which establishes relationships between the incoming and outgoing modes [38, 42, 73].

Therefore, this chapter presents a comprehensive design and mode-matching technique for analyzing a stepped SIW, specifically focusing on the behaviour of TE_{m0} modes. The proposed stepped SIW exhibits multi-bandpass filter characteristics within the frequency range of 4 to 22 GHz, making it highly relevant and beneficial for future microwave and millimeter wave circuits.

4.2 Design and MMT Analysis of Stepped SIW

The illustration in Figure 4.1 displays the schematic representation of the stepped SIW under consideration. The cross-sectional view of the structure is presented in the XZ plane, while the propagation direction of the electromagnetic wave occurs along the positive Y axis. To ensure effective confinement of the electromagnetic energy within the structure and to minimize radiation leakage, a careful selection is made for the vias diameter-to-pitch ratio. The chosen ratio falls within the range of 0.5 to 0.8, as specified in reference [10]. For the analysis of this designed structure, MMT are employed. This method involves dividing the structure into smaller, more manageable substructures, each possessing known or determinable eigen modes. The electric and magnetic fields within the structure are expressed as a summation of these individual eigen modes, with coefficients that will be determined during the analysis process. When MMT are utilized to find the eigen values, they are referred to as field matching techniques. By combining MMT with the generalized scattering matrix, a powerful tool for analyzing composite structures is created. This approach enables a detailed analysis of the stepped SIW and its scattering properties.

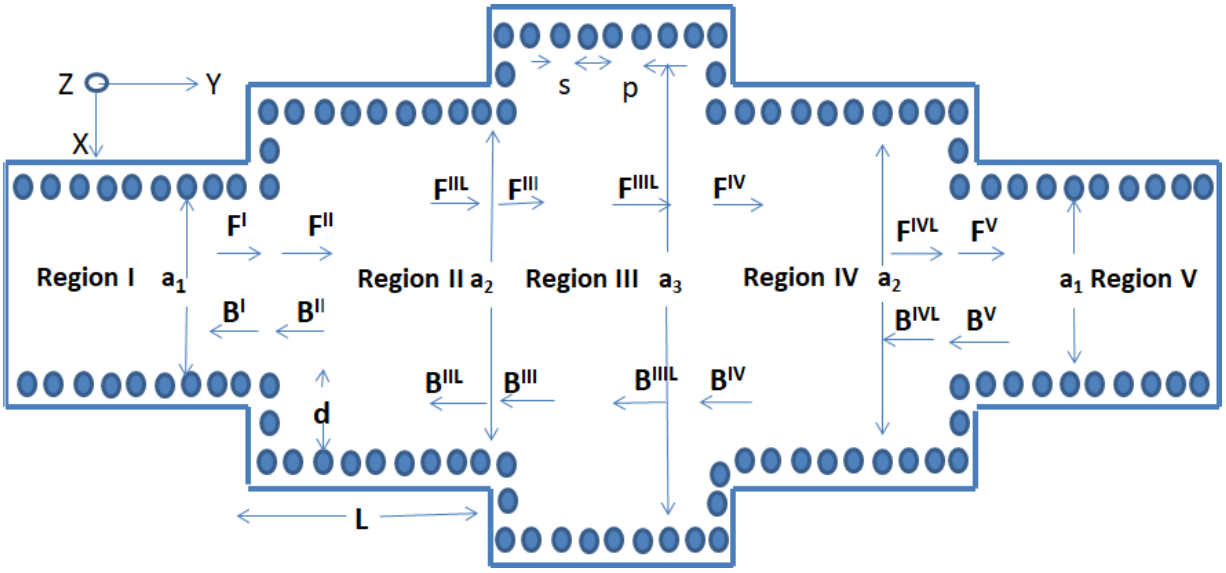

Figure 4.1. Schematic view of stepped SIW

The stepped SIW is divided into five regions, where, a_1 = width of the regions I and V, a_2= width of the regions II and IV, a_3 = width of the region III, L = length of each step, d = height of each step, F stands for the forward wave and B stands for the backward wave. The physical design parameters are shown in the Table 4.1

Table 4.1 Geometric design parameters of the stepped SIW

Parameters	**a_1**	**a_2**	**a_3**	**L**	**s**	**p**	**d**
In mm	12.25	15.89	19.53	10	0.61	0.91	1.82

The cascaded stepped SIW exhibits a generalized scattering matrix obtained by combining the individual regions' generalized scattering matrices. By incorporating mode matching with the generalized scattering matrix, additional modes of interaction between the step discontinuities are observed. Giving due consideration to the influence of supplementary modes becomes vital, particularly when the discontinuity is in proximity, as disregarding these modes, even if they are evanescent, can result in imprecise outcomes.

The structure is implemented on an RO 4350B dielectric substrate, which has a relative permittivity of 3.48. The substrate has a height of 0.762 mm. Each step in the structure has a

length (L) of 10 mm and a step height (d) of 1.82 mm. The average width of 15.89 mm is determined using a formula based on the equivalent rectangular waveguide model [73].

$$W_{SIW} = W_{RWG} + \frac{s^2}{0.95p} \tag{4.1}$$

The average width of the SIW is denoted as W_{SIW} , while the width of the equivalent rectangular waveguide is represented as W_{RWG}. The metallic vias have a diameter of s and are spaced at a pitch of p. For three different step sizes (1.32 mm, 1.82 mm, and 2.32 mm), the cut-off frequencies of the dominant TE_{10} mode are calculated as 4.8 GHz, 5.2 GHz, and 5.6 GHz, respectively. To obtain the dispersion curve, which illustrates the relationship between imaginary propagation and frequency, the HFSS software is utilized. HFSS is a finite element method-based software known for accurately determining waveguide propagation behaviour. Fig. 4.2 shows the dispersion curve of the stepped SIW.

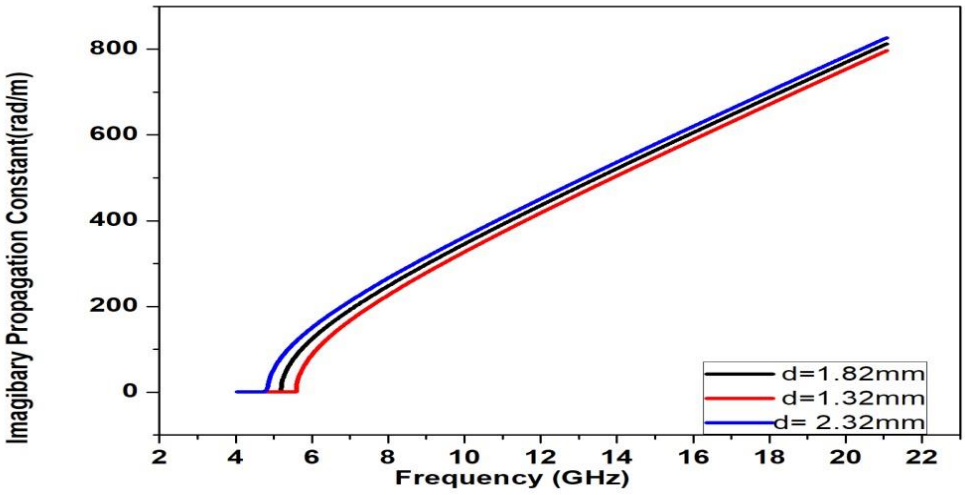

Figure 4.2 Dispersion curve of the stepped SIW

From the provided curves, it is evident that the HFSS simulated cut-off frequencies precisely match the calculated frequencies for the stepped SIW. Due to the small distance between the vias $(p = 0.91\,mm)$ compared to the guided wavelength $(\lambda_g = 30.9\,mm)$, the rows of metallic vias can be treated as continuous metal walls. Consequently, each region can be treated as an equivalent dielectric-filled RWG, allowing us to view the overall structure as a combination of dielectric-filled RWGs for analysis purposes. In every region, the forward

wave amplitude is represented by F, the backward wave amplitude is denoted by B, and the normalization coefficients are indicated by ψ. The subscript in the alphabets signifies the integer variable, while the superscript indicates the corresponding region.

The electric and magnetic fields consist only of the $E_{z,}$ H_x and H_y components at the discontinuity. In region I, the field components are expanded as [46].

$$E_Z^I(x,y)= \sum_{m=1}^{M} \psi_m^I Sin\left[\frac{m\pi(x-d)}{a_1}\right]\left(F_m^I\, e^{-jk_m^I y} + B_m^I e^{-jk_m^I y}\right) \tag{4.2a}$$

$$H_x^I(x,y) = -\sum_{m=1}^{M} \psi_m^I Y_m^I Sin\left[\frac{m\pi(x-d)}{a_1}\right]\left(F_m^I\, e^{-jk_m^I y} - B_m^I e^{-jk_m^I y}\right) \tag{4.2b}$$

The propagation constant k_m^I and wave admittance Y_m^I for the TE mode in region I are expressed as follows.

$$k_m^I = +\sqrt{\omega^2 \mu_0 \varepsilon_0 \varepsilon_r - \left(\frac{m\pi}{a_1}\right)^2} \quad \text{For propagating mode} \tag{4.3a}$$

Where ω indicates the angular frequency of the wave and ε_r indicates the relative dielectric constant of the substrate, μ_0 indicates permeability of the vacuum and ε_0 represents permittivity of the vacuum.

$$k_m^I = -j\sqrt{\left(\frac{m\pi}{a_1}\right)^2 - \omega^2 \mu_0 \varepsilon_0 \varepsilon_r} \quad \text{For evanescent mode} \tag{4.3b}$$

The magnitude of evanescent modes is significant only in the proximity of the discontinuities

$$k_m^I = Y_m^I \omega \mu_0 \tag{4.4a}$$

$$Y_m^I = \frac{k_m^I}{\omega \mu_0} \tag{4.4b}$$

In region II, the electric and magnetic fields are represented by the following expressions:

$$E_Z^{II}(x,y)= \sum_{n=1}^{N} \psi_n^{II} Sin\left[\frac{n\pi x}{a_2}\right]\left(F_n^{II}\, e^{-jk_n^{II} y} + B_n^{II} e^{-jk_n^{II} y}\right) \tag{4.5a}$$

$$H_x^{II}(x,y) = -\sum_{n=1}^{N} \psi_n^{II} Y_n^{II} Sin\left[\frac{n\pi x}{a_2}\right]\left(F_n^{II}\, e^{-jk_n^{II} y} - B_n^{II} e^{-jk_m^{II} y}\right) \tag{4.5b}$$

The propagation constant k_n^{II} and wave admittance Y_n^{II} for the TE mode in region II are expressed as follows [47].

$$k_n^{II} = +\sqrt{\omega^2 \mu_0 \varepsilon_0 \varepsilon_r - \left(\frac{n\pi}{a_2}\right)^2} \quad \text{For propagating mode} \tag{4.6a}$$

$$k_n^{II} = -j\sqrt{\left(\frac{n\pi}{a_2}\right)^2 - \omega^2 \mu_0 \varepsilon_0 \varepsilon_r} \quad \text{For evanescent mode} \tag{4.6b}$$

$$Y_n^{II} = \frac{k_n^{II}}{\omega \mu_0} \tag{4.6c}$$

In region III, the electric and magnetic fields are represented by the following expressions

$$E_Z^{III}(x,y) = \sum_{u=1}^{U} \psi_u^{III} Sin\left[\frac{u\pi(x+d)}{a_3}\right]\left(F_u^{III}\, e^{-jk_u^{III}y} + B_u^{III} e^{-jk_u^{III}y}\right) \tag{4.7a}$$

$$H_x^{III}(x,y) = -\sum_{u=1}^{U} \psi_u^{III} Y_u^{III} Sin\left[\frac{u\pi(x+d)}{a_3}\right]\left(F_u^{III}\, e^{-jk_u^{III}y} - B_u^{III} e^{-jk_u^{III}y}\right) \tag{4.7b}$$

The propagation constant k_n^{III} and wave admittance Y_n^{III} for the TE mode in region III are expressed as follows.

$$k_u^{III} = +\sqrt{\omega^2 \mu_0 \varepsilon_0 \varepsilon_r - \left(\frac{u\pi}{a_3}\right)^2} \quad \text{For propagating mode} \tag{4.8a}$$

$$k_u^{III} = -j\sqrt{\left(\frac{u\pi}{a_3}\right)^2 - \omega^2 \mu_0 \varepsilon_0 \varepsilon_r} \quad \text{For evanescent mode} \tag{4.8b}$$

$$Y_u^{III} = \frac{k_u^{III}}{\omega \mu_0} \tag{4.8c}$$

In region IV, the electric and magnetic fields are represented by the following expressions:

$$E_Z^{IV}(x,y) = \sum_{v=1}^{V} \psi_v^{IV} Sin\left[\frac{v\pi x}{a_2}\right]\left(F_v^{IV}\, e^{-jk_v^{IV}y} + B_v^{IV} e^{-jk_v^{IV}y}\right) \tag{4.9a}$$

$$H_x^{IV}(x,y) = -\sum_{v=1}^{V} \psi_v^{IV} Y_v^{IV} Sin\left[\frac{v\pi x}{a_2}\right]\left(F_v^{IV}\, e^{-jk_v^{IV}y} - B_v^{IV} e^{-jk_v^{IV}y}\right) \tag{4.9b}$$

The propagation constant k_n^{IV} and wave admittance Y_n^{IV} for the TE mode in region IV are expressed as follows:

$$k_v^{IV} = +\sqrt{\omega^2 \mu_0 \varepsilon_0 \varepsilon_r - \left(\frac{v\pi}{a_2}\right)^2} \quad \text{For propagating mode} \tag{4.10a}$$

$$k_v^{IV} = -j\sqrt{\left(\frac{u\pi}{a_2}\right)^2 - \omega^2 \mu_0 \varepsilon_0 \varepsilon_r} \quad \text{For evanescent mode} \tag{4.10b}$$

$$Y_v^{IV} = \frac{k_v^{IV}}{\omega\mu_0} \tag{4.10c}$$

The stepped SIW design has specific boundary conditions that are both necessary and sufficient. These conditions dictate that the tangential electric field components must become zero at the discontinuity point $(y = 0)$ and maintain continuity at the other apertures. Applying these boundary conditions ensures a smooth transition of the electric field across the discontinuity, allowing for consistent wave propagation in the stepped SIW design. These conditions are applied to analyze the waveguide behaviour in regions I and II [81].

$$E_Z^I(x, y = 0) = 0, \quad 0 \le x \le d \text{ and } (a_1 + d) \le x \le a_2 \tag{4.11a}$$

$$E_Z^I(x, y = 0) = E_Z^{II}(x, y = 0) = E_Z^{III}(x, y = 0) = E_Z^{IV}(x, y = 0),$$

$$d \le x \le (a_1 + d),\ 2d \le x \le (a_1 + 2d) \tag{4.11b}$$

$$H_x^I(x, y = 0) = H_x^{II}(x, y = 0) = H_x^{III}(x, y = 0) = H_x^{IV}(x, y = 0)$$

$$d \le x \le (a_1 + d), 2d \le x \le (a_1 + 2d) \tag{4.11c}$$

In the context of MMT ensuring consistent power levels across all modes is essential. This standardization of power allows for accurate comparisons between modes. Consequently, a maximum average power of 1W is considered for each propagating mode within the MMT framework. To achieve this power normalization, a specific coefficient is calculated. This coefficient adjusts the average power to align with the given maximum wave amplitude, represented as $F_m^I = 1W$ and $B_m^I = 0$. By applying this coefficient, the average power across different modes can be made uniform, enabling effective comparisons within the MMT. So the normalization coefficient is expressed as

$$\psi_m^I = \sqrt{\frac{4\omega\mu_0}{a_1 h k_m^I}} \tag{4.12a}$$

Where, h represents the height of the dielectric substrate. Similarly, the backward wave in region II is subjected to the same normalization. In this case $B_m^I = 1W$ and $F_m^I = 0$. By considering these values, the normalization coefficients can be defined as

$$\psi_n^{II} = \sqrt{\frac{4\omega\mu_0}{a_2 h k_n^{II}}} \tag{4.12b}$$

The normalization coefficients for regions III and IV are defined in a similar manner as:

$$\psi_u^{III} = \sqrt{\frac{4\omega\mu_0}{a_3 h k_u^{III}}}\ , \psi_v^{IV} = \sqrt{\frac{4\omega\mu_0}{a_2 h k_v^{IV}}} \tag{4.12c}$$

By applying the orthogonality principle and matching the values of E_z and H_x across the entire discontinuity, the equations (4.2a), (4.2b), (4.3a), and (4.3b) can be solved using the relations (4.11b) and (4.11c). This process leads to the following relation.

$$E_y: \ F_n^{II} + B_n^{II} = \sum_{m=1}^{M} (L_E)_{n,m} [\, F_m^I + B_m^I] \tag{4.13a}$$

$$F_v^{IV} + B_v^{IV} = \sum_{u=1}^{U} (L'_E)_{v,u} [\, F_u^{III} + B_u^{III}] \tag{4.13b}$$

$$H_x: \ F_m^I - B_m^I = \sum_{n=1}^{N} (L_H)_{m,n} [\, F_n^{II} - B_n^{II}] \tag{4.13c}$$

$$F_u^{III} - B_u^{III} = \sum_{v=1}^{V} (L'_H)_{u,v} [\, F_v^I - B_v^I] \tag{4.13d}$$

Where, $$(L_E)_{n,m} = 2\sqrt{\frac{k_n^{II}}{a_2 a_1 k_m^I}} \int_d^{a_1+d} Sin\left[\frac{m\pi(x-d)}{a_1}\right] Sin\left[\frac{n\pi x}{a_2}\right] dx \tag{4.14a}$$

$$(L_H)_{m,n} = 2\sqrt{\frac{k_n^{II}}{a_2 a_1 k_m^I}} \int_d^{a_1+d} Sin\left[\frac{m\pi(x-d)}{a_1}\right] Sin\left[\frac{n\pi x}{a_2}\right] dx \tag{4.14b}$$

$$(L'_E)_{v,u} = 2\sqrt{\frac{k_v^{IV}}{a_2 a_3 k_u^{III}}} \int_{2d}^{a_1+2d} Sin\left[\frac{u\pi(x+d)}{a_3}\right] Sin\left[\frac{v\pi x}{a_2}\right] dx \tag{4.14c}$$

$$(L'_H)_{u,v} = 2\sqrt{\frac{k_v^{IV}}{a_2 a_3 k_u^{III}}} \int_{2d}^{a_1+2d} Sin\left[\frac{u\pi(x+d)}{a_3}\right] Sin\left[\frac{v\pi x}{a_2}\right] dx \tag{4.14d}$$

The equations (4.13a) and (4.13b) can be expressed as follows:

$$F_n^{II} + B_n^{II} = L_E [F_m^I + B_m^I] \tag{4.15a}$$

$$F_n^I - B_n^I = L_H [F_m^{II} - B_m^{II}] \tag{4.15b}$$

The functions L_E and L_H contain data that are obtained from the matching conditions of E_z and H_x respectively. These functions incorporate the necessary information derived from the matching process to accurately describe the behaviour of the electric field and magnetic field components.

The scattering matrix, which serves as a mathematical representation of the reflection and transmission properties, characterizes the behaviour of electromagnetic waves at the H-plane discontinuity between region I and region II. This matrix is expressed as: [50].

$$\begin{bmatrix} B^I \\ F^{II} \end{bmatrix} = \begin{bmatrix} S_{11}^I & S_{12}^I \\ S_{21}^I & S_{22}^I \end{bmatrix} \begin{bmatrix} F^I \\ B^{II} \end{bmatrix} \tag{4.16a}$$

$$B^I = S_{11}^I F^I + S_{12}^I B^{II} \tag{4.16b}$$

$$F^{II} = S_{21}^I F^I + S_{22}^I B^{II} \tag{4.16c}$$

The scattering parameters of the matrix (4.16a) are defined as the sub-matrices and can be expressed as [48].

$$S_{11}^I = [U + L_E L_H]^{-1}[U - L_E L_H] \tag{4.17a}$$

$$S_{12}^I = 2[U + L_E L_H]^{-1} L_H \tag{4.17b}$$

$$S_{21}^I = 2[U + L_E L_H]^{-1} L_E \tag{4.17c}$$

$$S_{22}^I = [U + L_E L_H]^{-1}[L_E L_H - U] \tag{4.17d}$$

Where U is defined as the unitary matrix

The H-plane discontinuity between region II and region III is represented by the scattering matrix as follows:

$$\begin{bmatrix} B^{IIL} \\ F^{III} \end{bmatrix} = \begin{bmatrix} S_{11}^{II} & S_{12}^{II} \\ S_{21}^{II} & S_{22}^{II} \end{bmatrix} \begin{bmatrix} F^{IIL} \\ B^{III} \end{bmatrix} \tag{4.18a}$$

$$B^{IIL} = S_{11}^{II} F^{IIL} + S_{12}^{II} B^{III} \tag{4.18b}$$

$$F^{III} = S_{21}^{II} F^{IIL} + S_{22}^{II} B^{III} \tag{4.18c}$$

$$F^{IIL} = Diag[e^{-jk_n^{II}L}] F^{II} \tag{4.18d}$$

$$B^{II} = Diag[e^{-jk_n^{II}L}] B^{IIL} \tag{4.18e}$$

The scattering parameters of the matrix (4.18a) are defined as the sub-matrices and can be expressed as:

$$S_{11}^{II} = [U + L_E L_H]^{-1}[U - L_E L_H] \tag{4.19a}$$

$$S_{12}^{II} = 2[U + L_E L_H]^{-1} L_H \tag{4.19b}$$

$$S_{21}^{II} = 2[U + L_E L_H]^{-1} L_E \tag{4.19c}$$

$$S_{22}^{II} = [U + L_E L_H]^{-1} [L_E L_H - U] \tag{4.19d}$$

The equation (4.20a) represents the specific form of the generalized scattering matrix for the H-plane discontinuity, which is obtained from the interaction between regions I and II. This matrix provides a mathematical description of how the incident wave is scattered and transmitted at the H-plane boundary, including the reflection coefficients, transmission coefficients.

$$\begin{bmatrix} B^I \\ F^{III} \end{bmatrix} = \begin{bmatrix} S_{11}^A & S_{12}^A \\ S_{21}^A & S_{22}^A \end{bmatrix} \begin{bmatrix} F^I \\ B^{III} \end{bmatrix} \tag{4.20a}$$

$$B^I = S_{11}^A F^I + S_{12}^A B^{III} \tag{4.20b}$$

$$F^{III} = S_{21}^A F^I + S_{22}^A B^{III} \tag{4.20c}$$

Where S^A represents the resulting scattering parameters.

By substituting equations (4.16b), (4.16c), (4.18b), and (4.17b) into equations (4.20b) and (4.20c), we obtain the scattering parameters as given by equation (4.20a). This process combines the relevant equations to derive the specific values that characterize the scattering behaviour described in equation (4.20a).

$$S_{11}^A = S_{11}^I + S_{11}^{II} S_{12}^I S_{21}^I e^{-j2k_n^{II} L} W \tag{4.21a}$$

$$S_{12}^A = S_{12}^I S_{12}^{II} e^{-jk_n^{II} L} W \tag{4.21b}$$

$$S_{21}^A = S_{21}^I S_{21}^{II} e^{-jk_n^{II} L} W \tag{4.21c}$$

$$S_{22}^A = S_{22}^{II} + S_{22}^I S_{12}^{II} S_{21}^{II} e^{-j2k_n^{II} L} W \tag{4.21d}$$

Where $$W = (U - S_{11}^{II} S_{22}^I e^{-j2k_n^{II} L})^{-1} \tag{4.21e}$$

The scattering matrix representing the H plane discontinuity between region III and region IV is derived from the scattering parameters of the third region, and it is expressed as:

$$\begin{bmatrix} B^{IIIL} \\ F^{IV} \end{bmatrix} = \begin{bmatrix} S_{11}^{III} & S_{12}^{III} \\ S_{21}^{III} & S_{22}^{III} \end{bmatrix} \begin{bmatrix} F^{IIIL} \\ B^{IV} \end{bmatrix} \quad (4.22a)$$

$$B^{IIIL} = S_{11}^{III} F^{IIIL} + S_{12}^{III} B^{IV} \quad (4.22b)$$

$$F^{IV} = S_{21}^{III} F^{IIIL} + S_{22}^{III} B^{IV} \quad (4.22c)$$

$$F^{IIIL} = Diag[e^{-jk_u^{III}L}] F^{III} \quad (4.22d)$$

$$B^{III} = Diag[e^{-jk_u^{III}L}] B^{IIIL} \quad (4.22a)$$

The scattering parameters of the matrix (4.22a) are defined as the sub-matrices and can be expressed as:

$$S_{11}^{III} = [U + L'_E L'_H]^{-1}[U - L'_E L'_H] \quad (4.23a)$$

$$S_{12}^{III} = 2[U + L'_E L'_H]^{-1} L'_H \quad (4.23b)$$

$$S_{21}^{III} = 2[U + L'_E L'_H]^{-1} L'_E \quad (4.23c)$$

$$S_{22}^{III} = [U + L'_E L'_H]^{-1}[L'_E L'_H - U] \quad (4.23d)$$

The combined scattering matrix encompassing the first three discontinuities is obtained by cascading the matrix from equation (4.20a) with equation (4.21e), resulting in the following matrix:

$$\begin{bmatrix} B^{I} \\ F^{IV} \end{bmatrix} = \begin{bmatrix} S_{11}^{B} & S_{12}^{B} \\ S_{21}^{B} & S_{22}^{B} \end{bmatrix} \begin{bmatrix} F^{I} \\ B^{IV} \end{bmatrix} \quad (4.24a)$$

Where S^B indicates the resulting scattering parameters.

$$S_{11}^{B} = S_{11}^{A} + S_{11}^{III} S_{12}^{A} S_{21}^{A} e^{-j2k_u^{III}L} W' \quad (4.24b)$$

$$S_{11}^{B} = S_{11}^{A} + S_{11}^{III} S_{12}^{A} S_{21}^{A} e^{-j2k_u^{III}L} W' \quad (4.24c)$$

$$S_{21}^{B} = S_{21}^{A} S_{21}^{III} e^{-jk_u^{III}L} W' \quad (4.24d)$$

$$S_{22}^{B} = S_{22}^{III} + S_{22}^{A} S_{12}^{III} S_{21}^{III} e^{-j2k_u^{III}L} W' \quad (4.24e)$$

$$W' = (U - S_{11}^{III} S_{22}^{A} e^{-j2k_u^{III}L})^{-1} \quad (4.24f)$$

The expression for the scattering matrix of the entire cascaded H-plane discontinuity is as follows:

$$\begin{bmatrix} B^I \\ F^V \end{bmatrix} = \begin{bmatrix} S_{11} & S_{12} \\ S_{21} & S_{22} \end{bmatrix} \begin{bmatrix} F^I \\ B^V \end{bmatrix} \tag{4.25a}$$

$$B^I = S_{11}F^I + S_{12}B^V \tag{4.25b}$$

$$F^V = S_{21}F^I + S_{22}B^V \tag{4.25c}$$

The scattering parameters of the matrix (4.25a) is derived as:

$$S_{11} = S_{11}^B + S_{11}^{IV}S_{12}^B S_{21}^B e^{-j2k_v^{IV}L}W'' \tag{4.26a}$$

$$S_{12} = S_{12}^B S_{12}^{IV} e^{-jk_v^{IV}L}W'' \tag{4.26b}$$

$$S_{21} = S_{21}^B S_{21}^{IV} e^{-jk_v^{IV}L}W'' \tag{4.26c}$$

$$S_{22} = S_{22}^{IV} + S_{22}^B S_{12}^{IV} S_{21}^{IV} e^{-j2k_v^{IV}L}W'' \tag{4.27d}$$

Where $$W'' = (U - S_{11}^{IV}S_{22}^B e^{-j2k_v^{IV}L})^{-1} \tag{4.28e}$$

By substituting equations (4.24b), (4.24c), (4.24d), and (4.24e) into equations (4.26a), (4.26b), (4.26c), and (4.26e), we obtain the resulting equations.

$$S_{11} = (S_{11}^A + S_{11}^{III}S_{12}^A S_{21}^A e^{-j2k_u^{III}L}W') +$$
$$S_{11}^{IV}(S_{12}^A S_{12}^{III} e^{-jk_u^{III}L}W')(S_{21}^A S_{21}^{III} e^{-jk_u^{III}L}W')e^{-j2k_v^{IV}L}W'' \tag{4.27a}$$

$$S_{12} = S_{12}^A S_{12}^{III} e^{-jk_u^{III}L}W' S_{12}^{IV} e^{-jk_v^{IV}L}W'' \tag{4.27b}$$

$$S_{21} = S_{21}^A S_{21}^{III} e^{-jk_u^{III}L}W' S_{21}^{IV} e^{-jk_v^{IV}L}W'' \tag{4.27c}$$

$$S_{22} = S_{22}^{IV} + (S_{22}^{III} + S_{22}^A S_{12}^{III} S_{21}^{III} e^{-j2k_u^{III}L}W')S_{12}^{IV} S_{21}^{IV} e^{-j2k_v^{IV}L}W'' \tag{4.27d}$$

The equations (4.21a) to (4.21d) are inserted into equations (4.27a) to (4.27d), resulting in the final scattering parameters of the designed stepped SIW.

$$S_{11} = S_{11}^I + S_{11}^{II}S_{12}^I S_{21}^I e^{-j2k_n^{II}L}W +$$
$$S_{11}^{III}S_{12}^I S_{12}^{II} S_{21}^I S_{21}^{II} e^{-j2(k_n^{II}+k_u^{III})L}W^2W' +$$
$$S_{11}^{IV}S_{12}^I S_{12}^{II} S_{12}^{III} S_{21}^I S_{21}^{II} S_{21}^{III} e^{-j2(k_n^{II}+k_u^{III}+k_v^{IV})L}W^2W'^2W'' \tag{4.28a}$$

$$S_{12} = S_{12}^{I} S_{12}^{II} S_{12}^{III} S_{12}^{IV} e^{-j(k_n^{II}+k_u^{III}+k_v^{IV})L} WW'W'' \quad (4.28b)$$

$$S_{21} = S_{21}^{I} S_{21}^{II} e^{-jk_n^{II}L} W S_{21}^{III} e^{-jk_u^{III}L} W' S_{21}^{IV} e^{-jk_v^{IV}L} W'' \quad (4.28c)$$

$$S_{22} = S_{22}^{IV} + S_{22}^{III} S_{12}^{IV} S_{21}^{IV} W'' + S_{22}^{II} S_{12}^{III} S_{21}^{III} S_{12}^{IV} S_{21}^{IV} e^{-j2(k_u^{III}+k_v^{IV})L} W'W'' + S_{22}^{I} S_{12}^{II} S_{21}^{II} S_{12}^{III} S_{21}^{III} S_{12}^{IV} S_{21}^{IV} e^{-j2(k_n^{II}+k_u^{III}+k_v^{IV})L} WW'W'' \quad (4.29c)$$

So, Return Loss $S_{11}(dB) = -20\log|S_{11}|$ and Transmission Loss $S_{12}(dB) = -20\log|S_{12}|$

(4.30)

By solving the equations using the specified design parameters, we obtain the analytical results depicted in Figs. 4.4 and 4.5.

4.3 Stepped SIW Result Analysis

The MMT of the proposed stepped SIW with a step height of 1.82 mm and a linearly tapered microstrip transition has been carried out as described earlier. The stepped SIW prototype has been fabricated and subjected to measurements. The fabricated stepped SIW, with a step size of 1.82mm, is shown in Fig.4.3.

(a) (b)

Figure 4.3.Fabricated stepped SIW (a) Top view (b) Back view

To validate the preceding analysis, the obtained reflection coefficient $S_{11}(dB)$ and transmission coefficient $S_{12}(dB)$ are compared with the simulated results from HFSS and

CST-MWS, as well as the measured coefficients. The MMT is applied to analyze the four propagating modes: TE_{10}, TE_{20}, TE_{30}, and TE_{40} of the proposed stepped substrate integrated waveguide (SIW). Fig. 4.4 illustrates the frequency response curve of the transmission coefficient $S_{12}(dB)$ for the proposed stepped SIW.

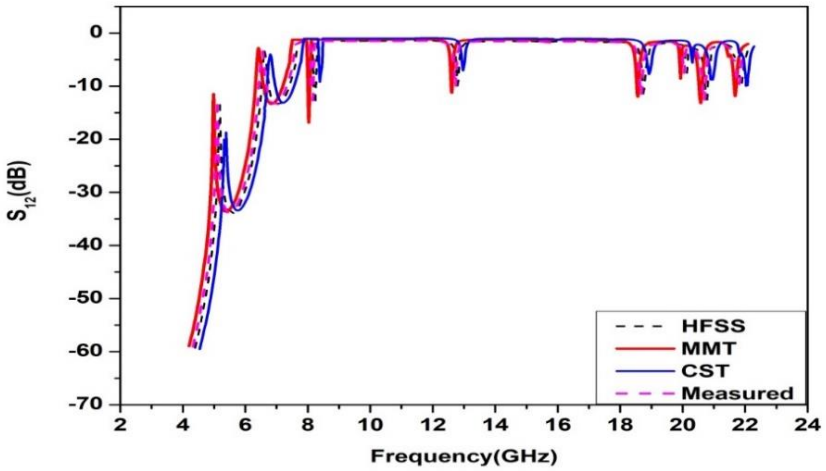

Figure 4.4 $S_{12}(dB)$ vs. frequency curves (d=1.82)

Fig. 4.5 presents the frequency response curve of the reflection coefficient $S_{11}(dB)$ for the proposed stepped SIW.

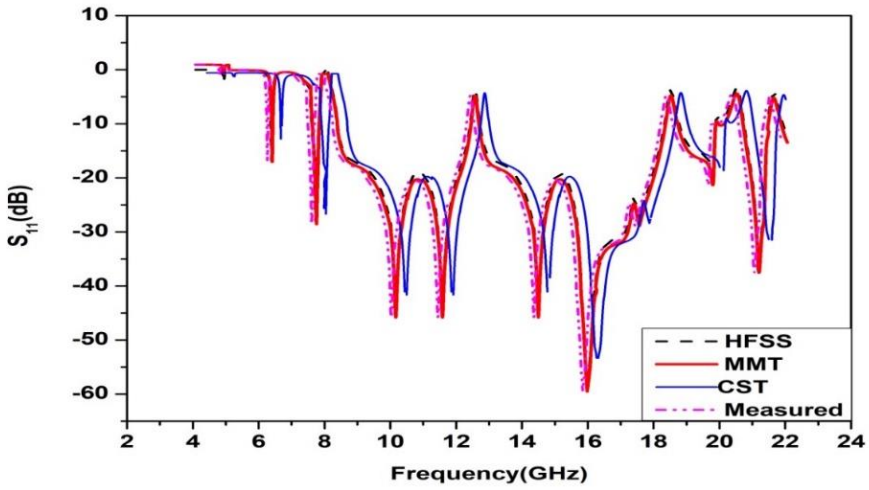

Figure. 4.5 $S_{11}(dB)$ Vs frequency curves (d=1.82)

The comparison of S-parameters obtained from the mode-matching technique (MMT) with those obtained from HFSS, CST-MWS, and measurements reveals a close agreement. The simulations were conducted on a machine equipped with an I3 CPU @ 2.00 GHz and 8 GB RAM. The MMT solution was implemented using MATLAB. Table 4.2 showcases the processor computational time in seconds, while

Table 4.2 Processor computational time (in sec.) of the stepped SIW

HFSS		**CST-MWS**		**MMT**
Meshing	**Frequency Point**	**Meshing**	**Frequency Point**	
468	175	450	163	17

Table 4.3 displays the comparison of memory usage in megabytes (MB).

Table 4.3. Memory used (in MB) in the proposed SIW

HFSS		**CST-MWS**		**MMT**
Meshing	**Frequency Point**	**Meshing**	**Frequency Point**	
1716	1658	1689	1651	320

The tables presented above demonstrate the high efficiency of the proposed analysis technique in terms of computational time and memory requirements. Additionally, its mesh-free nature makes it valuable for design optimization processes involving changes in geometric parameters. The findings depicted in Figures 4.4 and 4.5 demonstrate that the designed stepped SIW exhibits the characteristics of a band-pass filter, which can be attributed to its periodic design.

4.4 Conclusion

In this chapter, we have designed and fabricated a stepped SIW. The scattering parameters have been evaluated using a mode matching analysis. Comparative analysis reveals that the mode matching technique employed in this study outperforms the HFSS finite element method and CST-MWS finite integration method in terms of processor computation time, memory usage, as well as reflection and transmission characteristics. The band-pass filter characteristics exhibited by the designed stepped SIW make it well-suited for applications in

the X-band, Ku-band, and K-band. Additionally, the propagation curve indicates that the designed periodic SIW functions as a fast wave structure, making it suitable for the design of leaky wave antennas.

CHAPTER 5

Sinusoidally Modulated Substrate Integrated Folded Waveguide as a Filter

This chapter presents an in-depth analysis of the wave propagation properties of electromagnetic (EM) waves within a sinusoidally modulated substrate integrated folded waveguide (SMSIFW).The SMSIFW is a periodic structure with a varying width along its length, offering unique filter properties. This study aims to examine the electromagnetic (EM) field components, dispersion characteristics, and filter performance of the SMSIFW. The chapter starts by introducing the SMSIFW and its significance in waveguide engineering. The sinusoidal modulation of the waveguide's width modulation is discussed, highlighting its influence on EM wave propagation. The variational analysis technique is utilized to determine the propagation constant. Through theoretical derivations and simulations, the electromagnetic field properties and dispersion characteristics of the SMSIFW are analyzed. The results reveal the filter properties of the structure, which enable selective frequency transmission or rejection. The investigation focuses on two specific values of modulation indices to examine their impact on the filter performance. The results presented in this chapter enhance our comprehension of the potential applications of the SMSIFW in waveguide filters, signal processing, and communication systems. The theoretical analysis and simulation outcomes offer valuable insights into the electromagnetic wave propagation characteristics within the SMSIFW.

5.1 Introduction

In the past few years, there has been increasing interest in studying the behaviour of EM waves in periodic structures. Significant research has been conducted to understand the effects of these structures on EM wave propagation, and relevant early studies can be found in [81].The investigation of periodic effects on EM wave propagation has been comprehensive, demonstrating their potential applications in various EM devices. Periodic structures, which can be constructed using dielectric or conducting materials, exhibit a wide range of dimensional possibilities, including one, two, or three dimensions [38, 39]. The

inclusion of distributed loading allows for the alteration of the electromagnetic characteristics of a transmission line, leading to the achievement of periodicity. As an example, one can modify a traditional RWG by introducing a dielectric material with a variable permittivity. This modification leads to EM wave propagation within the waveguide that displays characteristics like to those of sinusoidally varying reactive walls.

The use of SIW has become increasingly popular in microwave and millimeter-wave circuits, with a wide range of applications, from filters to antennas. SIW is a structure similar to a planar RWG that incorporates dielectric material. It is characterized by metallic vias on its vertical side walls, while the horizontal walls are formed by the ground planes. This design offers numerous benefits, such as a high Q factor, minimal losses, cost-effectiveness, and efficient heat dissipation through the vias, enabling a high power handling capacity. Additionally, SIW allows for seamless integration of both active and passive components.

Nevertheless, when compared to other printed transmission lines like strip lines and microstrip lines, SIW components tend to possess wider widths, especially at lower frequencies. As a result, it becomes crucial to address the need for width reduction in SIW structures. Researchers, as exemplified in studies conducted by Che et al. [57] and Trong et al. [58], have extensively investigated SIFW. This involves the process of deriving equations to assist in calculating key parameters such as the propagation constant, cut-off frequency, and the central metal vane gap from the rows of vias. Additionally, variational analysis has been employed to explore the intricacies of SIW behavior. The need for compact, wide-frequency range, low signal loss and highly selective filters remains significant in recent microwave and millimeter wave systems. As a result, multiband filters have been developed to operate across multiple pass bands, reducing the overall module requirements [38]. Several studies in the field have explored the use of SIW technology for multiband filters [59-61, 82-84]. For instance, Guo et al. [59] introduced a design for SIW-based multiband band-pass filters by combining single-band/dual-band synthesis methods with multimode resonator theory, allowing for the generation of multiple filtering pass bands. Jankovic et al. [82] built multiple-mode resonators for a multiband filter using Hilbert fork resonators. Iqbal et al. [83] used two capacitively connected quarter-wavelength SIW cavities to create SIW filters for single and tri-band operations. S. Kumari et al. [60] concentrated on a slot-loaded SIFW filter for lower-frequency applications. S. Pelluri et al. [84] suggested band-pass filter with triple

band and based on a multi-mode HMSIW cavity, to establish the initial passband of the filter, a paired configuration of half-mode Defected Ground Structures (DGS) was utilized. This arrangement was instrumental in attaining the desired filter characteristics. Martinez Wt. et al. [61] designed a periodic structure-based band-pass filter utilizing SIW. Additionally, Kumar et al. [85] presented a sinusoidally modulated SIW (SMSIW) and analyzed it, which served as the foundation for the proposed SMSIFW.

In this chapter, we explore the creation and examination of a compact SMSIFW, which is a modified version of the SMSIW [85]. By comparing the phase constant curves of SMSIW and SMSIFW, we observe similar behaviour at a specific gap width. To better understand the proposed SMSIFW, we employ variational analysis, which reveals its capability to support multiple frequency bands within the millimeter wave range, making it a versatile solution. Given the ever-increasing demand for space-efficient and high-performance signal transmission in modern wireless systems, the significance of the SMSIFW becomes even more pronounced.

5.2 SMSIFW Design and Wave Equation

Fig. 5.1 provides an isometric view of both the SMSIW and SMSIFW within a cartesian coordinate system. The SMSIFW structure is obtained by transversely folding the SMSIW while incorporating a central metal vane within the *H*-plane configuration. The SMSIW [85] and the newly suggested SMSIFW are both built on dielectric substrates with a thickness of 0.762 mm and a relative permittivity of 3.48.

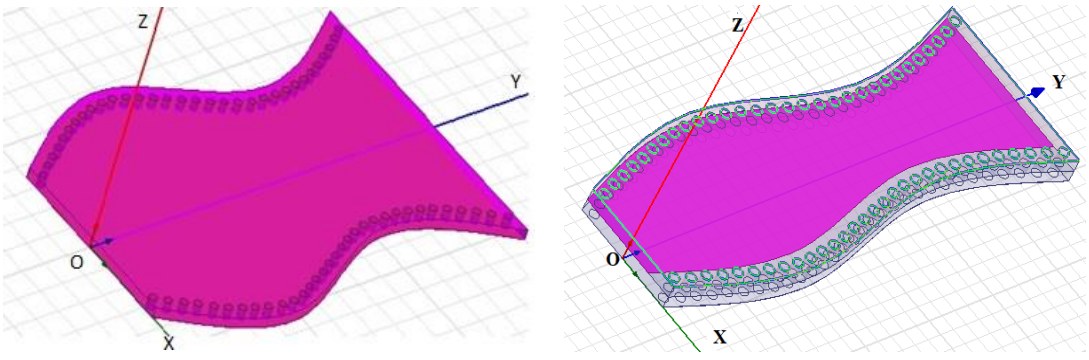

(a) (b)

Figure 5.1 Isometric View of (a) SMSIW (b) SMSIFW

Conducting vias with a diameter of 0.61 mm are employed in the design, and they are arranged at a separation of 0.91 mm. The dimensions of the vias are specifically selected to minimize the emission of radiation between them. The periodic sinusoidal wave present in the design possesses a wavelength (λ) of 20 mm, and the overall length of the waveguide is 1.5 times the wavelength (1.5λ). In order to calculate the modulation index under these circumstances, the following formula is utilized.

$$\mu = \frac{W_{max} - W_{min}}{W_{max} + W_{min}} \tag{5.1}$$

The terms W_{max} and W_{min} represent the maximum and minimum widths of the SMSIFW, respectively. The SMSIFW design introduced in this proposal achieves a compact cross-section area by reducing the width by half and increasing the height by double when compared to the SMSIW. Both the proposed SMSIFW and the SMSIW exhibit a modulation index of 0.25. The central partial H-plane metal vane undergoes sinusoidal modulation along the axial direction, applying the same modulation index to it. In Fig.5.1 (a) and (b), point 'O' is regarded as the reference point. The table 5.1 provides the specifications of the geometric properties for both the SMSIW and SMSIFW.

Table 5.1 Specification of geometric parameters of SMSIW and SMSIFW

Type	Wmax(mm)	Wmin(mm)	Modulation Index (μ)	Length (mm)	Height (mm)
SMSIW	20	12.1	0.25	30	0.762
SMSIFW	10	6.05	0.25	30	1.524

The Y-axis represents the wave propagation direction, while the X-axis. The X-axis captures the diversity in width, accounting for its variation, In the SMSIFW structure, the metallic vias, which undergo modulation, align with and adapt to one of the curved planar surfaces within a newly defined orthogonal coordinate system. This alignment ensures that the metallic vias conform to the specific curved surface, facilitating efficient wave propagation and manipulation within the SMSIFW. The coordinates within this newly defined coordinate system are denoted as (u_1, u_2, u_3) to indicate their corresponding values. Assuming uniform width, the average width is denoted as $\bar{u}_1$, and the corresponding x-coordinate is represented as [85].

$$\bar{x} = \bar{u}_1[1 + \mu f(2\pi y/p)] \tag{5.2}$$

Where μ represent the modulation index, and its range is $0 < \mu < 1$, and the function $f\left(\frac{2\pi y}{p}\right)$ demonstrates periodicity with a period p. To facilitate the analysis of the SMSIFW, it is divided into two distinct regions: one situated above the metal vane and another below it. Fig. 5.2 showcases the frontal perspective of the proposed SMSIFW, where the average width is represented as $\bar{x}$.

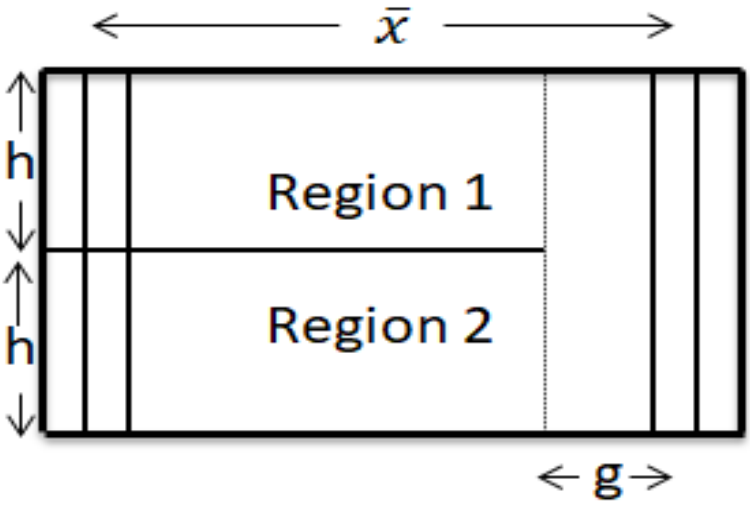

Figure 5.2 Frontal perspective of the proposed SMSIFW

The field components in both specified regions are obtained through the utilization of Hill's equations. Hill's equations are of significant importance in the study of periodic microwave systems [85]. These equations help describe the behavior and dynamics of electromagnetic fields within such systems. By solving Hill's equations, one can gain insights into the periodic variations, resonances, and stability properties of microwave fields. Understanding Hill's equations is essential for analyzing and designing periodic microwave structures, such as filters, resonators, and waveguides, to achieve desired performance characteristics and efficient signal transmission. The derived field components significantly contribute to determining the dispersion curve of the system. The derived field components in region 1 are as follows:

$$E_x^1 = E_y^1 = 0 \tag{5.3a}$$

$$E_z^1 = -j\omega\mu Cos(K_1 u_1) U_2 \tag{5.3b}$$

$$H_x^1 = Cos(K_1u_1)\frac{dU_2}{du_2} + \frac{\frac{2\pi}{p}u_1\mu f'\left(\frac{2\pi u_2}{p}\right)K_1}{1+\mu f\left(\frac{2\pi u_2}{p}\right)}Sin(K_1u_1)U_2 \quad (5.3c)$$

$$H_y^1 = \frac{K_1Sin(K_1\,u_1)U_2}{1+\mu f\left(\frac{2\pi u_2}{p}\right)} - \frac{2\pi}{p}u_1\mu f'\left(\frac{2\pi u_2}{p}\right)K_1\,Cos(K_1u_1)\frac{dU_2}{du_2} \quad (5.3d)$$

$$H_z^1 = 0 \quad (5.3e)$$

The field components within region 2 can be represented as

$$E_x^2 = E_y^2 = 0 \quad (5.4a)$$

$$E_z^2 = -j\omega\mu Cos(K_2u_1)U_2 \quad (5.4b)$$

$$H_x^2 = Cos(K_2u_1)\frac{dU_2}{du_2} + \frac{\frac{2\pi}{p}u_1\mu f'\left(\frac{2\pi u_2}{p}\right)K_2}{1+\mu f\left(\frac{2\pi u_2}{p}\right)}Sin(K_2u_1)U_2 \quad (5.4c)$$

$$H_y^2 = \frac{K_1Sin(K_1\,u_1)U_2}{1+\mu f\left(\frac{2\pi u_2}{p}\right)} - \frac{2\pi}{p}u_1\mu f'\left(\frac{2\pi u_2}{p}\right)K_2\,Cos(K_2u_1)\frac{dU_2}{du_2} \quad (5.4d)$$

$$H_z^2 = 0 \quad (5.4e)$$

The equations (5.3) and (5.4) represent the field components, with the superscript letters denoting the respective regions. The separation constants, K_1 and K_2 are obtained through the application of the boundary conditions and correspond to regions 1 and 2, respectively. Furthermore, the functions U_2 depend on the u_2 coordinates. The equation representing the propagation constant in a stationary state is derived based on the explanation given in reference [58].

$$\psi(\gamma) = \int_0^g \left(H_y^1 - H_y^2\right) du_2 = 0 \quad (5.5)$$

In the context of the proposed SMSIFW, the parameter g represents the width of the gap. Given the compact size of the gap in the suggested SMSIFW, it is presumed that the absolute value of the electric field component $|E_Z|$ is approximately equal to 1.This assumption is made based on the concept of the magnetic current, which is defined using the principle of field equivalence [85, 86].

$$\vec{M} = \vec{E}X\hat{N} \quad (5.6)$$

It is important to emphasize that in regions 1 and 2, the magnetic currents exhibit opposite directions, while the magnitudes of the magnetic field remain constant. By considering this

condition, the determination of the propagation constant can be achieved by solving equation (5.7).

$$\int_0^g \left(H_y^1\right) du_2 = 0 \tag{5.7}$$

The equation (5.7) is solved to obtain the closed-form solution for the propagation constant. In this context, H_y^1 is defined as per equation (5.3d).

$$\int_0^g \left(H_y^1\right) du_2 = \frac{j}{\omega\mu}\left[\frac{g^2}{\bar{x}}\cot(C_0 h) + 2\sum_{n=1}^{\infty} sin^2\frac{n\pi g}{\bar{x}}\cot\left\{(C_0 h)\left(\frac{ln\bar{x}}{n^2\pi^2} + \frac{1}{C_0\bar{x}}\right)\right\}\right] \tag{5.8}$$

Here, $C_0 = \sqrt{\varepsilon_r k^2 + \gamma^2 - \left(\frac{n\pi}{\bar{x}}\right)^2}$, $k = \frac{\omega}{c}$ with ω representing the angular frequency and c denoting the velocity of the electromagnetic wave in vacuum. By utilizing iterative methods, the equation (5.7) is solved to find the root(s) of the equation.

$$\gamma_0 = \sqrt{\left(\frac{\pi}{2\bar{x}}\right)^2 - \varepsilon_r k^2} \tag{5.9}$$

To validate the analysis, dispersion curves have been generated for three different gap widths ($g = 1mm$,$0.8\,mm$ and $1.2\,mm$). ultimately, when the gap size was set to 1 mm, the proposed folded SIW (SMSIFW) demonstrated a remarkably similar dispersion pattern to its unfolded counterpart, the SMSIW. These findings highlight the consistency between the dispersion curves obtained from simulations using HFSS, a finite element method-based electromagnetic simulator, and the analytical results. Figure 5.3 illustrates the dispersion curves, allowing for a visual comparison between the proposed SMSIFW and SMSIW.

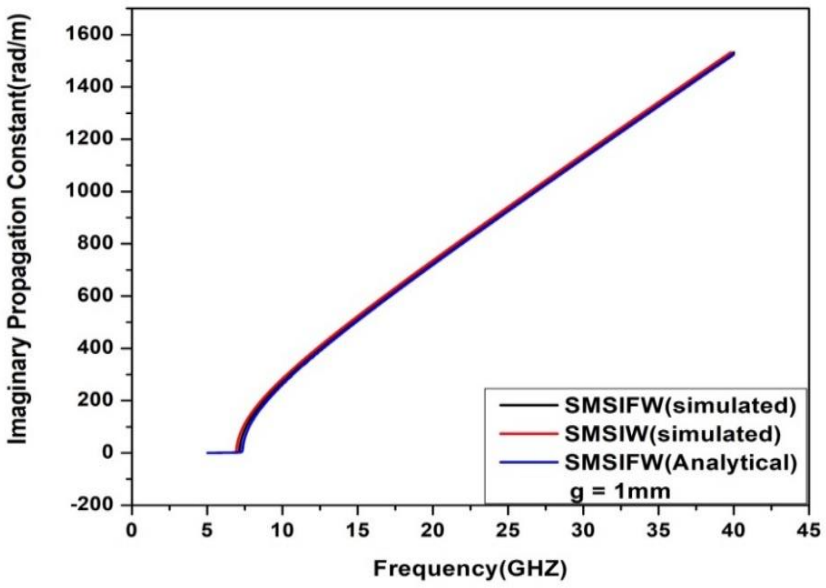
Imaginary Propagation Constant(rad/m)
1600
1400
1200
1000
800
600
400
200
0
-200
0
5
10
15
20
25
30
35
40
45
Frequency(GHZ)
SMSIFW(simulated)
SMSIW(simulated)
SMSIFW(Analytical)
g = 1mm

(a)

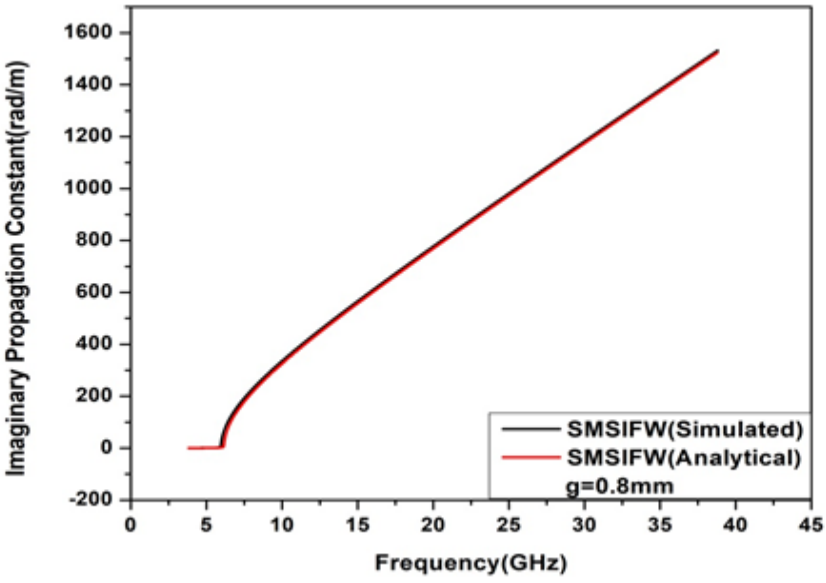
Imaginary Propagtion Constant(rad/m)
1600
1400
1200
1000
800
600
400
200
0
-200
0
5
10
15
20
25
30
35
40
45
Frequency(GHz)
SMSIFW(Simulated)
SMSIFW(Analytical)
g=0.8mm

(b)

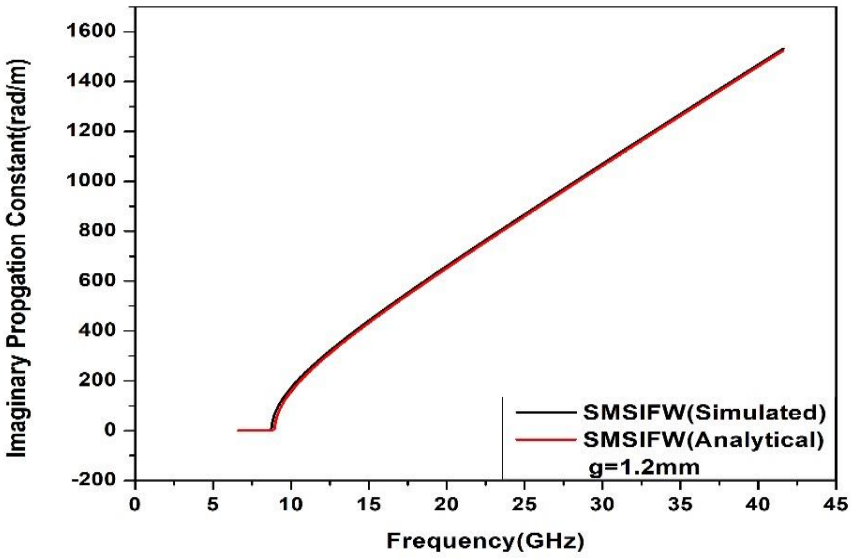

(c)

Figure 5.3 Dispersion curves of SMSIFW for various values of gap width (g) (a) $g = 1mm$ (b) $g = 0.8\ mm$, and (c) $g = 1.2\ mm$

Based on the dispersion curve analysis, it is observed that the cut-off frequency of SMSIW obtained through simulation, and the cut-off frequency of SMSIFW obtained through simulation and analysis are nearly identical. Additionally, the dispersion curves of SMSIW and SMSIFW exhibit a high degree of similarity. The imaginary propagation constant of SMSIFW is influenced by both the gap width and the modulation index. To assess the performance of the proposed SMSIFW, the S-parameters are analyzed at modulation index values of 0.25 and 0.15, and these results are depicted in Fig. 5.4.

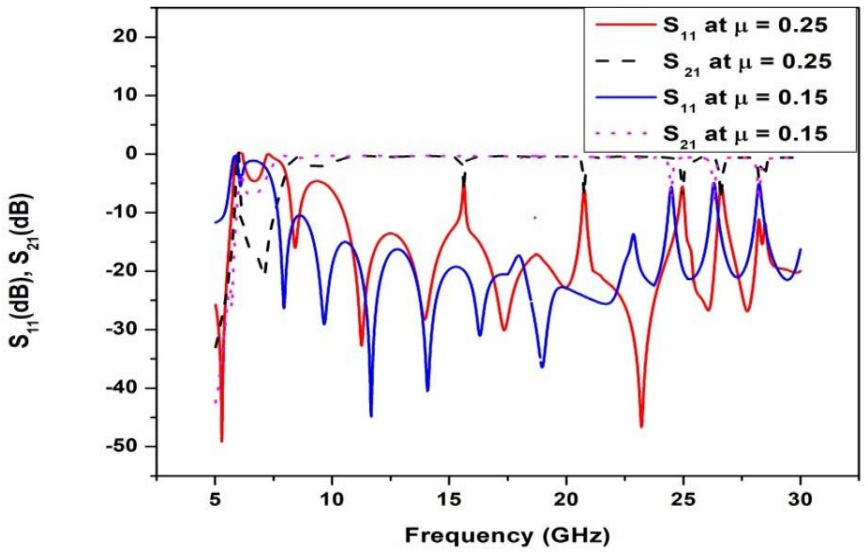

Figure 5.4 Frequency response of S_{11} and S_{21} for different modulation indices

The provided curve illustrates the relationship between the bandwidth and the modulation index. When the modulation index is set to 0.25, the initial transmission band occurs within the frequency range of 10.5 GHz to 15.4 GHz, followed by the subsequent transmission band from 15.8 GHz to 20.5 GHz, and the successive transmission band from 20.8 GHz to 24.6 GHz. Similarly, for a modulation index of 0.15, the primary transmission band extends from 7.5 GHz to 24 GHz, followed by the following transmission band from 24.5 GHz to 26.5 GHz, and the subsequent transmission band from 27 GHz to 28 GHz. By adjusting the modulation index, bandwidth tuning can be achieved.

5.3 Conclusion

In conclusion, this chapter has focused on the design and simulation of an SMSIFW. The modulation index and the gap width have been identified as key parameters for filtering performance. These parameters play a crucial role in determining the characteristics and functionality of the SMSIFW structure. By controlling and optimizing the modulation index and gap width, the desired filtering properties can be achieved. The analysis and investigation of these parameters contribute to advancing our understanding of the SMSIFW design and its potential applications in various filtering applications. Furthermore, through variational analysis, we have explored the propagation characteristics of the SMSIFW. The proposed

SMSIFW has exhibited comparable dispersion characteristics to the SMSIW, particularly when the gap width is set to 1 mm. The multi-passband filter capabilities of the SMSIFW hold significant potential for various applications in IOT sensors, as well as in future millimeter-wave systems. Moreover, the demonstrated support for fast wave propagation, as depicted in Fig. 5.3, indicates potential advantages in the design of leaky wave antennas.

CHAPTER 6

Cavity-Backed Slot Loaded SIW Self-Diplexing Antenna

In this chapter, a unique antenna design for self-diplexing mechanism is introduced, which utilizes a SIW loaded with a slot in the upper ground plane and backed by a cavity. The antenna configuration includes a rectangular slot located behind an SIW cavity, enabling resonance at two distinct frequencies. It employs two inset microstrip lines feed that are offset from each other for independent feeding at each frequency. The investigation encompasses key parameters such as reflection coefficient, total gain, antenna radiation efficiency, and 2D radiation patterns in both the E-plane and H-plane. The antenna exhibits resonances at two frequencies: 6.5 GHz and 7 GHz. In the broadside direction, it provides gains of 4.8 dBi at 6.5 GHz and 6.4 dBi at 7 GHz. The outstanding feature of the design being referred to is its ability to achieve an isolation of over 30 dB. This level of isolation is vital to ensure successful diplexing. The chapter highlights the antenna's potential for applications requiring simultaneous transmission and reception at different frequencies, offering a robust dual-frequency solution with efficient isolation. The utilization of dual feed and a slot created in the upper conducting plane endows the proposed antenna with leaky wave self-diplexing capabilities.

6.1 Introduction

The ongoing advancements in wireless communication systems are driving a surge in the demand for compact, economical, and high-performing planar dual-band antennas [51]. To cater to the needs of wireless handheld devices, integrated receiver systems with wireless antennas, and communication systems with distinct uplink and downlink channels, the significance of dual-band antennas with exceptional isolation cannot be overstated [52, 87]. These antennas play a vital role in ensuring efficient signal transmission and reception by providing strong isolation between the uplink and downlink channels. Moreover, their compact size and affordability make them highly desirable for various applications. The continuous development of low-profile, cost-effective, and high-performance planar dual-

band antennas is essential to keep pace with the evolving wireless communication landscape and meet the diverse requirements of wireless devices and systems. Recently, there has been significant attention towards the design of self-diplexing antennas, mainly due to their capability of eliminating the need for complex diplexers with higher order functionality. In addition to cost reduction and enhancing the efficiency of radio frequency front-end systems, this approach also decreases the number of components required [51, 52]. Self-diplexing antennas provide numerous benefits, such as unidirectional radiation patterns, cost-effectiveness, minimized signal losses, and simplified mode excitation. The presence of self-diplexing antennas is also recognized in the literature [52, 53, 87-89, 91].For example, in reference [52], a circular-shaped printed antenna with high isolation and orthogonal polarization. This design incorporates a dielectric substrate with a high permittivity. In references [87] and [88], an advanced microstrip patch antenna with multiple layers is developed, integrating additional filtering techniques to enhance isolation. The SIW has also gained prominence as a favoured option for self-diplexing antenna design [89, 90]. Furthermore, non-planar structures have been explored for self-diplexing antennas in references [89] and [90]. Additionally, reference [91] presents a design where T-shaped stubs are used to load the microstrip patch. The SIW is a modified variant of the traditional rectangular waveguide, where the upper and lower part of the substrate are enveloped with metal cladding, forming the top and bottom walls correspondingly. The sidewalls of the SIW structure are vertically defined using conductive vias. SIW technology offers the advantage of integrating active elements, passive components, and various devices onto a single substrate, making it well-suited for the construction of diverse wireless systems [72, 85].

Numerous slotted cavity backed SIW antennas with unidirectional radiation pattern have been reported [54, 55]. Moreover, the literature describes high-gain dual-band antennas based on SIW technology, which incorporate cavities and slots [54, 92, 93]. In RF front-end transceiver systems, these antennas are often accompanied by diplexing circuits that are commonly employed in the transmitter and receiver sections.

Within this chapter, we present a unique antenna design that combines a cavity-backed structure with slot loading in SIW configuration. The proposed antenna utilizes inset microstrip line feeding techniques to achieve exceptional isolation between the feed lines. To ensure strong isolation, offset feed lines are employed, resulting in the generation of two

resonant modes within the SIW cavities. By incorporating slot loading in the upper ground plane, the antenna operates as a leaky wave antenna, providing enhanced performance and radiation characteristics. This leaky wave operation is made possible through the combination of the dual feed lines and slot loading technique. Furthermore, the integration of the cavity structure within the SIW design not only contributes to achieving high antenna gain but also ensures the structural planarity is maintained. The distinctive combination of features in the proposed antenna renders it highly suitable for wireless communication systems operating within the C-band spectrum. It demonstrates compatibility with sub-6 GHz and 5G wireless communication technologies, which are increasingly prevalent in modern networks. Additionally, the antenna's performance extends to the sub-7 GHz spectrum, catering to satellite communication applications involving uplink and downlink frequencies [54, 92, 93].

6.2 Antenna Configuration

The proposed SIW antenna design utilizes an RT duroid 5880 dielectric substrate with a thickness of 0.787 mm. This substrate has a relative permittivity of 2.2 and a loss tangent of 0.004. The proposed antenna's geometrical arrangements are depicted in Fig. 6.1, illustrating the presence of two feed line ports designated as F_1 and F_2. These feed lines are positioned in an orthogonal manner and are deliberately offset from each other.

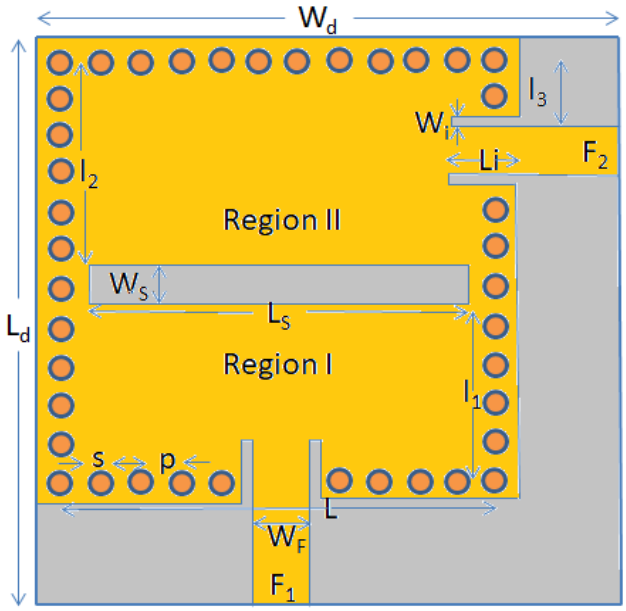

Figure 6.1 Geometrical configuration of the antenna

The physical antenna parameters are shown in Table 6.1.

Table 6.1 Physical parameters of the proposed antenna

Parameters	L_d	W_d	**L**	**Li**	l_1	l_2	l_3	L_S	W_S	W_F	**s**	**p**	W_i
In mm.	29	29	22	3	9	11	3.3	20	2	2.33	1	2	0.5

The cavity resonator is ingeniously designed in a square shape, utilizing four rows of conductive vias that serve as the conducting walls of the SIW. Two inset feed microstrip lines, configured in an offset arrangement, exhibit a characteristic impedance of 50 Ω each. On the top ground surface, a rectangular slot is introduced, effectively dividing it into two uneven radiating apertures, commonly referred to as region I and region II. These apertures are responsible for radiating at two distinct resonating frequencies. The resonating frequencies depend on the lengths of region I (l_1) and region II (l_2), as well as the slot length (L_S).In order to minimize energy leakage between the conductive vias, the pitch (p) and diameter (s) must be carefully selected. It is crucial that $\frac{s}{\lambda}$ is less than or equal to 1/10, and $\frac{P}{s}$is less than 2, with λ denoting the operating wavelength [94]. By adhering to these considerations the antenna's performance is optimized. The size specifications of the SIW cavity resonator are determined to be $0.52\ \lambda_g\ X\ 0.52\ \lambda_g$, where λ_g represents the guided wavelength.

6.3 Results and Discussions

The newly developed SIW antenna underwent meticulous design and simulation using HFSS, an electromagnetic solver that employs the finite element method for analyzing electromagnetic structures. The antenna comprises two radiating regions, I and II, with deliberately different dimensions, resulting in the generation of distinct resonating modes within the cavity, each accompanied by its unique perturbed fields. When feed line F_1 is excited, region I, with its shorter length, exhibits resonance at a higher frequency of 7 GHz. Notably, this resonance does not compromise the impedance matching for feed line F_2, which remains at 50 Ω. Similarly, when feed line F_2 is excited, region II, with its longer length, resonates at a lower frequency of 6.5 GHz. During this resonance, feed line F_1 maintains a matched 50 Ω impedance. This detailed explanation offers a comprehensive comprehension

of the functioning of the radiation mechanism. Fig. 6.2 (a) presents the distribution of surface current at 7 GHz, illustrating the prevalence of surface current in region I when feed line F_1 is activated. The maximum surface current occurs at the lower edge of the slot, while region II remains insignificantly affected. In Fig. 6.2 (b), the depiction of surface current distribution at 6.5 GHz showcases the dominance of region II when feed line F_2 is activated, with the peak surface current observed at the upper edge of the slot while region I remains negligibly influenced. These visual representations provide valuable insights into the behaviour of the antenna's surface current at different resonating frequencies.

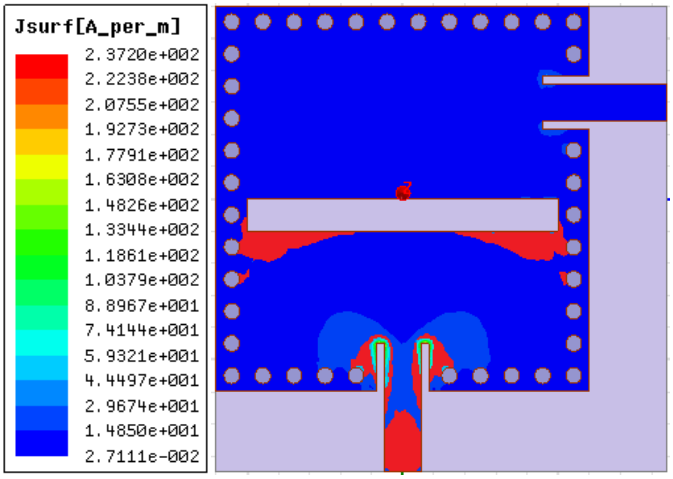

(a)

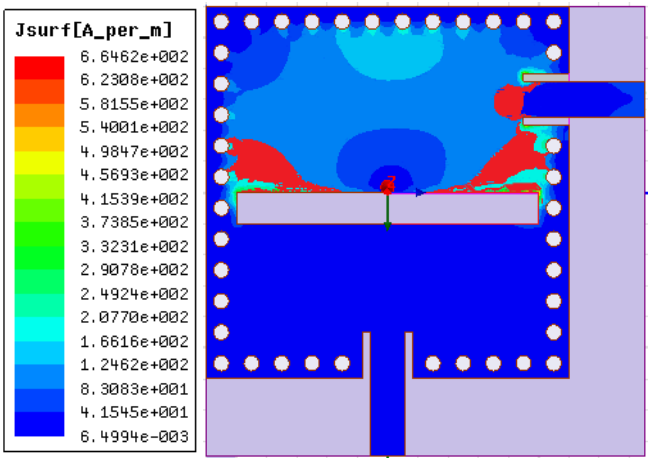

(b)

Figure 6.2 (a) Distribution of surface current, if feeding line F_1 is activated (at 7 GHz) (b) Distribution of surface current , if feeding line F_2 is activated (at 6.5 GHz)

Figure 6.3 shows how the proposed antenna performs at different frequencies. At 6.5 GHz frequency the reflection coefficient $|S_{22}|$ is 14 dB, meaning very little power is reflected back. Similarly, at 7 GHz, the reflection coefficient $|S_{11}|$ is 13 dB, suggesting a good match with the impedance at that frequency. The antenna design also achieves impressive isolation, over 30 dB between the antenna input ports. This is significant accomplishment. By carefully positioning the feed lines, the design reduces unwanted interactions and maximizes isolation. The addition of metalized vias in the substrate helps counter the negative effects of surface waves, ensuring that the energy stays concentrated beneath the radiating patch. This significantly improves the antenna's overall performance, making it more efficient and effective.

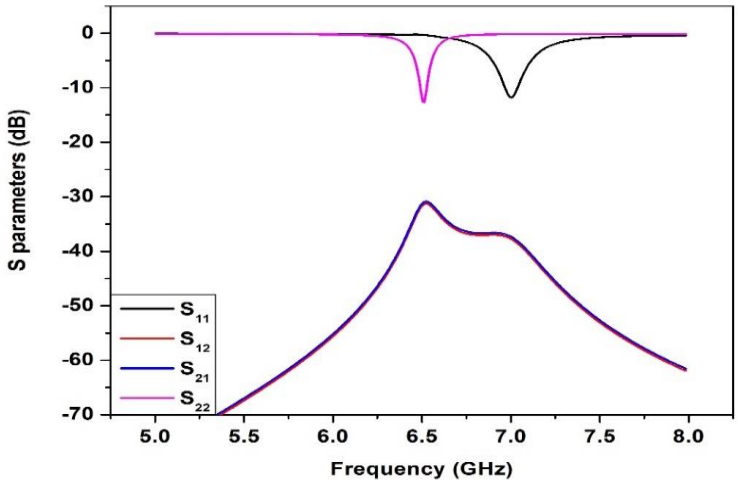

Figure 6.3 S-parameters of the proposed antenna, where the parameter (l_1 = 9 mm)

The placement of the slot in the upper ground plane has a notable influence on the resonating characteristics of the proposed antenna. Fig. 6.4 displays a comparison of the antenna S-parameters for different values of the parameter l_1. Decreasing the value of l_1 causes the lower resonating frequency to decrease while the upper resonating frequency increases. For instance, with l_1 set to 8.5 mm, the lower resonating frequency shifts to 6.3 GHz, and the upper resonating frequency shifts to 7.3 GHz. Further reducing l_1 to 8 mm leads to a lower resonating frequency of 6.1 GHz and an upper resonating frequency of 7.6 GHz. Additionally, the isolation between the two feed line ports, exceeding 30 dB, also changes according to the resonating frequencies.

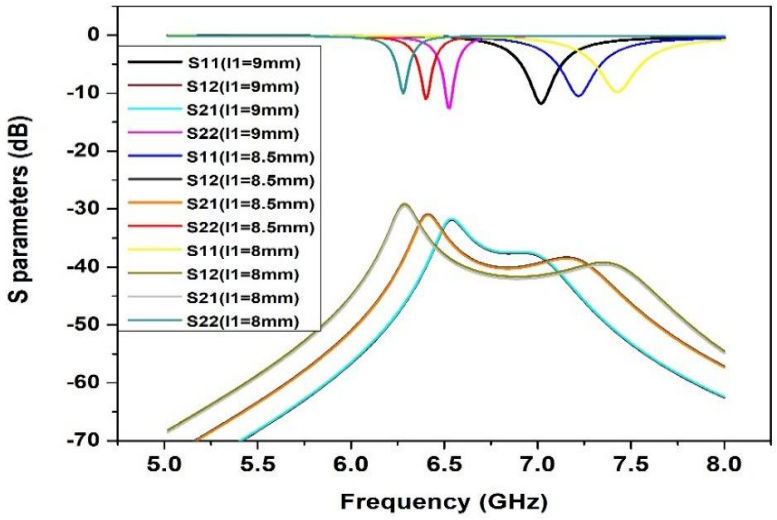

Figure 6.4. The comparison curve of S-parameters for varying slot positions (l_1=9 mm, 8.5 mm, and 8 mm)

To achieve a self-diplexing operation on a planar dielectric substrate, it is crucial to maintain specific feeding configurations. This ensures that most of the energy fed into the antenna is radiated from its specific region, while only a small amount is transmitted to another port. The antenna's radiation patterns in the E-plane and H-plane at 6.5 GHz and 7 GHz, respectively, are shown in Fig. 6.5(a, b).

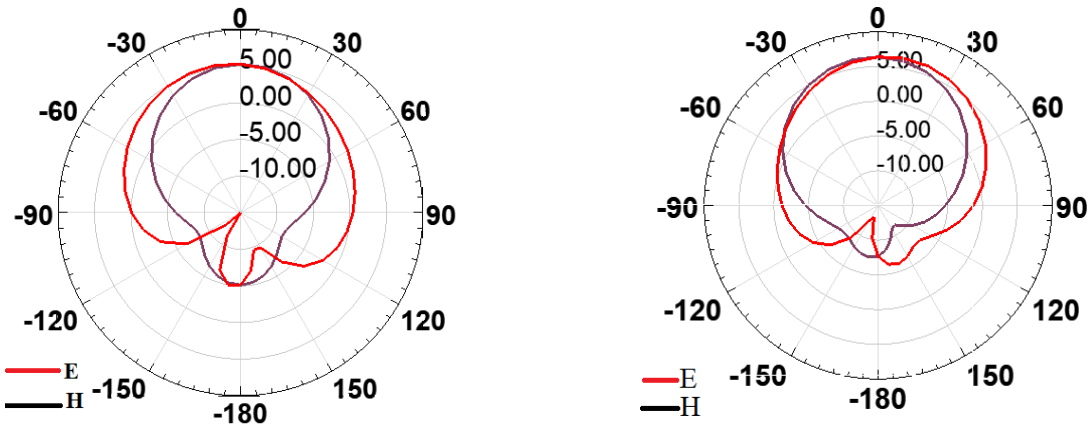

(a) (b)

Figure 6.5. The E-plane and H-plane radiation patterns at two different frequencies: (a) 6.5 GHz and (b) 7 GHz.

These patterns offer valuable insights into the antenna's performance. They showcase the radiation characteristics of the proposed antenna under the specified configuration, where the l_1 parameter is set to 9 mm. In Region II, the feed position is asymmetrical relative to the rectangular slot, and this asymmetry is a contributing factor to the tilt and asymmetry observed in the E-plane radiation pattern at 6.5 GHz.

The antenna under consideration demonstrates outstanding performance at its lower resonant frequency of 6.5 GHz, boasting a remarkable total gain of 4.8 dBi, which highlights its efficiency in capturing and transmitting electromagnetic energy. Likewise, at the higher resonating frequency of 7 GHz, the antenna attains an even more elevated total gain of 6.4 dBi, signifying a notable enhancement in radiation efficiency. Both the E-plane and H-plane radiation patterns exhibit a close alignment, indicating minimal side lobes. This characteristic ensures unidirectional broadside radiation, focusing the majority of the radiated energy in the desired direction. With its remarkable radiation efficiency and directional behaviour, the proposed antenna holds great promise for enhancing the performance of C-band transceiver systems.

To conduct a more in-depth assessment of the antenna's performance, Fig. 6.6 illustrates the radiation efficiency curve. This curve offers a comprehensive analysis of how efficiently the antenna converts input power into radiated energy at various frequencies, providing valuable insights into its overall effectiveness.

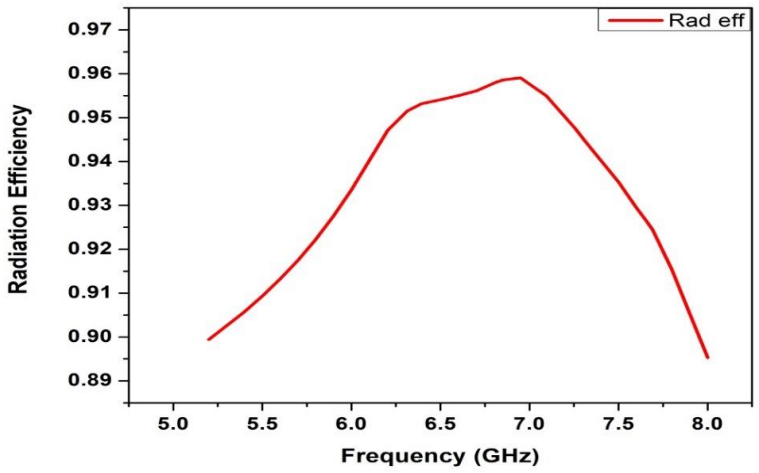

Figure 6.6 The radiation efficiency versus frequency curve

The radiation efficiency of the proposed antenna has been assessed at various resonating frequencies. At the lower resonating frequency of 6 GHz, the antenna demonstrates an impressive radiation efficiency of 92.7%. As we transition to the higher resonating frequency of 7 GHz, the efficiency continues to improve, reaching a remarkable 95.5%.This high level of radiation efficiency distinguishes the proposed antenna from dipole and microstrip patch antennas, surpassing their performance levels. With efficiencies exceeding 90% across various resonating frequencies, this achievement can be attributed to the carefully considered design parameters such as the lengths (l_1 and l_2) of different regions in the antenna.

Table 6.2 displays a comparative analysis of the proposed antenna with previously published designs, highlighting its distinctive attributes. Ultimately the proposed antenna demonstrates superior total gain, showcasing its exceptional capacity to emit signals effectively. Furthermore, it showcases a unidirectional radiation pattern, a valuable characteristic for enabling self-diplexing within a transceiver system. This pattern ensures that the antenna concentrates most of its energy in a specific direction, resulting in improved performance and reduced interference. Based on these findings, the proposed antenna emerges as a superior solution, offering efficient and effective performance for various communication applications.

Table 6.2 Performance comparison of the proposed antenna

Ref. No.	**Resonating Freq.(GHz)**	**Gain (dB)**	**Radaition Pattern**	**$\|S_{21}\|$(dB), $\|S_{12}\|$(dB)**
51.	8.26/10.46	3.56/5.24	Unidirectional	27.9
91.	2.45/5.5	1.9/4.4	Bidirectional	25
53.	9/11.2	4.3/4.2	Unidirectional	25
Proposed Work	6.5/7	4.8/6.4	Unidirectional	30

6.4 Conclusion

Within this chapter, we have investigated a self-diplexing antenna with leaky wave characteristics, utilizing a cavity-backed SIW structure. To achieve this, we introduced a rectangular slot in the top conducting layer, effectively dividing it into two distinct regions. This innovative design approach allows for enhanced control over the radiation properties and beam steering capabilities of the antenna. Additionally, we implemented two inset

microstrip feed lines with an offset configuration, strategically placed for optimal performance. Through our design, we have achieved resonance at two different frequencies, providing versatility in operation. Additionally, our antenna's isolation performance has been exceptional, with more than 30 dB of isolation among the two separate feeding line. This level of isolation minimizes undesired interactions and enhances the antenna's overall performance.

Moreover, our investigation comprises an extensive parametric analysis that centers on the placement of the slots. This analysis has allowed us to fine-tune the antenna's characteristics and optimize its performance, particularly in terms of leaky wave radiation. Based on our findings, we conclude that the designed antenna exhibits leaky wave characteristics, which enables controlled radiation and beam steering capabilities. These features make the antenna highly suitable for C-band wireless applications, where precise and directional communication is crucial. The combination of leaky wave characteristics, resonance capabilities, and effective isolation makes our proposed antenna a promising solution for various wireless communication scenarios.

CHAPTER 7

Half-Mode SIW Band-Pass Filter and Leaky Wave Antenna

In this chapter, we explore the practical implementation and use of a half-mode substrate integrated waveguide (HMSIW) in X-band wireless systems. The versatility of the HMSIW is showcased as it serves both as a filter and a leaky wave antenna. By capitalizing on the advantages of the HMSIW structure, which allows for a smaller size while maintaining propagation characteristics similar to full-mode substrate integrated waveguides, we open up new possibilities. The primary focus of the chapter is on the design and performance of the HMSIW filter. To ensure exceptional performance, a defected ground structure (DGS) is incorporated, resulting in outstanding selectivity and an impressively low insertion loss of only 1.3 dB. Operating within the frequency range of 7.5 GHz to 8.6 GHz, with a center frequency of 7.25 GHz, the HMSIW filter demonstrates its effectiveness.

Furthermore, the chapter explore into the utilization of the HMSIW as a leaky wave antenna. This achievement is realized through the integration of parallel slots in the upper ground plane, enabling the antenna to effectively serve its purpose. By adopting this dual-purpose component in X-band wireless systems, we aim to enhance overall system performance and efficiency.. These slots resonate at 7.9 GHz and 9 GHz, resulting in a high gain exceeding 8.5 dBi at both resonating frequencies. The proposed HMSIW filter and leaky wave antenna are evaluated in the context of X-band wireless systems, demonstrating their suitability for efficient signal filtering and radiation. The chapter concludes by highlighting the potential applications and future directions for further research and development in this field.

7.1 Introduction

In the field of millimeter and microwave component designs, SIWs have captured significant attention in recent years. Their exceptional advantages, including low loss, high quality factor (especially at millimeter wave frequencies), and the ability to fabricate complete circuits on a single substrate, have led to their rapid rise in popularity [49, 85, 95, 96]. However, one limitation of SIW-based components is their relatively larger size compared to planar

transmission line-based components. Therefore, size reduction is crucial for practical applications, and the HMSIW offers a compelling solution by reducing the size by approximately half while maintaining the same cutoff frequency as the full-mode SIW (FMSIW) [15, 97, 98]. Furthermore, HMSIW-based band-pass filters demonstrate comparable performance to FMSIW filters but with a smaller physical footprint [15, 97, 98]. To achieve specific frequency responses in planar lines and SIWs, defected ground structures (DGS) are employed. The implementation of DGS disrupts the propagation of surface currents and can be regarded as a form of metamaterial, particularly when the structure's period is considerably shorter than the wavelength of passing electromagnetic waves [99, 100]. Numerous studies have been conducted on the design and analysis of HMSIW filters, employing various techniques [63, 75, 101]. Additionally, LWAs have garnered popularity due to their simpler design and reduced losses in comparison to conventional planar lines, especially at millimeter wave frequencies. The HMSIW-based LWA inherits the advantages of the full-mode SIW LWA while offering a nearly halved size [102, 103, 104]. Researchers have proposed and investigated different designs of HMSIW LWAs, including the incorporation of umbrella-shaped slots and periodic slots in the upper ground plane [102, 103]. HMSIW antennas in the Ku-band frequency range have been investigated, and one approach involves exploring the implementation of cross slots on the upper ground plane [104]. This chapter centers on the design and simulation of HMSIW structures using the High-Frequency Structure Simulator (HFSS). We begin by creating and contrasting the dispersion curves of HMSIW and FMSIW. Following this, we explore the utilization of the HMSIW structure to develop a band-pass filter and a leaky wave antenna, capitalizing on its benefits. Throughout the design and simulation process, the HFSS software plays a vital role, enabling comprehensive analysis and optimization of these components for enhanced performance.

7.2 HMSIW and HMSIW Filter Design

The proposed HMSIW design utilizes an RT duroid dielectric substrate with a relative permittivity of 2.2 and a height of 0.5 mm. To ascertain the width of the FMSIW, an equivalent rectangular waveguide is employed as a reference, following the methodology outlined in the cited source [96].

$$W_{siw} = W_{RG} + \frac{d^2}{0.95s} \quad (7.1)$$

The provided equation outlines the parameters utilized in the context of the FMSIW, HMSIW, and equivalent rectangular waveguide designs. Within the equation, W_{siw} represents the width of the FMSIW, W_{RG} denotes the width of the equivalent RWG, d signifies the diameter of the metallic vias, and s stands for the spacing between the vias. Moreover, when evaluating the equivalent rectangular waveguide, FMSIW, and HMSIW, the cut-off frequency is determined for the dominant TE_{10} mode of wave propagation. This mode is of particular importance in analyzing the behavior and characteristics of these waveguide structures. Additionally, Fig.7.1 provides a visual representation of the geometrical configuration of the upper part of the proposed HMSIW. It illustrates the layout and arrangement of components and vias within the HMSIW design.

Figure 7.1. Geometrical configuration of the top of HMSIW (W_{ml} = 1.5, W_{HMSIW} = 7, d = 0.4 and s = 0.8; all in mm)

The FMSIW, with a width of 14 mm, exhibits a cut-off frequency of 7.4 GHz. Verification using the finite element method-based HFSS shows that the HMSIW, having a width of 7 mm, has an almost identical cut-off frequency. Fig. 7.2 illustrates the dispersion characteristics of both waveguides, visually presenting their frequency responses and propagation modes, allowing for a comprehensive comparison of their performance.

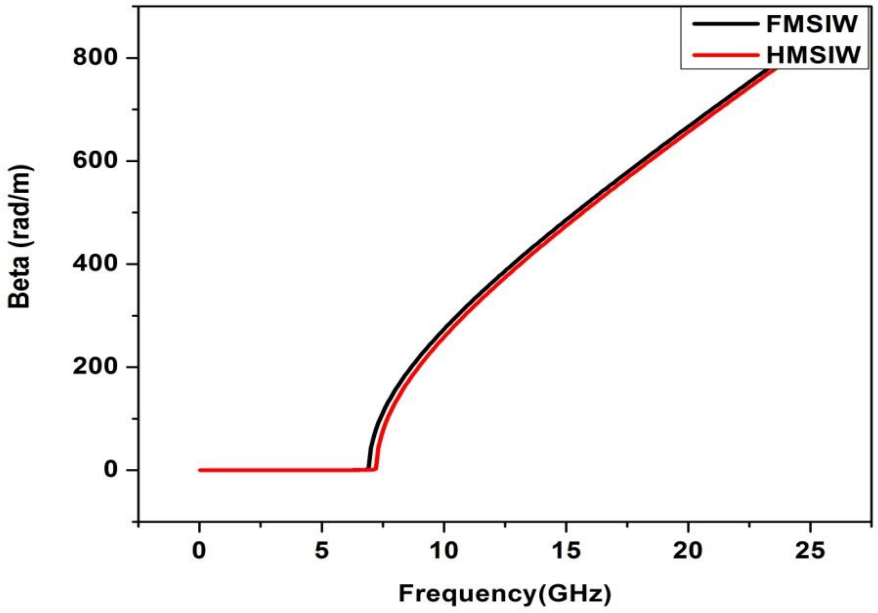

Figure 7.2 Dispersion characteristics of FMSIW and HMSIW

To convert the HMSIW into a band-pass filter, a DGS cell is incorporated into the center of the lower ground plane. Fig.7.3 illustrates the configuration of the DGS cell in the lower ground plane. This diagram provides a visual representation of the layout and structure of the DGS cell within the filter design.

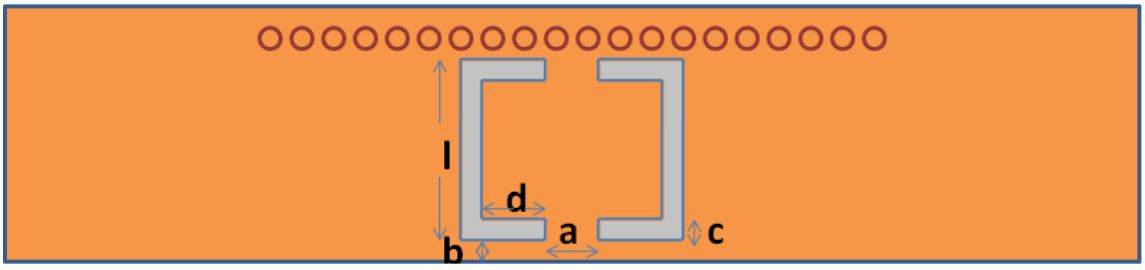

Figure 7.3. Geometrical configuration of DGS (a = 1, b = 0.7, c = 0.5, d = 1.2, and l = 4.8 all in mm)

The DGS employed in a bandpass filter modifies the surface currents in the lower ground plane, resulting in changes in inductance and capacitance. The DGS can be represented as a parallel LC resonant circuit. The values of the inductor (L) and capacitor (C) significantly

influence resonance frequency, shaping the frequency response, and enabling efficient transmission within the desired frequency range while attenuating unwanted frequencies. The DGS parameters, "l" and "d," have a direct impact on the higher cutoff frequency and the frequency range where the filter exhibits a band gap. Adjusting these parameters allows for fine-tuning of the filter's performance. Additionally, the parameter "a" influences the rejection of sidebands, while the parameter "h" affects the overall bandwidth of the filter. By carefully adjusting and customizing these DGS parameters, the bandpass filter can be fine-tuned to optimize the desired frequency response. This involves refining the resonance frequency, bandwidth, sideband rejection, and attenuation of unwanted frequencies to precisely meet the required specifications.

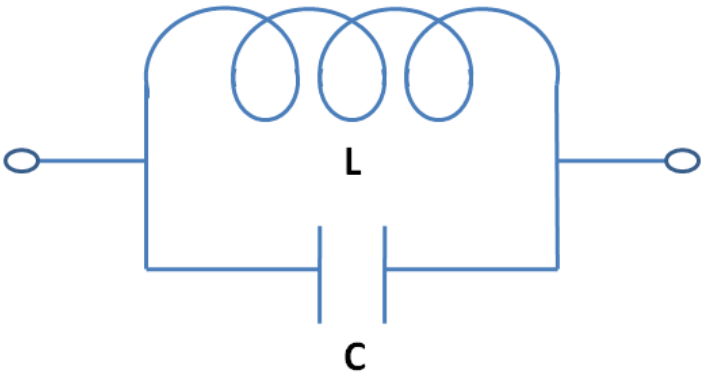

Figure 7.4 DGS equivalent circuit

In Fig. 7.5, the filter's performance is illustrated, revealing a peak insertion loss of 1.3 dB. The presence of minor ripples within the passband can be attributed to the impact of the DGS. Operating at a central frequency of 8.25 GHz, the filter offers a bandwidth ranging from 7.5 GHz to 8.6 GHz.

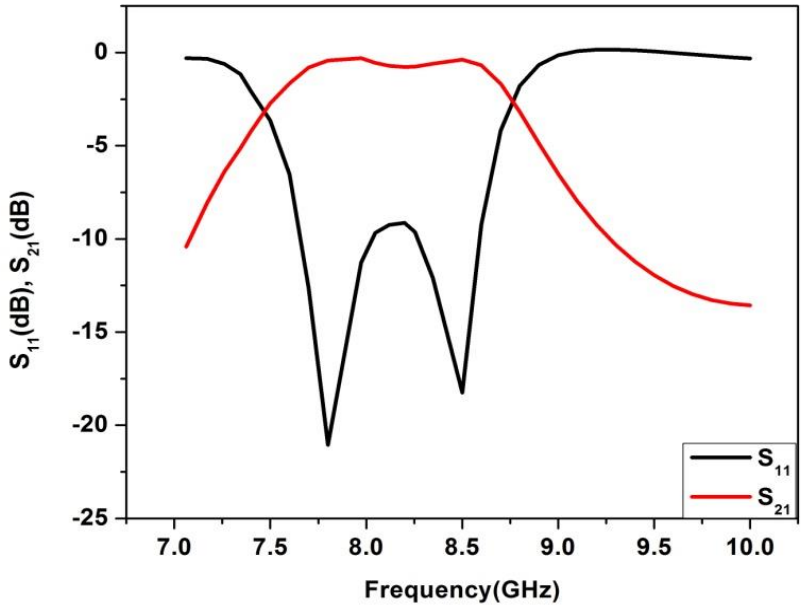

Figure 7.5 S_{11} (dB) and S_{21} (dB) curve of HMSIW filter

7.3 HMSIW Leaky Wave Antenna Design

The conversion of the HMSIW to a LWA requires the introduction of collinear slots in the upper ground plane. These slots are characterized by a length of $\frac{\lambda_0}{4\sqrt{\varepsilon_r}}$ and a width smaller than $\frac{\lambda_0}{8\sqrt{\varepsilon_r}}$, where λ_0 represents the cut-off wavelength of the HMSIW. The central slot is positioned with an offset from the other two slots, maintaining longitudinal and transversal spacing smaller than $\frac{\lambda_0}{4\sqrt{\varepsilon_r}}$. The geometrical arrangement of the LWA is visually represented in Fig. 7.6.

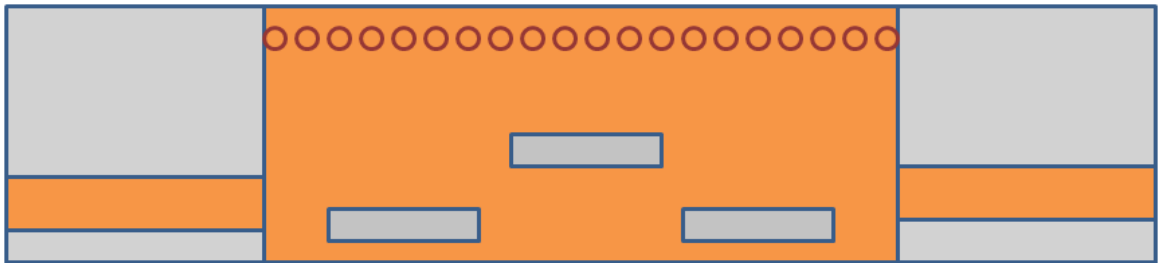

Figure 7.6 Geometrical configuration of LWA

Using the PNA-X Agilent N5247A microwave network analyzer, measurements were performed on the fabricated LWA. The physical appearance of the manufactured LWA is illustrated in Figure 7.7.

Figure 7.7 Fabricated LWA

In Fig. 7.8, a comparison is shown between the $S_{11}(dB)$ versus frequency curves obtained from simulation and measurement. The graphical representation in this plot enables the evaluation of the concurrence or divergence between the simulated and experimentally measured values of the reflection coefficient at various frequencies.

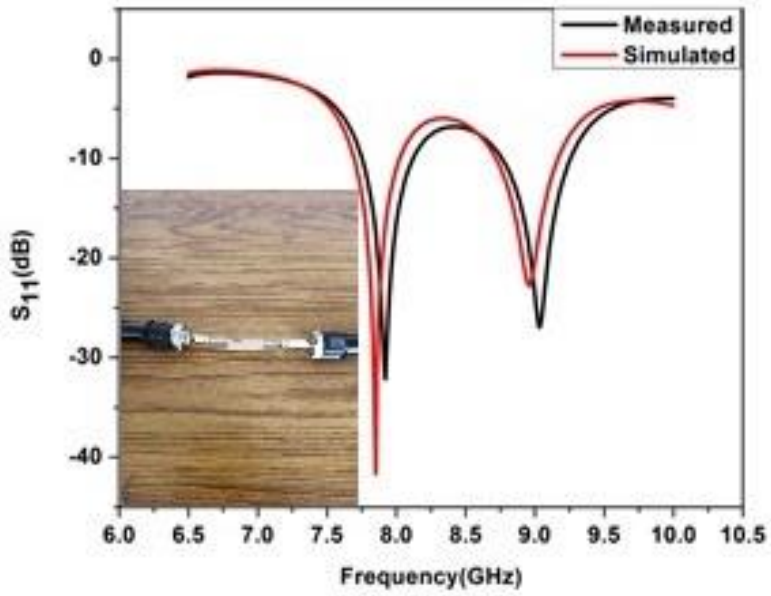

Figure 7.8. Simulated and measured reflection coefficient vs. frequency curve

The LWA demonstrates resonance at two specific frequencies: 7.9 GHz and 9 GHz. When operating at 7.9 GHz, the reflection coefficient $S_{11}(dB)$ reads -37 dB, while at 9 GHz, it measures -24 dB. These values signify the extent of power reflected at each frequency.

To visually depict the radiation patterns of the proposed LWA, we present Fig. 7.9 (a) showing the radiation pattern at 7.9 GHz, and Fig. 7.9 (b) displaying the radiation pattern at 9 GHz. These figures offer a graphical representation of how the antenna emits electromagnetic energy in different directions at the corresponding frequencies. The simulated radiation pattern is strongly correlated with the measured patterns in every direction.

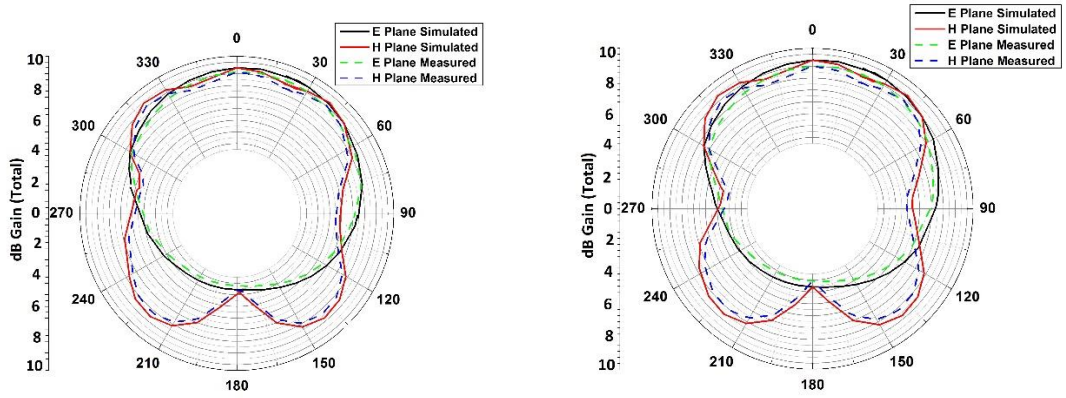

(a) (b)

Figure 7.9. E and H plane patterns at (a) 7.9 GHz (b) 9 GHz

The total gain of the LWA at both resonating frequencies, 7.9 GHz and 9 GHz, surpasses 8.5 dBi. This indicates that the antenna provides a gain of more than 8.5 decibels relative to an isotropic radiator, which implies omnidirectional radiation pattern and improved radiation efficiency.

7.4 Conclusion

In this research, we have successfully designed an HMSIW and analyzed its dispersion curve. The incorporation of DGS allowed for the transformation of the HMSIW into a band-pass filter. Furthermore, by introducing parallel rectangular slots, the HMSIW was converted into a LWA. The S-parameter analysis of the filter received thorough investigation, while the reflection coefficient and radiation pattern of the LWA were subject to detailed examination. HFSS, a software utilizing the finite element method, has been employed for all simulations. Based on our findings, we conclude that the proposed filter and LWA are suitable for various X-band wireless applications

CHAPTER 8

Conclusion and Future Scope

In this thesis, an extensive exploration has been carried out to assess the potential of SIW technology in advancing wireless communication systems. The primary focus of this research has been on the creation, simulation, and experimental validation of diverse SIW filters. Moreover, the study has delved into the investigation and design of leaky wave antennas and half-mode SIW filters. Special attention has also been devoted to exploring smooth transitions between SIW and other planar transmission lines in the prototypes. This exploration aims to seamlessly integrate SIW technology with existing transmission line technologies. Additionally, the research has delved into tunable filtering, wherein physical parameters have been manipulated to achieve desired filtering characteristics.

The findings and outcomes of this research have proven to be highly significant. Demonstrating the potential of SIW technology, this study offers a promising solution for fulfilling the requirements of advanced wireless systems. By leveraging the benefits of metallic waveguides and planar transmission lines, SIW technology allows for the development of compact multiband bandpass filters and antennas that occupy minimal space. Furthermore, this technology offers cost-effective fabrication and facilitates easy integration with other components. The key contributions of this dissertation encompass the following points: Comprehensive exploration of SIW technology, including various SIW configurations and analysis techniques.

- Extensive exploration of the multi-band filter properties in different SIW configurations, including sinusoidally modulated SIW, step-sized SIW, and sinusoidally modulated substrate-integrated folded waveguide (SMSIFW), showcasing their unique design and analysis.

- Comparative study of mode matching techniques (MMT) against commercially available simulators, specifically for the analysis of periodic structures and waveguides with varying cross-sections.
- Design and analysis of a novel cavity-backed slot-loaded SIW self-diplexing antenna tailored for C-band applications, emphasizing its distinctive resonances, gains, and isolation characteristics.
- Innovation in the design of half-mode SIW filters with tunable center frequencies through the incorporation of defected ground structures and leaky wave antenna elements.

Moving forward, there are several potential areas for future research and exploration in the field of SIW technology. Some of the possible avenues for further investigation include:

- Advancement of SIW filters and antennas to cater to higher frequency ranges, specifically millimeter-wave and terahertz frequencies, expanding the capabilities of wireless communication systems.
- Research and exploration of innovative SIW structures and configurations to augment the performance and functionalities of SIW-based components.
- Investigation into novel fabrication methods and materials aimed at enhancing the cost-effectiveness and seamless integration potential of SIW technology.
- Exploration of cutting-edge signal processing techniques and algorithms tailored for SIW-based systems, fostering higher data rates and improved signal quality.
- Seamless integration of SIW technology with emerging wireless communication technologies, including 5G, Internet of Things (IOT), and other upcoming advancements in the field.

In conclusion, this thesis has provided valuable insights into the design, analysis, and application of SIW technology in advanced wireless systems. The research conducted has demonstrated the potential of SIW for developing compact, cost-effective, and high-performance microwave filters and antennas. The findings and outcomes of this thesis lay the foundation for further advancements in SIW technology and its integration into future wireless communication networks.

REFERENCES

1. F. Shigeki, “Waveguide line,” Japan Patent 06-53 711, Feb. 25, 1994.
2. J. Hirokawa and M. Ando, "Single-layer feed waveguide consisting of posts for plane TEM wave excitation in parallel plates," in IEEE Transactions on Antennas and Propagation, vol. 46, no. 5, pp. 625-630, May 1998.
3. H. Uchimura, T. Takenoshita and M. Fujii, "Development of a "laminated waveguide"," in IEEE Transactions on Microwave Theory and Techniques, vol. 46, no. 12, pp. 2438-2443, Dec. 1998.
4. A. O. Nwajana and E. R. Obi, “A Review on SIW and Its Applications to Microwave Components,” Electronics, vol. 11, no. 7, p. 1160, Apr. 2022,
5. D. Deslandes, and K. Wu, “Single-Substrate Integration Technique of Planar Circuits and Waveguide Filters,” IEEE Trans. Microwave Theory Tech., Vol. 51, No. 2, 2003, pp. 593–596.
6. Feng Xu and K. Wu, "Guided-wave and leakage characteristics of substrate integrated waveguide," in IEEE Transactions on Microwave Theory and Techniques, vol. 53, no. 1, pp. 66-73, Jan. 2005.
7. D. Liu, C. Baks and X. Gu, "SIW design considerations for mm Wave applications," IEEE International Symposium on Antennas and Propagation (APSURSI), Fajardo, PR, USA, 2016, pp. 1229-1230, 2016.
8. M. Bozzi, L. Perregrini and K. Wu, "Analysis, design, and sensitivity study of substrate integrated waveguide circuits by using equivalent circuit models," 2014 XXXIth URSI General Assembly and Scientific Symposium (URSI GASS), Beijing, China, 2014, pp. 1-4.
9. R.E. Collin., Field Theory of Guided Waves, Wiley-IEEE Press, 1991.
10. R Garg, M. Bozzi and I. Bahl, “Microstrip Lines and Slotlines” Third Edition, Artech, 2013.
11. G. L. Chen, T. L. Owens and J. H. Whealton, "Theoretical study of the folded waveguide," in IEEE Transactions on Plasma Science, vol. 16, no. 2, pp. 305-311, April 1988.

12. N. Grigoropoulos, B. Sanz-Izquierdo and P. R. Young, "Substrate integrated folded waveguides (SIFW) and filters," in IEEE Microwave and Wireless Components Letters, vol. 15, no. 12, pp. 829-831, Dec. 2005.
13. W. Che, K. Deng, D. Wang and Y. L. Chow, "Analytical equivalence between substrate-integrated waveguide and rectangular waveguide", IET Microw. Antennas Propag., vol. 2, no. 1, pp. 35-41, 2008.
14. W. Hong et al., "Half Mode Substrate Integrated Waveguide: A New Guided Wave Structure for Microwave and Millimeter Wave Application," 2006 Joint 31st International Conference on Infrared Millimeter Waves and 14th International Conference on Teraherz Electronics, Shanghai, China, pp. 219-219, 2006.
15. Q. Lai, C. Fumeaux, W. Hong and R. Vahldieck, "Characterization of the Propagation Properties of the Half-Mode Substrate Integrated Waveguide," in IEEE Transactions on Microwave Theory and Techniques, vol. 57, no. 8, pp. 1996-2004, Aug. 2009.
16. G. H., Zhai, et al., “Folded Half Mode Substrate Integrated Waveguide 3 dB Coupler,” IEEE Microwave Wireless Comp. Lett., Vol. 18, No. 8, pp. 512–514, Aug. 2008.
17. M. Bozzi, D. Deslandes, P. Arcioni, L. Perregrini, K. Wu and G. Conciauro, "Efficient analysis and experimental verification of substrate-integrated slab waveguides for wideband microwave applications", Int. J. RF Microw. Comput.-Aided Eng., vol. 15, no. 3, pp. 296-306, 2005.
18. D. Deslandes, M. Bozzi, P. Arcioni and K. Wu, "Substrate integrated slab waveguide (SISW) for wideband microwave applications," IEEE MTT-S International Microwave Symposium Digest, 2003, Philadelphia, PA, USA, 2003, vol. 2 pp. 1103-1106.
19. S. B. Cohn, "Properties of Ridge Wave Guide," in Proceedings of the IRE, vol. 35, no. 8, pp. 783-788, Aug. 1947.
20. W. Che, C. Li, P. Russer and Y. L. Chow, "Propagation and band broadening effect of planar integrated ridged waveguide in multilayer dielectric substrates," 2008 IEEE MTT-S International Microwave Symposium Digest, Atlanta, GA, USA, pp. 217-220,2008.

21. W. Che, C. Li, D. Zhang and Y. L. Chow, "Investigations on propagation and the band broadening effect of ridged rectangular waveguide integrated in a multilayer dielectric substrate", Microw. Antenna Propag., vol. 4, pp. 674-684, 2010.
22. M. Bozzi, S. A. Winkler and K. Wu, "Broadband and compact ridge substrate-integrated waveguides", IET Microw. Antennas Propag., vol. 4, no. 11, pp. 1965-1973, 2010.
23. D. Deslandes, M. Bozzi, P. Arcioni and K. Wu, "Substrate integrated slab waveguide (SISW) for wideband microwave applications," IEEE MTT-S International Microwave Symposium Digest, Philadelphia, PA, USA, vol.2. pp.1103, 2003.
24. D. Deslandes and K. Wu, "Single-substrate integration technique of planar circuits and waveguide filters," in IEEE Transactions on Microwave Theory and Techniques, vol. 51, no. 2, pp. 593-596, Feb. 2003.
25. G.-Y. Du and L. Jin, "Neural network of calibrated coarse model and application to substrate integrated waveguide filter design", Int. J. RF Microw. Comput.-Aided Eng., vol. 30, no. 10, pp. 1-17, Oct. 2020.
26. L. Silvestri, E. Massoni, C. Tomassoni, A. Coves, M. Bozzi and L. Perregrini, "Substrate Integrated Waveguide Filters Based on a Dielectric Layer With Periodic Perforations," in IEEE Transactions on Microwave Theory and Techniques, vol. 65, no. 8, pp. 2687-2697, Aug. 2017.
27. Z. C. Hao, W. Hong, J. X. Chen, H. X. Zhou, and K. Wu, " Single-layer substrate integrated waveguide directional couplers," IEE Proc-Microw. Antennas Propag., Vol. 153, No.5, pp. 426-432, October 2006.
28. T. Djerafi and K. Wu, "Super-Compact Substrate Integrated Waveguide Cruciform Directional Coupler," in IEEE Microwave and Wireless Components Letters, vol. 17, no. 11, pp. 757-759, Nov. 2007.
29. Ji-Xin Chen, W. Hong, Zhang-Cheng Hao, Hao Li and K. Wu, "Development of a low cost microwave mixer using a broad-band substrate integrated waveguide (SIW) coupler," in IEEE Microwave and Wireless Components Letters, vol. 16, no. 2, pp. 84-86, Feb. 2006.

30. Y. Cassivi and K. Wu, "Low cost microwave oscillator using substrate integrated waveguide cavity," in IEEE Microwave and Wireless Components Letters, vol. 13, no. 2, pp. 48-50, Feb. 2003.
31. F. F. He, K. Wu, W. Hong, L. Han and X. Chen, "A Low Phase-Noise VCO Using an Electronically Tunable Substrate Integrated Waveguide Resonator," in IEEE Transactions on Microwave Theory and Techniques, vol. 58, no. 12, pp. 3452-3458, Dec. 2010.
32. A. Georgiadis, S. Via, A. Collado and F. Mira, "Push-push oscillator design based on a substrate integrated waveguide (SIW) resonator," 2009 European Microwave Conference (EuMC), Rome, Italy, 2009, pp. 1231-1234.
33. M. Abdolhamidi and M. Shahabadi, "X-Band Substrate Integrated Waveguide Amplifier," in IEEE Microwave and Wireless Components Letters, vol. 18, no. 12, pp. 815-817, Dec. 2008.
34. A.O. Nwajana, A. Dainkeh and K.S.K. Yeo, “Substrate integrated waveguide (SIW) diplexer with novel input/output coupling and no separate junction.” Prog. Electromagn. Res. M, 67, pp.75–84, 2018.
35. Y. Leviatan, P. G. Li, A. T. Adams, and J. Perini, “Single-post inductive obstacle in rectangular waveguide,” IEEE Trans. Microwave Theory Tech., vol. MTT-31, pp. 806–812, Oct. 1983.
36. F. Taringou, D. Dousset, J. Bornemann and K. Wu, "Substrate-integrated waveguide transitions to planar transmission-line technologies," 2012 IEEE/MTT-S International Microwave Symposium Digest, Montreal, QC, Canada, pp. 1-3.2012.
37. X. -P. Chen and K. Wu, "Low-loss ultra-wideband transition between conductor-backed coplanar waveguide and substrate integrated waveguide," 2009 IEEE MTT-S International Microwave Symposium Digest, Boston, MA, USA, pp. 349-352,2009.
38. F. Grine, T. Djerafi, M. T. Benhabiles, K. Wu and M. L. Riabi, "High-Q Substrate Integrated Waveguide Resonator Filter With Dielectric Loading," in IEEE Access, vol. 5, pp. 12526-12532, 2017.

39. A. K. Mallick and G. S. Sanyal, "Electromagnetic Wave Propagation in a Rectangular Waveguide with Sinusoidally Varying Width," in IEEE Transactions on Microwave Theory and Techniques, vol. 26, no. 4, pp. 243-249, Apr. 1978.
40. L. Huang and N. Yuan, “A Compact Wideband SIW Band-pass Filter with Wide Stop band and High Selectivity” MDPI, Electronics , 8, 440, 2019.
41. Y. Cassivi, L. Perregrini, P. Arcioni, M. Bressan, K. Wu, and G. Conciauro, “Dispersion characteristics of substrate integrated rectangular waveguide,” IEEE Microwave. Wireless Compon. Letter, vol. 12, no. 9, pp. 333–335, September, 2002.
42. D. Deslandes and K. Wu, “Integrated microstrip and rectangular waveguide in planar form,” IEEE Microw. Wireless Compon. Lett., vol. 11, no. 2, Feb. 2001, pp. 68–70, Feb. 2001.
43. P. Moon and D.E. Spencer, “Field Theory for Engineers”. New York Van Norstrand, pp 303-309, 1961.
44. E. T. Whittaker and G.N. Watson, “Modern Analysis” 4th Ed. 1962. Cambridge University Press. London, p 413-417.
45. A. Iqbal, J. J. Tiang, S. K. Wong, M. Alibakhshikenari, F. Falcone and E. Limiti, "Miniaturization Trends in Substrate Integrated Waveguide (SIW) Filters: A Review," in IEEE Access, vol. 8, pp. 223287-223305, 2020.
46. Z. Kordiboroujeni and J. Bornemann, "Designing the Width of Substrate Integrated Waveguide Structures," in IEEE Microwave and Wireless Components Letters, vol. 23, no. 10, pp. 518-520, Oct. 2013.
47. Z. Kordiboroujeni and J. Bornemann, “Mode-matching analysis and design of substrate integrated waveguide T-junction diplexer and corner filter” International Journal of Numerical Modelling: Electronic Networks, Devices and Fields Int. J. Numer. Model. 28:497–507, 2015.
48. J. Bornemann and R. Vahldieck, “Characterization Of A Class Of Waveguide Discontinuities Using A Modified TExmn Mode Approach” IEEE Transactions On Microwave Theory Techniques Vol. 38, No. 12, Dlclmuek, pp 1816-182, 1990.
49. D. Deslandes and K. Wu., “Accurate modeling, wave mechanisms, and design considerations of a substrate integrated waveguide”. IEEE Transactions on Microwave Theory and Techniques; 54(6):2516–2526, 2006

50. A.V. Labay and J. Bornemann, “Generalized Modal Scattering Matrix Of Discontinuity-Distorted Waveguide Multiport Junctions” international journal of numerical modeling: electronic networks, devices and fields, Vol. 10, 153–167, 1997.
51. S. Nandi and A. Mohan, “An SIW Cavity-Backed Self-Diplexing Antenna,” in IEEE Antennas and Wireless Propagation Letters, vol. 16, pp. 2708-2711, October 2013.
52. D. K. Park, R. Waterhouse, Y. Qian, and T. Itoh, “Self-diplexed integrated antenna transceiver for wireless applications,” in Proc. IEEE Antennas Propag. Soc. Int. Symp., vol. 3, pp. 444–447, 2001.
53. S. Mukherjee and A. Biswas, “Design of self-diplexing substrate integrated waveguide cavity backed slot antenna,” IEEE Antennas Wireless Propag. Lett., vol. 15, pp. 1775–1778, 2016.
54. G. Q. Luo, Z. F. Hu, L. X. Dong and L. L. Sun, “Planar slot antenna backed by substrate integrated waveguide cavity,” IEEE Antennas Wireless Propag. Lett, vol. 7, pp. 235–239, 2008.
55. S. Mukherjee, A. Biswas and K. V. Srivastava, “Bandwidth enhancement of Substrate Integrated Waveguide Cavity backed slot antenna by offset feeding technique”, IEEE Applied Electromagnetics. Conf. (AEMC), pp. 1-2, 2013.
56. G. Q. Luo, Z. F. Hu, W. J. Li, X. H. Zhang, L. L. Sun and J. F. Zheng, "Bandwidth-Enhanced Low-Profile Cavity-Backed Slot Antenna by Using Hybrid SIW Cavity Modes," in IEEE Transactions on Antennas and Propagation, vol. 60, no. 4, pp. 1698-1704, April 2012.
57. W. Che, L. Geng, K. Deng and Y. L. Chow, “Analysis and experiments of compact folded substrate integrated waveguide” IEEE Transactions on Microwave Theory and Techniques, Vol. 56 No.1 January 2008.
58. N. N. Trong, T. Kaufmann, L. Hall and C. Fumeaux, "Variational analysis of folded substrate-integrated waveguides," IEEE Microwave and Wireless Components Letters, vol. 25, no. 6, pp. 352-354, June 2015.
59. X. Guo, L. Zhu and W. Wu, "Design Method for Multiband Filters With Compact Configuration in Substrate Integrated Waveguide," in IEEE Transactions on Microwave Theory and Techniques, vol. 66, no. 6, pp. 3011-3018, June 2018.

60. S. Kumari, V.R Gupta, and S. Srivastava, “Folded Substrate Integrated Waveguide Based Multiband Filter for Wi-Fi6E Application” Wireless Pers. Commun 119, 1607–1618, 2021.
61. J. Mart´ınez, A. Coves, E. Bronchalo, A. A. S. Blas, and M. Bozzi, “Band-pass filters based on periodic structures in SIW technology,” AEU Int. J. Electron. Commun., vol. 112, p. 152942, 2019.
62. Q. Lai, C. Fumeaux, W. Hong and R. Vahldieck, "Characterization of the Propagation Properties of the Half-Mode Substrate Integrated Waveguide," in IEEE Transactions on Microwave Theory and Techniques, vol. 57, no. 8, pp. 1996-2004, Aug. 2009.
63. J. Xu, W. Hong, H. Tang, Z. Kuai and K. Wu, "Half-Mode Substrate Integrated Waveguide (HMSIW) Leaky-Wave Antenna for Millimeter-Wave Applications," in IEEE Antennas and Wireless Propagation Letters, vol. 7, pp. 85-88, 2008.
64. S. Kurudere and V. B. Ertürk, "Novel SIW based interdigital bandpass filter with harmonic suppression," 2014 44th European Microwave Conference, Rome, Italy, pp. 845-848, 2014.
65. M. Li, C. Chen and W. Chen, "Miniaturized Dual-Band Filter Using Dual-Capacitively Loaded SIW Cavities," in IEEE Microwave and Wireless Components Letters, vol. 27, no. 4, pp. 344-346, April 2017.
66. X. Wang , X. W. Zhu , Z. H. Jiang , Z.C. Hao , Yi. W. Wu and W. Hong , “Analysis of Eighth-Mode Substrate-Integrated Waveguide Cavity and Flexible Filter Design” IEEE Transactions On Microwave Theory And Techniques, Vol. 67, No. 7, July 2019.
67. X. Chen, W. Hong, T. Cui, J. Chen, and K. Wu, “Substrate integrated waveguide (SIW) linear phase filter,” IEEE Microwave. Wireless Compon. Lett., vol. 15, no. 11, pp. 787–789, Nov. 2005.
68. C. J. You, Z. N. Chen, X. W. Zhu, and K. Gong, “Single-layered SIW post-loaded electric coupling-enhanced structure and its filter applications,” IEEE Trans. Microw. Theory Techn., vol. 61, no. 1, pp. 125–130, Jan. 2013.
69. Z.C. Hao, W.Q. Ding, and W. Hong, “Developing low-cost W-band SIW bandpass filters using the commercially available printed-circuit board technology,” IEEE Trans. Microw. Theory Techn., vol. 64, no. 6, pp. 1775–1786, Jun. 2016.

70. P. Chu et al., “Dual-mode substrate integrated waveguide filter with flexible response,” IEEE Trans. Microw. Theory Techn., vol. 65, no. 3, pp. 824–830, Mar. 2017.
71. F. Zhu, W. Hong, J. X. Chen, and K. Wu, “Wide stopband substrate integrated waveguide filter using corner cavities,” Electron. Lett., vol. 49, no. 1, pp. 50–52, Jan. 2013.
72. L. Perregrini, C. Tomassoni,”A Review of Compact Substrate Integrated Waveguide (SIW) Interconnects and Components” IEEE 23 signal workshop on signal and power integrity 2019.
73. M. Bozzi, A. Georgiadis and K. Wu, “Review of Substrate Integrated Waveguide Circuits and Antennas”, Special Issue on RF/Microwave Communication Subsystems for Emerging Wireless Technologies. 2010.
74. R. F. Harrington, “Time Harmonic Electromagnetic fields” The IEEE Press on Electromagnetic Wave Theory, P 129, 1968.
75. M. H. Weng, C.Y. Tsai, D. Li. Chen, Yi. C. Chung and R. Y. Yang, “A Bandpass Filter Using Half Mode SIW Structure with Step Impedance Resonator” Electronics, 10, 51. 2021.
76. X.L. Huang, L. Zhou, Y. Huang, L. F. Qiu and J. Fa. Mau, “Quintuple-mode Wideband Packaged Filter Based on a Modified Quarter-Mode Substrate Integrated Waveguide Cavity” IEEE Transactions on Components, Packaging and Manufacturing Technology, vol. 9, no. 11, pp. 2237–2247, 2019.
77. M. Bozzi, L. Perregrini, K. Wu and P. Arcioni, “Current and Future trends in substrate integrated waveguide Technology” Radioengineering”, vol. 18, no. 2, pp. 201-209. June 2009.
78. A. Khan and M. K. Mandal, “Narrowband substrate integrated waveguide bandpass filter with high selectivity” IEEE Microwave Wireless Component Letters, vol. 28, no. 5, p. 416–418, 2018.
79. J. li, Y. Huang, H. Wang, P. Wang and G. Wen, “38 GHz SIW filter based on the stepped-impedance face-to-face E-shaped DGSs for 5G application” Microwave Optical Technology Letters, vol. 61, no. 6, p. 1500–1504, 2019.

80. A. R. Azad, D. K. Jhariya and A. Mohan, “Substrate-integrated waveguide cross-coupled filters with mixed electric and magnetic coupling structure” International of Journal Microwave and Wireless Technologies, vol. 10, no. 8, pp. 896–903, 2018.
81. L. Brillouin, “Wave Propagation in Periodic Structures,” 1st ed.; McGraw-Hill Book Co., Inc.: New York, NY, USA; London, UK, 1946.
82. N. Janković, R. Geschke and V. Crnojević-Bengin, "Compact Tri-Band Bandpass and Bandstop Filters Based on Hilbert-Fork Resonators," in IEEE Microwave and Wireless Components Letters, vol. 23, no. 6, pp. 282-284, June 2013.
83. A. Iqbal, J. J. Tiang, S. K. Wong, S. W. Wong and N. K. Mallat, "QMSIW-Based Single and Triple Band Bandpass Filters," in IEEE Transactions on Circuits and Systems II: Express Briefs, vol. 68, no. 7, pp. 2443-2447, July 2021.
84. S. Pelluri and M. Kartikeyan “Compact triple-band bandpass filter using multi-mode HMSIW cavity and half-mode DGS” International Journal of Microwave and Wireless Technologies, 13(2), pp. 103-110, 2021.
85. S. Kumar and A. De, “Design and analysis of sinusoidally modulated substrate integrated waveguide and filters” Int. J of RF microw comput Aided Eng.,32(e), 22912,2022.
86. C.A. Balanis, “Advanced Engineering Electromagnetic” Wiley: second edition, pp. 330, 2012.
87. J. M. de. Paz, E. U. Munoz, F. J. H. Martinez, V. G. Posadas, L. E. G. Munozand and D. S. Vargas, "Multifrequency Self-Diplexed Single Patch Antennas Loaded with Split Ring Resonators," Progress In Electromagnetics Research, Vol. 113, 47-66, 2011.
88. F. J. Herraiz-Martinez, E. Ugarte-Munoz, V. Gonzalez-Posadas, L. E. Garcia-Munoz and D. Segovia-Vargas, "Self-Diplexed Patch Antennas Based on Metamaterials for Active RFID Systems," in IEEE Transactions on Microwave Theory and Techniques, vol. 57, no. 5, pp. 1330-1340, May 2009.
89. K. R. Boyle, M. Udink, A. de Graauw and L. P. Ligthart, "A Dual-Fed, Self-Diplexing PIFA and RF Front-End," in IEEE Transactions on Antennas and Propagation, vol. 55, no. 2, pp. 373-382, Feb. 2007.

90. C. -Y. -D. Sim, C. -C. Chang and J. -S. Row, "Dual-Feed Dual-Polarized Patch Antenna With Low Cross Polarization and High Isolation," in IEEE Transactions on Antennas and Propagation, vol. 57, no. 10, pp. 3321-3324, Oct. 2009.
91. Y. -C. Lu and Y. -C. Lin, "A Mode-Based Design Method for Dual-Band and Self-Diplexing Antennas Using Double T-Stubs Loaded Aperture," in IEEE Transactions on Antennas and Propagation, vol. 60, no. 12, pp. 5596-5603, Dec. 2012.
92. S. Mukherjee, A. Biswas and K. V. Srivastava, "Broadband Substrate Integrated Waveguide Cavity-Backed Bow-Tie Slot Antenna," in IEEE Antennas and Wireless Propagation Letters, vol. 13, pp. 1152-1155, 2014.
93. T. Zhang, W. Hong, Y. Zhang and K. Wu, "Design and Analysis of SIW Cavity Backed Dual-Band Antennas With a Dual-Mode Triangular-Ring Slot," in IEEE Transactions on Antennas and Propagation, vol. 62, no. 10, pp. 5007-5016, Oct. 2014.
94. R. Garg, I. Bahl and M. Bozi, “Microstrip lines and slot linrs” Artech House, Third edition. Artech House. pp. 513, 2013.
95. Y. J. Cheng, H. Xu, D. Ma, J. Wu, L. Wang, and Y. Fan, “Millimeter-wave shaped-beam substrate integrated conformal array antenna,” IEEE Transactions on Antennas and Propagation, vol. 61, no. 9, pp. 4558–4566, 2013.
96. S .Kumar and A. De, “Design and Mode Matching Analysis of stepped substrate integrated waveguide and filter” IETE Journal of research. Published on line Feb. 2023.
97. Y. Wang, W. Hong, Y. Dong et al., “Half mode substrate integrated waveguide (HMSIW) bandpass filter,” IEEE Microwave and Wireless Components Letters, vol. 17, no. 4, pp. 265–267, 2007.
98. S. Kumar and A. De, "Sinusoidally Modulated Substrate Integrated Folded Waveguide as a Filter for Multiband Applications," 2022 International Conference on Computing, Communication, and Intelligent Systems (ICCCIS), Greater Noida, India, pp. 328-331. 2022
99. Q. Y. Song, H. R. Cheng, X. H. Wang, L. Xu, X. Q. Chen & X. W. Shi “ Novel Wideband Bandpass Filter Integrating HMSIW with DGS” Journal of Electromagnetic Waves and Applications, 23:14-15, pp. 2031-2040, 2009.

100. C. Wang, Z. Wang and Y. M. Huang, "Size-miniaturized half-mode substrate integrated waveguide bandpass filter incorporating E-shaped defected ground structure for wideband communication and radar applications," 20th International Conference on Advanced Communication Technology (ICACT), Chuncheon, Korea (South), pp. 12-16, 2018.
101. M.-H. Ho, C.-I. G. Hsu, K.-H. Tang, and W. Hong, “Miniaturized Band Pass Filter Design Using Half Mode Substrate Integrated Coaxial Resonators,” Micromachines, vol. 13, no. 3, p. 389, Feb. 2022.
102. P. Belwal, R. Agrawal, and S. C.Gupta "Half mode substrate integrated waveguide based leaky wave antenna with low cross polarisation" Frequenz, vol. 74, no. 7-8, 2020, pp. 239-245. 2020.
103. Y. Geng, J. Wang, Y. Li, Z. Li, M. Chen and Z. Zhang, "A Ka-Band Leaky-Wave Antenna Array With Stable Gains Based on HMSIW Structure," in IEEE Antennas and Wireless Propagation Letters, vol. 21, no. 8, pp. 1597-1601, Aug. 2022.
104. R Agarwal, P. Belwal and S. Gupta, “Half Mode Substrate Integrated Waveguide Leaky Wave Antenna with Broadside Gain Enhancement for Ku-Band Applications” Radio engineering, vol.28, no.3, 2019.

List of Publications

Journal Publications

1. S. Kumar and A. De, “Design and analysis of sinusoidally modulated substrate integrated waveguide and filter” Int J RF Microw Comput Aided Eng.; 32(1):e22912, 2022. doi:10.1002/mmce.22912.

2. S. Kumar and A. De, “Design and Mode Matching Analysis of stepped substrate integrated waveguide and filters” IETE Journal of Research, https://doi.org/10.1080/03772063.2023.2171917
3. S. Kumar and A. De, “Design and Analysis of Substrate Integrated Folded Waveguide and Waveguide” submitted in Sadhana Journal, Springer (Under review after revision).

Conference publications

1. S. Kumar and A. De, "Cavity-Backed Slot Loaded Substrate Integrated Waveguide Self-Diplexing Antenna for C Band Applications," 2022 IEEE 6th Conference on Information and Communication Technology (CICT), Gwalior, India, 2022, pp. 1-4, doi: 10.1109/CICT56698.2022.9997872.
2. S. Kumar and A. De, "Sinusoidally Modulated Substrate Integrated Folded Waveguide as a Filter for Multiband Applications," 2022 International Conference on Computing, Communication, and Intelligent Systems (ICCCIS), Greater Noida, India, 2022, pp. 328-331, doi: 10.1109/ICCCIS56430.2022.10037718.
3. S. Kumar and A. De, “Design of a Half-Mode SIW Band-Pass Filter and Leaky Wave Antenna for X-Band “Application” 3rd International Conference on Advancement in Electronics & Communication Engineering, 2023, Ghaziabad, India (Accepted).

Curriculum Vitae

Sudarshan Kumar received his B.E. in Electronics and Communication Engineering from Meerut University and M.Tech in Digital Communication from UPTU, Lucknow. He is currently pursuing a Ph.D. from Delhi Technological University, New Delhi. Additionally, he works as an Assistant Professor at Maharaja Agrasen Institute Of Technology, New Delhi. He has published more than 20 research articles in international journals and conferences, with his primary areas of interest being electromagnetic theory, antenna design, and substrate integrated waveguide components